GRADUATE AERONAUTICAL LABORATORIES
CALIFORNIA INSTITUTE OF TECHNOLOGY

Turbulence, fractals, and mixing

Paul E. Dimotakis and Haris J. Catrakis

GALCIT Report FM97-1

17 January 1997

Firestone Flight Sciences Laboratory

Guggenheim Aeronautical Laboratory

Karman Laboratory of Fluid Mechanics and Jet Propulsion

Pasadena

Turbulence, fractals, and mixing*

Paul E. Dimotakis and Haris J. Catrakis

Graduate Aeronautical Laboratories
California Institute of Technology
Pasadena, California 91125

Abstract

Proposals and experimental evidence, from both numerical simulations and laboratory experiments, regarding the behavior of level sets in turbulent flows are reviewed. Isoscalar surfaces in turbulent flows, at least in liquid-phase turbulent jets, where extensive experiments have been undertaken, appear to have a geometry that is more complex than (constant-D) fractal. Their description requires an extension of the original, scale-invariant, fractal framework that can be cast in terms of a variable (scale-dependent) coverage dimension, $D_d(\lambda)$. The extension to a scale-dependent framework allows level-set coverage statistics to be related to other quantities of interest. In addition to the pdf of point-spacings (in 1-D), it can be related to the scale-dependent surface-to-volume (perimeter-to-area in 2-D) ratio, as well as the distribution of distances to the level set. The application of this framework to the study of turbulent-jet mixing indicates that isoscalar geometric measures are both threshold and Reynolds-number dependent. As regards mixing, the analysis facilitated by the new tools, as well as by other criteria, indicates enhanced mixing with increasing Reynolds number, at least for the range of Reynolds numbers investigated. This results in a progressively less-complex level-set geometry, at least in liquid-phase turbulent jets, with increasing Reynolds number. In liquid-phase turbulent jets, the spacings in one-dimensional records, as well as the size distribution of individual "islands" and "lakes" in two-dimensional isoscalar slices, are found in accord with lognormal statistics in the inner-scale range. The coverage dimension, $D_d(\lambda)$, derived from such sets is also in accord with lognormal statistics, in the inner-scale range. Preliminary three-dimensional (2-D space + time) isoscalar-surface data provide further evidence of a complex level-set geometrical structure in scalar fields generated by turbulence, at least in the case of turbulent jets.

---

* Presented at the NATO Advanced Study Institute series, "Mixing: Chaos and Turbulence," Cargèse (Corsica, France), 7–20 July 1996.

1. Introduction

Turbulent flow, or turbulence, is found to have two important and interrelated properties. It is *chaotic* and it can *transport, stir, and mix* its constituents with great effectiveness.

By chaotic, we mean that it is characterized by irregular temporal and spatial dynamics that are unstably related to its initial and boundary conditions. The Random House Dictionary of the English Language (1971), for example, offers as a definition of *turbulent flow*,

> "The flow of a fluid past an object such that the velocity at any fixed point in the fluid varies irregularly."

We may remove the requirement that an object is necessary for turbulent flow, as noted in a discussion on turbulence (cited in Hinze 1975) by von Karman (1937), who was quoting a 1927 lecture by G. I. Taylor:

> "Turbulence is an irregular motion which in general makes its appearance in fluids, gaseous or liquid, when they flow past solid surfaces or even when neighboring streams of the same fluid flow past or over each other."

If viscous effects are small enough, it is sufficient to impose shear on the flow, by any means, for hydrodynamic instabilities, unsteady flow, and turbulence to be sustained. While the zero-relative-velocity boundary condition on solid boundaries will suffice to generate the shear and vorticity in the flow to trigger turbulence, there are other means to do so, without recourse to solid bodies. We may also remove the restriction from the definition above that the shear zone must be sustained between "neighboring streams of the same fluid". A shear layer between two different fluids, *e.g.*, helium and nitrogen, for example, will also be turbulent.

Irregular motion, however, is an indisputable characteristic of turbulence. As we sit here on ancient Mediterranean shores, Heracleitos comes to mind, on the banks of a small river near the ancient Greek town of Ephesos, in Asia Minor, tossing little sticks on the turbulent river water, two and a half millennia ago, watching them float irregularly downstream, and remarking,**

> "Twice into the same river you could not enter."

** Δὶς εἰς τὸν αὐτὸν ποταμὸν οὐκ ἂν ἐμβαίης.

Despite initial conditions defined a long time in the past (relative to the time it takes the water to reach our observation station from the spring) and steady boundary conditions (the banks are not changing), the unsteady, turbulent (flow in the) river is not the same twice. The caveat of Heracleitos summarizes a quandary of the "turbulence problem." If the goal of science and the study of natural phenomena is the ability to predict their evolution, in what sense does one "predict" turbulence, for a given set of initial and boundary conditions?

For a particular turbulent-flow configuration (initial/boundary conditions), we may list the following possible scenaria, ranging from the more to the less pessimistic:

I. The turbulent flow need not be uniquely related to its initial and boundary conditions, in any sense.

II. The turbulent flow is a unique function of the boundary and initial conditions only in a statistical (mean) sense.

III. There exists a time, long enough for the effects of the initial conditions to have been forgotten, after which the resulting turbulent flow, in a mean sense, is determined by the boundary conditions alone.

IV. For flows in a domain of extent L that is large compared with Λ, the local outer scale of the turbulent-flow region, not only (temporally) initial conditions (after a sufficiently long time), but also inflow (spatially "initial") conditions have a negligible effect.

Scenario II, for example, would accommodate a particular turbulent flow that develops statistics that are well defined, but a function of both the boundary and initial conditions. In such a flow, different initial conditions, for the same boundary conditions, would evolve into a different flow configuration, as $t \to \infty$.† Finally, we must accept that these possibilities need not be universal; what applies to one turbulent flow geometry need not apply to another.

Batchelor (1953) introduces his discussion of homogeneous turbulence with the observation of its irreproducible character, but includes a statement of belief:

---

† As P. Tabeling noted in the discussion, one may wish to consider a fifth scenario in which universal behavior may be anticipated in the limit of very high Reynolds numbers, irrespective of initial/boundary conditions.

> "It is a well-known fact that under suitable conditions, which normally amount to a requirement that the kinematic viscosity ν be sufficiently small, some of these motions are such that the velocity at any given time and position in the fluid is not found to be the same when it is measured several times under seemingly identical conditions. In these motions, the velocity takes random values which are not determined by the ostensible, or controllable, or 'macroscopic', data of the flow, although we believe that the *average* properties of the motion are uniquely determined by the data."

The requirement that the (kinematic) viscosity, $\nu = \mu/\rho$, *i.e.*, viscous effects, must be small should, of course, be interpreted in a relative sense, *i.e.*, in terms of a criterion associated with the dimensionless Reynolds number,

$$Re \equiv \frac{U\Lambda}{\nu} , \tag{1.1}$$

with U and Λ the characteristic velocity and length scale of the flow, respectively. The same fluid may be turbulent, or not, depending on the flow parameters. A "small viscosity" is assessed in comparison of (the fluid property) ν and the product (flow property) $U\Lambda$. That the Reynolds number should be large, must be accepted as a *necessary* requirement for turbulence to be sustainable.

Batchelor, who states that the irregular-flow behavior is "... not determined by the ... data of the flow", here inclusively interpreted as the complete initial and boundary conditions, assumes Scenario IV. To quote Frisch (1995):

> "Batchelor's (1953) *Homogeneous Turbulence* was a landmark in the field, written after considerable experimental and theoretical work had been done in Cambridge in the years after World War II. This monograph contributed to bringing the idea of a 'universal equilibrium' theory of turbulence (one aspect of Kolmogorov's contribution) to a wide scientific audience."

Hinze (1975), in his book on turbulence, is also concerned about the implied extension of the caveat and offers the following:

> "Turbulent fluid motion is an irregular condition of flow in which the various quantities show a random variation with time and space coordinates, so that statistically distinct average values can be discerned."

Scenario I must be excluded altogether from the proper study of turbulent flow, in his opinion, with the discussion in the body of the book itself predicated on Scenario IV. Nevertheless, solutions of the deterministic Navier-Stokes equations of

fluid motion, that we typically accept as containing all the dynamics of turbulence,‡ admit the possibility of non-unique solutions. Depending on the particular flow configuration, the sensitivity of the solutions to initial and boundary conditions can be such as to potentially render even average values of the resulting flow properties a non-unique function of those conditions. Batchelor's belief that the "*average* properties of the motion are uniquely determined by the data," must be accepted as an assumption. It has not been shown that chaotic solutions of the Navier-Stokes equations are ergodic, *i.e.*, that they describe stationary stochastic processes with well-defined statistics. We note the caveat(s) and proceed.

The second characteristic of turbulence is that it *can transport, stir, and mix* its constituents with great effectiveness. Such constituents can be its momentum (density), in which case efficient stirring and mixing of low-momentum fluid originating near no-slip-condition boundaries on a solid surface, for example, produces the many manifestations of drag; flow scalars, such as temperature, leading to heat transport; or chemical reactants, in which case turbulence can produce high chemical reaction rates and combustion heat release.

These two characteristics are the consequence of the dynamics of unsteady vortical structures; the hallmark of turbulence. Indeed, the two notions were intertwined in the minds of the ancient Greeks, who coined the roots of the word. *Turbulence* (situation where eddies abound), derives from the ancient Greek word, *τὐρβη* (eddy, swirl), whence *turban* (swirled headdress), *turbine, turbid* (as in unclear water, in recognition of turbulent flow's ability to pick up dirt and muddy it), *turpitude* (lack of moral clarity), and other unspeakables.♯ At the same time, the Greek verb, *τυρβάζειν*, means: to stir things up, make a mess of, mix.*

---

‡ Feynman, always fascinated by vortices and turbulence, states this belief: "We have no reason to think that there are any terms missing from these equations." (Feynman 1964, Ch. 41, p. 11). Frisch also comments on this, stating that the N-S equation "probably contains all of turbulence." (Frisch 1995, p. 1).

♯ Also related is *tornado, turn, etc.*, from the Greek *τὸρνος* for lathe (wood-/metal-turning tool), or spinning wheel (as for cotton). Euripides: "*Τροχὸς τὸρνου γραφὸμενος*," or, "Wheel, written by the lathe." Aeschylos: "*Βὸμβυκας τὸρνου κὰματον*," or, "Cotton, the spinning wheel's labor." Apropos turbulence and vorticity, the root also connotes twisting/bending. The word *τορνεία* (as in structural lumber) was used for the twisted (bent) main structural ribs of a ship.

* Aristophanes: "*Τον πυλὸν τυρβάζεις βαδίζων*," or, "You are dis*turb*ing the clay/dirt by walking," or, ever sarcastic, "You are making a mess by (simply) walking." In everyday speech, *turbulent* is derogatory. "Turbulent times" are times characterized by great dis*turb*ances. The Latin *turba* derives from the closely-related, ancient Greek *τὐρβα*, *i.e.*, *pêle-mêle* (pell-mell), helter-skelter, messy/unruly (crowd).

At least in incompressible turbulence, mixing of a scalar field, $c(\mathbf{x},t)$, *e.g.*, the jet-fluid concentration field in turbulent-jet flow, which tends to drive scalar values to their (local) spatial average, can be thought of as the result of a process involving "more or less distinct stages," as described by Eckart (1948). The scalar to be mixed may be regarded as first *injected* through a bounding surface (as in a jet), or *entrained* at the largest spatial scales of the flow, as in a shear layer (Brown & Roshko 1974). It is then *stirred* as it is convected by the velocity field associated with unsteady, fusing and fissioning eddies. Finally, it is *mixed* by molecular diffusion, or Brownian motion, in the case of a cloud of particles.

We will attempt a discussion of these phenomena from the vantage point of the properties of isoscalar surfaces, or (scalar) isosurfaces, *i.e.*, the instantaneous three-dimensional surface on which the value of the scalar field of interest is a constant, *i.e.*,

$$c(\mathbf{x},t) = c_0 \ . \tag{1.2}$$

The irregularity in turbulent-flow motions results in scalar level-set surfaces whose geometry is exceedingly complex and suggests that an approach based on fractal ideas and analysis may be appropriate, as was suggested by Mandelbrot (1975a).

Scalar transport and mixing phenomena in unsteady flow, as well as the many manifestations of chaotic advection, are interesting and worthy of study in their own right (*e.g.*, Aref 1984; Ottino 1989 and 1990; and Rom-Kedar *et al.* 1990). We will restrict the present discussion to transport and mixing in turbulent flows, however, at Reynolds numbers that are sufficiently high for the turbulence to be in a fully-developed state. An estimate for the minimum Reynolds number required to achieve this state will be discussed below.

1.1 Fully-developed turbulence

As Batchelor noted, turbulence requires that viscous effects should be small. In practice, one finds that as one increases the Reynolds number of the flow, from very low values, a transition occurs from laminar to unsteady flow and, eventually, turbulence. In a free shear layer, for example, this transition will take place at a value of the local Reynolds number, based on outer flow variables,

$$\mathrm{Re}_\Lambda(x) = \frac{U(x)\,\Lambda(x)}{\nu} \ , \tag{1.3}$$

where, for this flow, $U(x) = \Delta U \equiv U_1 - U_2$ is the difference between the two freestream velocities and $\Lambda(x) = \delta(x)$ is the local width of the shear layer, that is close to $Re_\delta = 40$, or so (Betchov & Szewczyk 1963). This is not too different from the minimum value required for vortex shedding from a smooth, circular cylinder (Roshko 1954), that is triggered by unsteadiness in the separation bubble behind the cylinder, *i.e.*, again, some distance from the closest solid boundary.

In wall-bounded flows, transition from steady to unsteady flow occurs at higher values of the Reynolds number and is, generally, hysteretic. For such flows, a more appropriate criterion for a critical Reynolds number can be based on values below which turbulence cannot be sustained. In circular-pipe flow, for example, this critical value of the Reynolds number, based on the average mass-flow velocity and pipe diameter, is $Re_d \simeq 2 \times 10^3$, or a Reynolds number based on pipe radius of, $Re_R \simeq 1 \times 10^3$ (the latter might be regarded as the more appropriate as it is based on the length scale across which the shear is sustained). For a flat-plate boundary layer, the corresponding value, based on the free-stream velocity, U_∞, and local boundary-layer thickness, δ, is given by (Shen 1954), $Re_\delta \simeq 1.2 \times 10^3$.

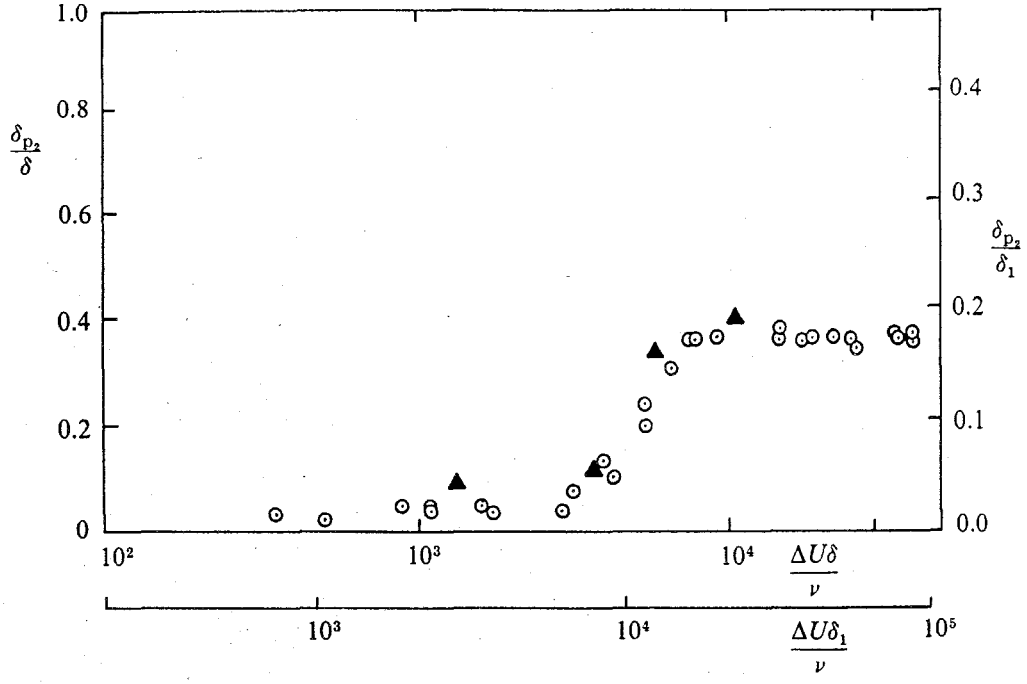

FIG. 1.1 Reynolds number dependence of estimated chemical product volume fraction, in liquid-phase shear layers (Koochesfahani & Dimotakis 1986).

At Reynolds numbers beyond (but close to) these critical values, even though the flow may be unsteady, the effects of viscosity, even though insufficient to main-

tain steady flow, are, nevertheless, still significant and the resulting turbulent flow cannot be described as fully-developed. In all these flows, wall-bounded or not, we typically find a second transition, as the local Reynolds number is further increased, and it is beyond this second transition that the flow may be regarded as *bona fide* turbulent.

In the case of free-shear-layer flows, such a transition was documented by Konrad (1976), who found a clear manifestation, as measured by the amount of fluid in the turbulent region mixed to compositions intermediate between those in the two free streams. This *mixing transition* occurred at a shear-layer Reynolds number of $Re_\delta \simeq 10^4$ and was identified as associated with a large increase in the three-dimensional interfacial area between the entrained freestream fluids (Bernal *et al.* 1979).

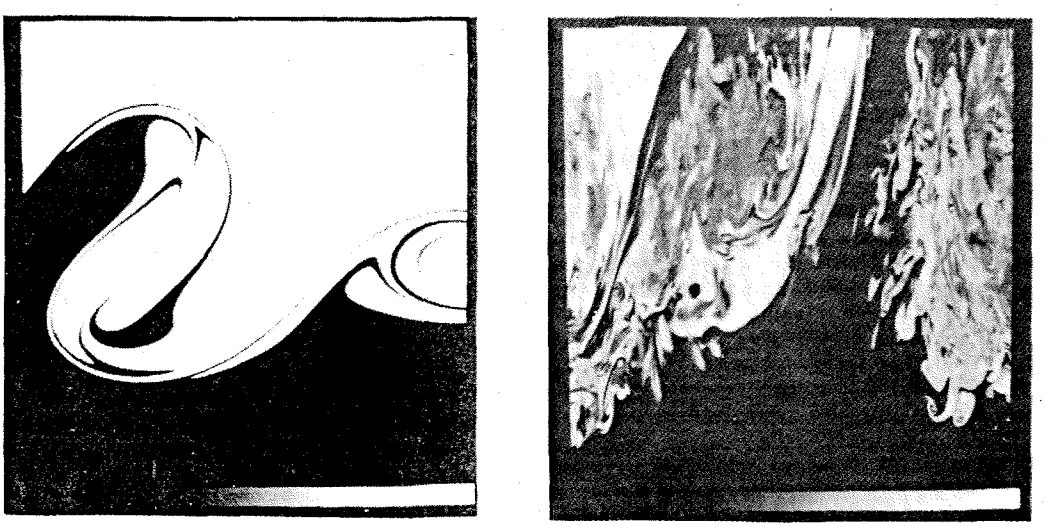

FIG. 1.2 Laser-induced fluorescence space-time images in a liquid-phase shear layer. Left: $Re_\delta \simeq 1.75 \times 10^3$. Right: $Re_\delta \simeq 23 \times 10^3$. (Koochesfahani & Dimotakis 1986, Figs. 7 and 9, respectively).

The shear layer studied by Konrad was a gas-phase shear layer in the original Brown-Roshko apparatus. A similar mixing transition was identified in liquid-phase shear layers (Breidenthal 1981, Koochesfahani & Dimotakis 1986), in the vicinity of the same Reynolds number (see Fig. 1.1). This was also related to a large increase in interfacial surface area and mixing in direct flow-visualization slices of the flow (see Fig. 1.2). As the Schmidt number, *i.e.*,

$$Sc \equiv \frac{\nu}{\mathcal{D}} , \tag{1.4}$$

where ν is the kinematic viscosity of the turbulent fluid and $\mathcal{D}$ is the species diffusivity, for the gas-phase shear-layer flows was of order unity, whereas for the liquid-phase flows of order 10^3, these results indicated that this transition was not a Schmidt-number-dependent phenomenon.

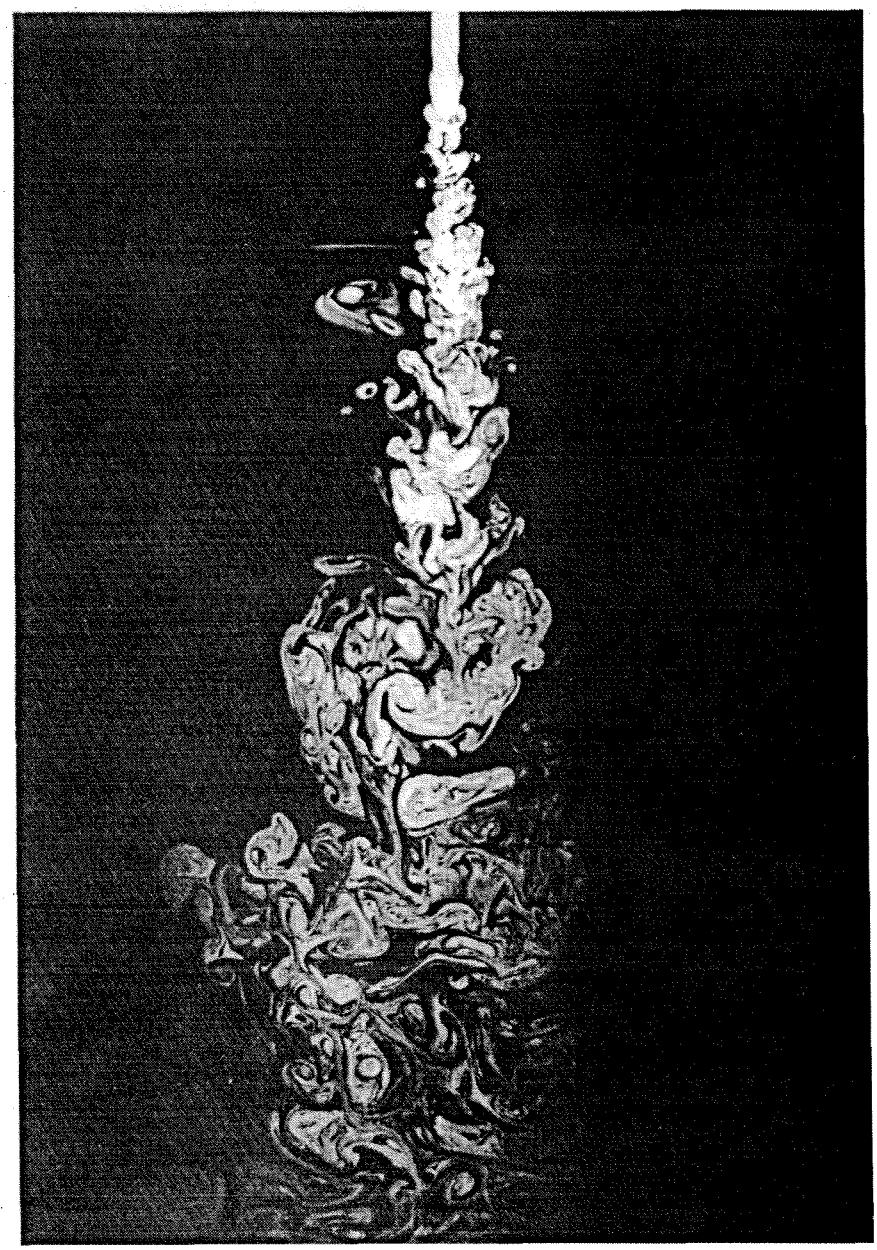

FIG. 1.3a Liquid-phase turbulent jet ($0 \lesssim z/d_j \lesssim 35$) at $Re \simeq 2.5 \times 10^3$.

A transition in mixing behavior can also be observed in turbulent jets, as shown in Figs. 1.3a and 1.3b (reproduced from Dimotakis *et al.* 1983, Figs. 5 and 9, respectively). Figure 1.3a, below, depicts the jet-fluid concentration scalar field

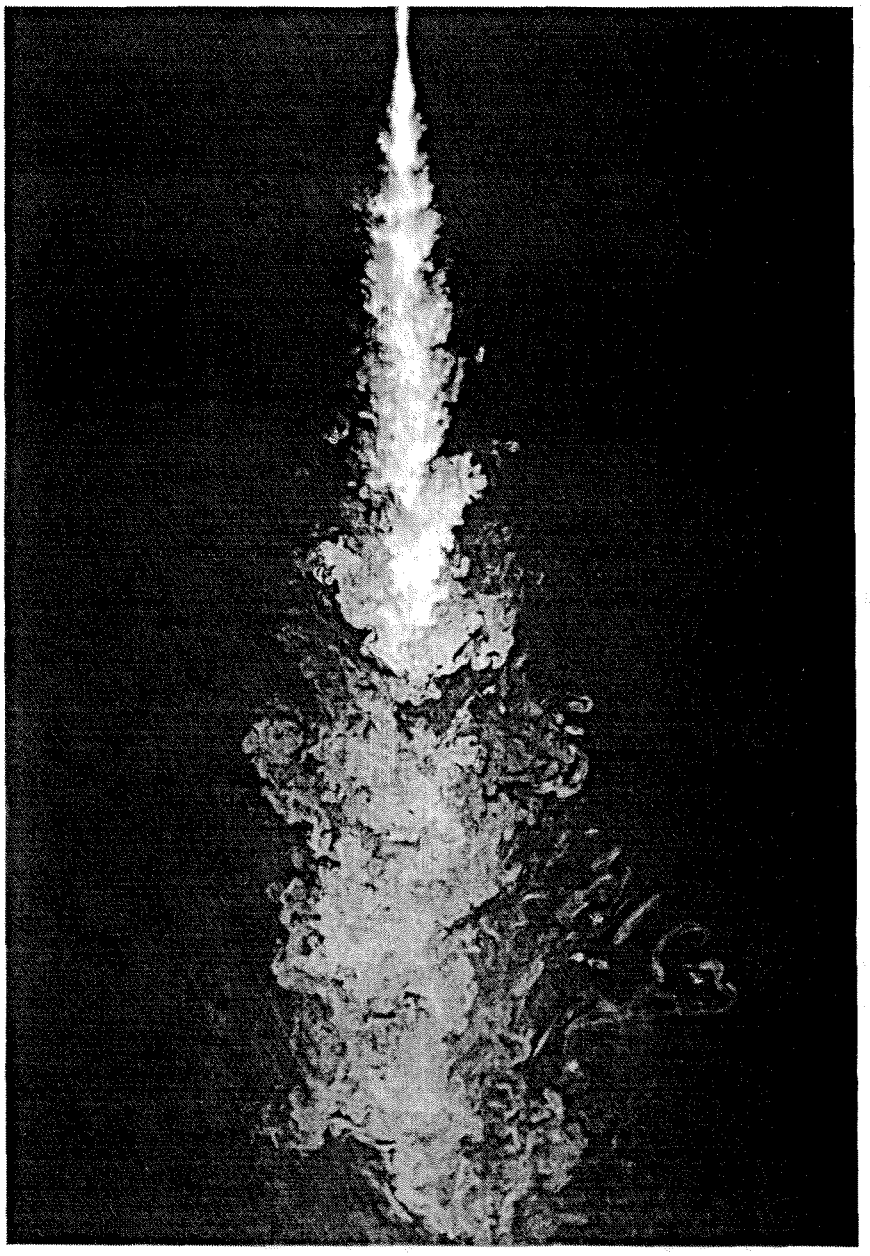

FIG. 1.3b Liquid-phase turbulent jet ($0 \lesssim z/d_j \lesssim 200$) at $Re \simeq 10^4$.

($0 \lesssim z/d_j \lesssim 35$), in the plane of symmetry of the jet, recorded using laser-induced fluorescence of the jet-plenum dye, for a jet Reynolds number of $Re \simeq 2500$. Figure 1.3b is similar, also depicting the far field of a turbulent jet, albeit with a larger field of view ($0 \lesssim z/d_j \lesssim 200$), at a Reynolds number of $Re \simeq 10^4$. As can be seen, there is a qualitative difference in the scalar field behavior, as depicted in Fig. 1.3a, at $Re < 10^4$, and Fig. 1.3b, at $Re \approx 10^4$, respectively. The former indicates a substantial probability of finding unmixed reservoir fluid all the way to the axis of the jet, whereas mixing is substantially more effective at $Re \simeq 10^4$ with the jet able to

homogenize the entrained fluid sufficiently quickly for that probability to be negligible. In the latter, $Re \simeq 10^4$ jet, one can also see regions of nearly homogeneous composition, gradually *decreasing* in jet-fluid concentration from downstream to upstream, separated by a progression of relatively sharp boundaries, indicating entrainment from the upstream boundary of large-scale vortical structures (*cf.* Dahm & Dimotakis 1987). This transitional behavior is also confirmed by chemically-reacting experiments in which the dependence of flame length, *i.e.*, the distance required to mix and react the discharged jet fluid with the entrained reservoir fluid (Gilbrech 1991, Gilbrech & Dimotakis 1992).

Such transitions, albeit not always as conspicuous, have been reported to occur at similar values of the local critical Reynolds number, *i.e.*, at $Re \approx 10^4$. In flows characterized in terms of the Taylor microscale Reynolds number,

$$Re_\mathrm{T} \equiv \frac{u' \lambda_\mathrm{T}}{\nu} , \tag{1.5}$$

where u' is the streamwise root-mean-square (rms) velocity fluctuation level and λ_T is the Taylor microscale, a transition is reported to occur at $Re_\mathrm{T} \approx 70$. In particular, in addition to shear layers and jets, as noted above, transitions to a fully-developed turbulent state, in which flow properties are not as strongly Reynolds-number dependent, have been documented in both the near field (Liepmann & Gharib 1992) and far field of turbulent jets (as discussed above), in lifted jet flames (Hammer 1993); in pipe flow (Wygnanski & Champagne 1973); in flat-plate boundary layers (Collins *et al.* 1978), as manifested in the behavior of the Coles' turbulent boundary layer wake parameter, Π (Coles 1956); in the base-pressure coefficient in circular cylinder wakes (Roshko 1992); in the behavior of the scaled kinetic energy-dissipation rate,

$$\alpha(Re_\mathrm{T}) = \frac{\varepsilon \Lambda}{u'^3} , \tag{1.6}$$

in the flow behind a grid (Sreenivasan 1984), and in numerical simulations of homogeneous, cube-periodic turbulent flow (Jimenez *et al.* 1992); in the transition from "soft" to "hard" turbulence in thermal convection (Hezlot *et al.* 1978); as well as the Reynolds-number-dependence of the torque required to sustain a constant rotation rate in Couette-Taylor flow (Lathrop *et al.* 1992a, 1992b).

This list of (second) transitions, which is probably not exhaustive, indicates that there exists a property of turbulence that results in a more-or-less distinct transition from an unsteady-flow state, at relatively low Reynolds numbers, to a state in which viscous forces are less important. That this transition occurs in

such a wide variety of flows suggests that it is not a consequence of the large-scale behavior of the flow, which varies substantially from one flow to the next. It is more likely the consequence of inner-scale dynamics, that may be regarded as less sensitive to outer-flow dynamics. This hypothesis is also supported by the observation that all these transitions occur at, roughly, the same Reynolds number. An argument in support of this hypothesis, based on the significance and relative magnitude of the various spatial scales of turbulence, was discussed by Dimotakis (1993) and is summarized below for completeness.

The dynamics of turbulence may be regarded as contained between the flow outer scale, δ, and an inner scale in the vicinity of the kinetic-energy-dissipation (Kolmogorov 1941a) scale,

$$\lambda_{\rm K} \equiv \left(\frac{\nu^3}{\varepsilon}\right)^{1/4} . \tag{1.7}$$

At high Reynolds numbers, the two scales will be well separated, *i.e.*, the ratio $\lambda_{\rm K}/\delta \sim Re^{-3/4}$ will be large. In that case, we expect that intermediate-scale behavior may be approximated as (more-or-less) uncoupled and independent of the outer-scale dynamics, as well as inviscid, for spatial scales, λ, small compared to δ, but large compared to $\lambda_{\rm K}$, *i.e.*, for

$$\lambda_{\rm K} \ll \lambda \ll \delta . \tag{1.8}$$

To refine the upper bound of this range, outer-scale-independent dynamics requires a scale of interest, λ, that is small compared to one that can be generated directly from the outer-scales of the flow. Such a scale would be the laminar boundary-layer thickness, $\lambda_{\rm L}$, that can be generated by a single δ-size sweep across the turbulent region, for example. The size of this scale may be estimated by the 99%-thickness of a Blasius (1908) boundary layer, for example, that has been developing for a length δ, or (see Fig. 1.4),

$$\frac{\lambda_{\rm L}}{\delta} \simeq 5.0\, Re^{-1/2} . \tag{1.9}$$

As noted by Liepmann, in private conversation many years ago, this carries the same Reynolds-number dependence and is closely-related to the Taylor scale, $\lambda_{\rm T}$. We will accept that outer-scale independence, *i.e.*, no viscous coupling to outer-scale dynamics, imposes the much stricter spatial-scale-separation requirement, at large Re, of $\lambda \ll \lambda_{\rm L}$.

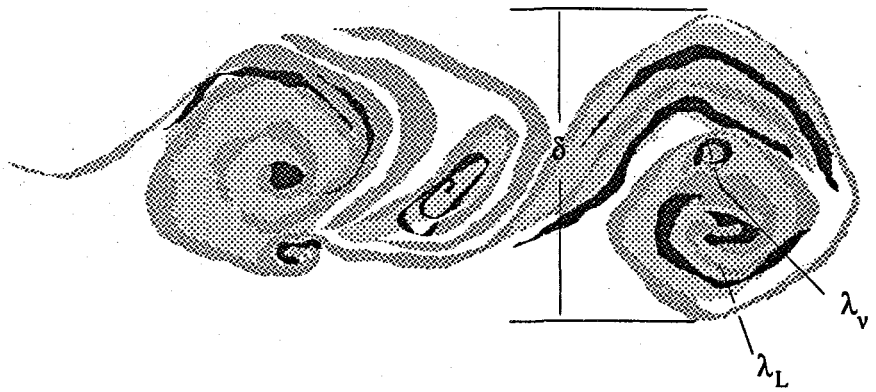

FIG. 1.4 Schematic of the outer scale, δ; the Liepmann boundary-layer scale, λ_L; and the viscous scale, λ_ν, in a sheared turbulent region.

To refine the lower bound in Eq. 1.8, inviscid dynamics dictate that the scale of interest, λ, must be large compared to some viscous scale, λ_ν. This can be related to the Kolmogorov scale, λ_K, and estimated in terms of the wavenumber, k_ν, where the energy spectrum has been found to deviate from a near-$^5/_3$ power-law behavior, or $k_\nu \lambda_K \simeq 1/8$ (*cf.* Chapman 1979, Saddoughi & Veeravalli 1994). To the extent that this may be regarded as a universal dimensionless factor, this yields a value that is a multiple of the (defined) Kolmogorov scale (*cf.* Eq. 1.7), *i.e.*,

$$\lambda_\nu \simeq \frac{2\pi}{k_\nu} \simeq 50\,\lambda_K \ . \tag{1.10}$$

At least on the centerline of a turbulent jet, for which experimental estimates of the kinetic-energy dissipation, ε, are available (Friehe *et al.* 1971), the Kolmogorov scale, λ_K, can be related to the outer-scale (local jet diameter), $\delta(x)$, to yield (*cf.* Eq. 1.7 and discussion in Dimotakis 1993),

$$\frac{\lambda_K}{\delta} \simeq 0.95\,Re^{-3/4} \ , \tag{1.11}$$

and, therefore, if the viscous scale is estimated as the wavelength associated with k_ν, we have, at least for turbulent jets,

$$\frac{\lambda_\nu}{\delta} \simeq 50\,Re^{-3/4} \ . \tag{1.12}$$

We will accept that inviscid dynamics impose the stricter inner-scale requirement of $\lambda_\nu \ll \lambda$.

Combining the refined inner- and outer-scale bounds (Eqs. 1.9 and 1.12), we then have,

$$\frac{\lambda_{\rm min}}{\delta} \simeq \frac{\lambda_\nu}{\delta} \approx 50\,Re^{-3/4} \ll \frac{\lambda}{\delta} \ll \frac{\lambda_{\rm max}}{\delta} \simeq \frac{\lambda_L}{\delta} \approx 5.0\,Re^{-1/2} \ , \tag{1.13}$$

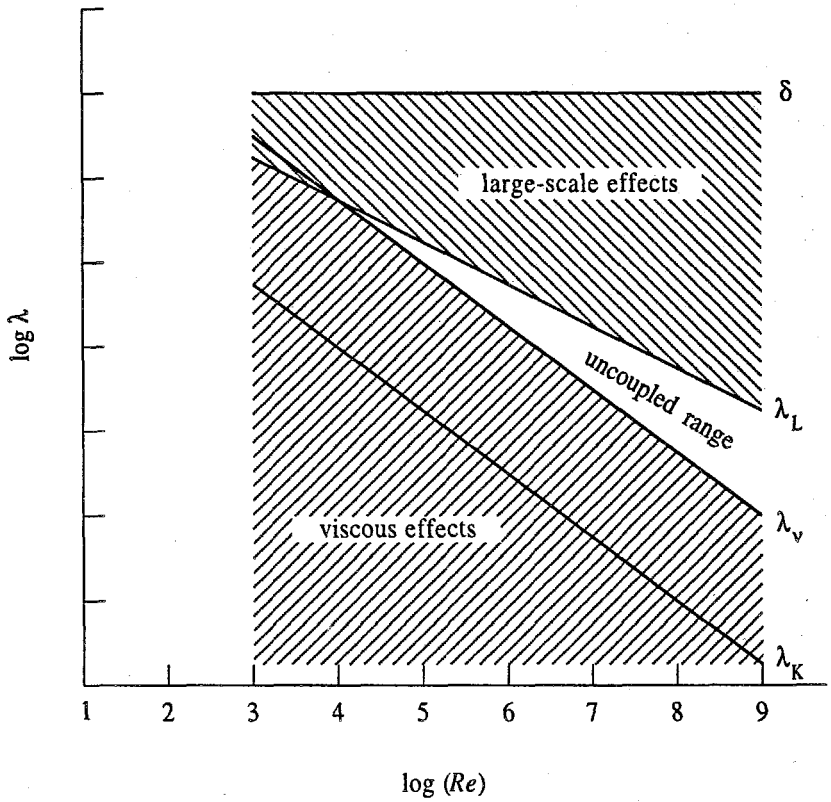

FIG. 1.5 Reynolds number dependence of spatial scales for a turbulent jet.

as estimated for a turbulent jet. This condition is satisfied if,

$$\frac{\lambda_{\mathrm{L}}}{\lambda_{\nu}} \simeq \frac{\lambda_{\mathrm{max}}}{\lambda_{\mathrm{min}}} \simeq 0.1\, Re^{1/4} > 1 \ , \tag{1.14}$$

or, if,

$$Re \gtrsim 10^4 \ . \tag{1.15}$$

These relations are summarized in Fig. 1.5.

While the numerical estimate for the energy dissipation rate, ε, was made based on empirical data for a turbulent jet, the other constants were not flow-specific. As a consequence, we may expect that the two factors of 50 and 5.0, in the λ_{ν}/δ and $\lambda_{\mathrm{L}}/\delta$ scaling, respectively, should not depend strongly on the flow geometry. As indicated by the list above of flows where such a transition has been reported, it appears to be a flow-independent value.

We may conclude that a minimum Reynolds number, approximately equal to 10^4, is required for the outer scales of the flow to be regarded as inviscid and for an intermediate range of scales to exist in which the dynamics may be approximated

as inviscid and outer-scale independent. It is in such an intermediate range of scales that one may expect the self-similar dynamics hypothesized by Richardson (1926), Kolmogorov (1941a), and others to be applicable and, perhaps, produce level-sets with the scale-invariant geometric similarity described by Mandelbrot as the defining characteristic of fractals (Mandelbrot 1989), as we'll discuss below. We will revisit this similarity property in the context of our discussion of experimental observations of scalar level-set geometrical properties.

1.2 Scalar transport and mixing

The convection-diffusion equation that describes the transport and mixing of a scalar field, $c(\mathbf{x},t)$, is given by,

$$\frac{\partial c}{\partial t} + \mathbf{u}\cdot\frac{\partial c}{\partial \mathbf{x}} = \mathcal{D}\frac{\partial}{\partial \mathbf{x}}\cdot\frac{\partial c}{\partial \mathbf{x}} , \tag{1.16}$$

where $\mathcal{D}$ is the species diffusivity (Eq. 1.4), here assumed constant, or,

$$\hat{\mathcal{L}}_{\mathcal{D}}(\mathbf{u})\, c(\mathbf{x},t) \equiv \left\{ \frac{\partial}{\partial t} + \left(\mathbf{u} - \mathcal{D}\frac{\partial}{\partial \mathbf{x}} \right)\cdot\frac{\partial}{\partial \mathbf{x}} \right\} c(\mathbf{x},t) = 0 . \tag{1.17}$$

Temperature, $T(\mathbf{x},t)$, is also a scalar field with a transport described by the same equation, but with its own diffusivity, $\mathcal{D}_T$, *i.e.*,

$$\hat{\mathcal{L}}_{\mathcal{D}_T}(\mathbf{u})\, T(\mathbf{x},t) \equiv \left\{ \frac{\partial}{\partial t} + \left(\mathbf{u} - \mathcal{D}_T\frac{\partial}{\partial \mathbf{x}} \right)\cdot\frac{\partial}{\partial \mathbf{x}} \right\} T(\mathbf{x},t) = 0 . \tag{1.18}$$

The convection-diffusion equation is linear, *e.g.*, for a scalar species whose concentration field is given by $c(\mathbf{x},t)$, we have $\hat{\mathcal{L}}_{\mathcal{D}}(\mathbf{u}) \neq \mathrm{fn}[c(\mathbf{x},t)]$ and, similarly, for the temperature field. Given the evolution of the complete velocity field, $\mathbf{u}(\mathbf{x},t)$, for a particular flow realization, and a set of initial and boundary conditions on the scalar field, it is instructive to consider the calculation, potentially after the fact, in which we compute the realization-specific evolution of a scalar field, $c(\mathbf{x},t)$, as it would have been transported and diffused in the spatio-temporal environment defined by $\mathbf{u}(\mathbf{x},t)$. Even in the case of a passive scalar, *i.e.*, if the scalar field does not influence the velocity field and could be computed after it, however, this would still be a task of some complexity.

In fully-developed turbulence, constant-c (iso)surfaces are characterized by a very large growth rate in area, as well as a rapid increase in geometric complexity. Furthermore, in the case of a convecting-diffusing field characterized by a *high Schmidt* number (Eq. 1.4), *i.e.*, $Sc \gg 1$, we have to contend with an additional difficulty. The Schmidt number is close to unity for gas-phase species diffusion and of the order of 10^3 for liquid-phase diffusion of moderate molecular-mass species. The smallest spatial scale of the scalar field, say, $\lambda_{\mathcal{D}}$, will be smaller than the smallest (viscous) scale, λ_ν, that characterizes the velocity (vorticity) field. In the case of heat diffusion (convection-diffusion of temperature), the quantity corresponding to the Schmidt number is the *Prandtl* number,

$$Pr \equiv \frac{\nu}{\mathcal{D}_T} , \tag{1.19}$$

with $\mathcal{D}_T$ the diffusivity of temperature (Eq. 1.18), is close to unity for heat diffusion in air, and close to 7 for water.

In the case of convection-diffusion of a high-Schmidt-number species in turbulence, one may expect (Batchelor 1959),

$$\lambda_{\mathcal{D}} \approx \lambda_\nu / Sc^{1/2} , \tag{1.20}$$

where λ_ν is the viscous scale (Eq. 1.10), and equivalently for temperature. By way of example, in the case of the diffusion of moderately large organic molecules in water, such as disodium fluorescein, which is often used in laser-induced fluorescence studies, $Sc \simeq 1900$ (Ware *et al.* 1983) and $\lambda_{\mathcal{D}} \approx \lambda_\nu / 44$. Smaller spatial scales would also render a numerical simulation temporally stiffer. The smallest Eulerian time scales associated with the scalar field would be smaller than the smallest Eulerian time scales of the convecting velocity field, by (very nearly) the same factor.

The convection-diffusion equation can be written with respect to a local coordinate system that is fixed on the scalar isosurface by noting that the only component of the local velocity that enters is the one selected by the direction of the scalar gradient. In particular, if,

$$\zeta(\mathbf{x},t) \equiv \frac{\partial}{\partial \mathbf{x}} c(\mathbf{x},t) = \hat{\mathbf{n}} \frac{\partial c}{\partial n} = \hat{\mathbf{n}}\, \zeta , \tag{1.21}$$

where $\hat{\mathbf{n}}$ is a local unit vector normal to the isosurface (in the direction of the scalar gradient), $\zeta(\mathbf{x},t)$, and n is the arc length along the space-curve tangent to it, then,

$$\mathbf{u} \cdot \frac{\partial c}{\partial \mathbf{x}} = u_n \frac{\partial c}{\partial n} . \tag{1.22}$$

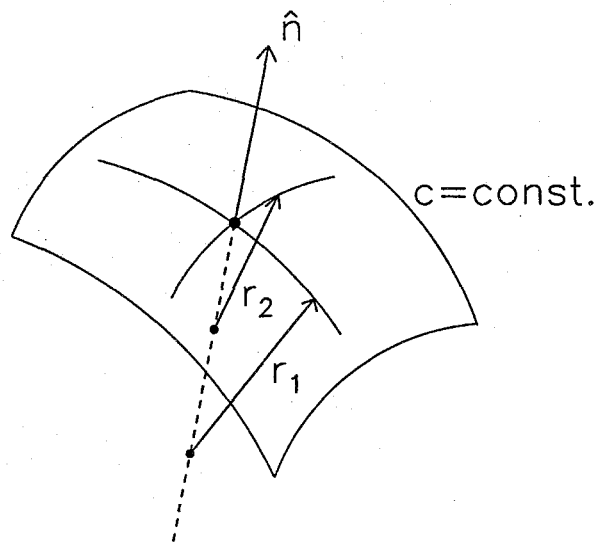

FIG. 1.6 Isoscalar surface patch.

The scalar transport equation can then be written as, (*cf.* Eq. 1.16), *i.e.*,

$$\frac{\partial c}{\partial t} + \mathbf{u}_c \cdot \frac{\partial c}{\partial \mathbf{x}} = 0 \ , \tag{1.23a}$$

where

$$\mathbf{u}_c = \mathbf{u} + \mathbf{u}_\mathcal{D} \ , \tag{1.23b}$$

and where $\mathbf{u}_\mathcal{D}$ is the diffusive contribution to the isosurface transport velocity, given by,

$$\mathbf{u}_\mathcal{D} = -\mathcal{D} \frac{\nabla^2 c}{|\partial c/\partial n|} \hat{\mathbf{n}} \ . \tag{1.23c}$$

as noted by Gibson (1968). More recently, Pope (1988) reported on isosurface propagation, relating $\mathbf{u}_\mathcal{D}$ to the local isosurface geometry (local curvature tensor), and Pope *et al.* (1989), and Girimaji & Pope (1992) pursuing its relation to scalar transport using velocity fields derived from direct numerical simulation of isotropic turbulence. The analysis of isosurface propagation can be simplified further, however, as illustrated below.

The isoscalar transport velocity, $\mathbf{u}_c$ involves only projections along the local scalar gradient. This allows the scalar transport equation to be written as,

$$\frac{\partial c}{\partial t} + u_c \frac{\partial c}{\partial n} = 0 \ , \tag{1.24a}$$

with

$$u_c = u_n + u_\mathcal{D} \ , \tag{1.24b}$$

and

$$u_{\mathcal{D}} = -\mathcal{D}\,\frac{\nabla^2 c}{\partial c/\partial n} \ . \tag{1.24c}$$

The preceding indicates that isoscalar surfaces are conserved on space curves along the local scalar gradient, in a frame moving along these paths given by,

$$n(t) = n(0) + \int_0^t u_c(t')\,\mathrm{d}t' \ , \tag{1.25}$$

with a transport velocity, u_c, that is the sum of a convective and diffusive contribution, with the latter dependent on the local isosurface geometry. In particular, writing the Laplacian in terms of the local isosurface coordinates, we have,

$$\nabla^2 c = \frac{\partial}{\partial \mathbf{x}} \cdot \left(\hat{\mathbf{n}}\,\frac{\partial c}{\partial n} \right) = \left(\frac{\partial}{\partial \mathbf{x}} \cdot \hat{\mathbf{n}} \right) \frac{\partial c}{\partial n} + \frac{\partial^2 c}{\partial n^2} \ , \tag{1.26a}$$

where,

$$\frac{\partial}{\partial \mathbf{x}} \cdot \hat{\mathbf{n}} = \kappa = \frac{1}{r_1} + \frac{1}{r_2} \ . \tag{1.26b}$$

with κ the (invariant) local mean curvature.** In this expression, r_1 and r_2 are the local principal radii of curvature of the scalar isosurface (or the radii of curvature along any orthogonal plane-pair cut). We then have,

$$\nabla^2 c = \kappa \frac{\partial c}{\partial n} + \frac{\partial^2 c}{\partial n^2} \ . \tag{1.26c}$$

A sign choice for r_1 and r_2, as they enter in the expression for the mean curvature, κ, is implicit in this expression, depending on whether the curvature in the corresponding direction is convex in the direction $+\hat{\mathbf{n}}$, of the scalar gradient, or in the direction $-\hat{\mathbf{n}}$, *i.e.*, opposite the scalar gradient. By way of example, for the geometry depicted in Fig. 1.6, both curvatures are convex in the $+\hat{\mathbf{n}}$ direction and both signs are plus. For a saddle point, the two signs would be opposite and if the two radii of curvature are equal (in magnitude) the two terms would cancel and κ would be zero. These expressions allow us to express $u_{\mathcal{D}}$ (Eq. 1.24c) in terms of the diffusivity and the local scalar-field geometry, *i.e.* (in the nondegenerate case),

$$u_{\mathcal{D}} = -\mathcal{D}\left(\kappa + \frac{1}{\zeta}\,\frac{\partial \zeta}{\partial n} \right) \ , \tag{1.27}$$

** This result (Eq. 1.26b) was communicated to one of us (PD) by G. B. Whitham, some years ago (pvte. comm.). J. M. Ottino (1989, p. 36) offers a similar result, expressing it in terms of the in-surface divergence only.

with $\zeta = \partial c/\partial n$ (Eq. 1.21). Combining these relations leads to a scalar-transport equation that can be written as (*cf.* Eq. 1.24),

$$\frac{\partial c}{\partial t} + \left[u_n - \mathcal{D}\left(\kappa + \frac{1}{\zeta}\frac{\partial \zeta}{\partial n} \right) \right] \frac{\partial c}{\partial n} = 0 \ . \tag{1.28}$$

This formulation must be amended at points where the local scalar gradient (instantaneously) vanishes (Gibson 1968). Such points are singular, in this sense,† with the scalar transport equation reducing to a local simple diffusion equation, *i.e.*,

$$\frac{\partial c}{\partial t} = \mathcal{D}\frac{\partial}{\partial \mathbf{x}} \cdot \frac{\partial c}{\partial \mathbf{x}} \ , \qquad \text{wherever} \qquad \frac{\partial c}{\partial \mathbf{x}} = 0 \ . \tag{1.29}$$

It is interesting to scale, $u_{\mathcal{D}}$, the diffusive contribution to the isosurface transport velocity. Accepting the diffusion scale, $\lambda_{\mathcal{D}}$ (Eq. 1.20), as the appropriate scaling length along the scalar gradient arc-length, n, we have (Eq. 1.27),

$$\frac{u_{\mathcal{D}}}{u'} = -\frac{\mathcal{D}}{u'\,\lambda_{\mathcal{D}}}\left(\lambda_{\mathcal{D}}\,\kappa + \frac{\lambda_{\mathcal{D}}}{\zeta}\frac{\partial \zeta}{\partial n} \right) \ . \tag{1.30a}$$

The prefactor is the reciprocal of a Peclet number based on the flow diffusion-scale. This can be estimated as,

$$\frac{u'\,\lambda_{\mathcal{D}}}{\mathcal{D}} \sim \left(\frac{u'}{U} \right) Re^{1/4}\, Sc^{1/2} \ . \tag{1.30b}$$

For fully-developed turbulent flow, the ratio, u'/U, of the rms velocity to the outer velocity scale, can be taken as Re-independent, to an excellent approximation. Consequently, this contribution can be seen to be only weakly dependent on the Reynolds number and is lower in liquid-phase scalar transport (high Sc), for example, than in gas-phase scalar transport.

We see that local isosurface curvature, alone, contributes to isosurface transport, even in the absence of a local convecting field and a vanishing second derivative of the scalar field in the direction normal to the isosurface, *i.e.*, wherever $\partial^2 c/\partial n^2 = \partial \zeta/\partial n = 0$. It can also lead to local counter-gradient scalar transport. Conversely, in regions where isosurface curvature can be ignored, *i.e.*, if r_1 and r_2 are large, or, more precisely, if,

$$|\kappa| = \left| \frac{1}{r_1} + \frac{1}{r_2} \right| \ll \left| \frac{1}{\zeta}\frac{\partial \zeta}{\partial n} \right| \ , \tag{1.31a}$$

† We should note, however, that they are likely to be (very) rare in a three-dimensional scalar field.

a locally-flat approximation can be employed. This simplifies the local convection-diffusion equation to,

$$\frac{\partial c}{\partial t} + u_n \frac{\partial c}{\partial n} \simeq \mathcal{D} \frac{\partial^2 c}{\partial n^2} \ . \tag{1.31b}$$

If diffusion occurs in a thin layer straddling, say, the $n = 0$ point along the scalar-gradient path and a local Taylor-expansion in employed, we may write,

$$u_n = u_0 + n \left(\frac{\partial u_n}{\partial n} \right)_{n=0} + O(n^2) \simeq u_0 - \sigma n \ , \tag{1.32a}$$

where $\sigma = -(\partial u_n / \partial n)_{n=0}$ is the local strain rate on the $n = 0$ (iso)surface, provides an adequate approximation for the local velocity component along the scalar gradient, the convection-diffusion equation can be simplified further to yield, locally, in a frame moving with u_0,

$$\frac{\partial c}{\partial t} - \sigma n \frac{\partial c}{\partial n} \simeq \mathcal{D} \frac{\partial^2 c}{\partial n^2} \ . \tag{1.32b}$$

This equation possesses solutions in closed form (*e.g.*, Carrier *et al.* 1975; Karagozian & Marble 1986) These were used in a model that estimated chemical-product formation in turbulent shear-layers, in the limit of high Damköhler numbers, *i.e.*, diffusion-limited reactions, in high Reynolds number flows, in which high local strain rates may be expected, with the preponderant fraction of molecular diffusion also expected to occur in thin diffusion layers (Dimotakis 1987).

As an aside, it would appear that only the velocity component in the direction of the scalar gradient, *i.e.*, $u_n = \hat{\mathbf{n}} \cdot \mathbf{u}$, enters in the scalar-field transport (Eq. 1.16). This is not correct, however, as can be seen by writing the equation for the transport of the scalar gradient, *i.e.*,

$$\frac{\partial \boldsymbol{\zeta}}{\partial t} + \mathbf{u} \cdot \frac{\partial \boldsymbol{\zeta}}{\partial \mathbf{x}} = \boldsymbol{\omega} \times \boldsymbol{\zeta} - \left(\boldsymbol{\zeta} \cdot \frac{\partial}{\partial \mathbf{x}} \right) \mathbf{u} + \mathcal{D} \frac{\partial}{\partial \mathbf{x}} \cdot \frac{\partial \boldsymbol{\zeta}}{\partial \mathbf{x}} \ , \tag{1.33}$$

where $\boldsymbol{\omega} = \boldsymbol{\omega}(\mathbf{x}, t)$ is the local vorticity field. The convected scalar gradient is rotated by the local vorticity; is amplified by a favorable local strain rate, with a term akin to the stretching term in the vorticity-transport equation; and is diffused. See also equivalent formulation in the article by P. Haynes, in this series, who used tensor notation to express the transport equation.

The preceding suggests that the local transport and mixing of a scalar field, $c(\mathbf{x}, t)$, can be described in terms of the evolution of the c-isosurfaces and, in turn, their local geometrical properties. While such a description also requires knowledge of the convecting velocity field, the geometrical description of the isosurfaces and, in particular, such properties as the local surface-to-volume ratio distribution, distribution of spatial scales that measure the distance to the isosurface, local-curvature distribution, *etc.*, provide essential information, from this point of view.

The geometry of isosurfaces also arises, in a natural way, in the context of mixing in chemically-reacting systems and combustion. In the case of non-premixed, hydrocarbon diffusion flames in the high Damköhler number (diffusion-limited) regime, for example, high-activation-energy chemical kinetics confine the instantaneous burning to the unsteady, three-dimensional, stoichiometric isosurface (Burke & Schumann 1928). While premixed combustion is more complicated, it can be cast in a similar language, with a burning surface that can be described as a constant-property surface. This surface, however, in addition to being propagated by the effects of the local convecting velocity field and diffusion, as in the case of a passive scalar discussed above, advances perpendicular to itself into regions of the flow occupied by unburnt reactant mixture with its own (laminar-flame) Lagrangian speed, as augmented and modified by the local, unsteady-flow, composition, and radiation environment. See discussion of premixed and nonpremixed turbulent combustion in the article by Lasheras *et al.* (1996) in this series.

2. Fractals

Characterizations of the geometry of isocontours and isosurfaces, *i.e.*, constant-property (level) sets, in turbulence and other phenomena in which complex structures are encountered, require an extension of the notions of conventional geometry. If regarded as possessing a complexity that extends over the whole range of scales, *e.g.*, the two Koch islands in two dimensions (*cf.* Figs. 2.1a,b), such objects are not *rectifiable*, *i.e.*, they are not differentiable and do not possess a finite arc length (*e.g.*, Mandelbrot 1977, p. 27). They may, however, be analyzed using the language of *fractals*, an extension to conventional geometry proposed by Mandelbrot to apply to a host of natural phenomena (Mandelbrot 1967, 1975a, 1975b, 1977, and 1982).

In this extension, fractional (non-integer) dimensions can be used to describe the geometrical object. The word *fractal* was coined by Mandelbrot (1975a, 1975b)

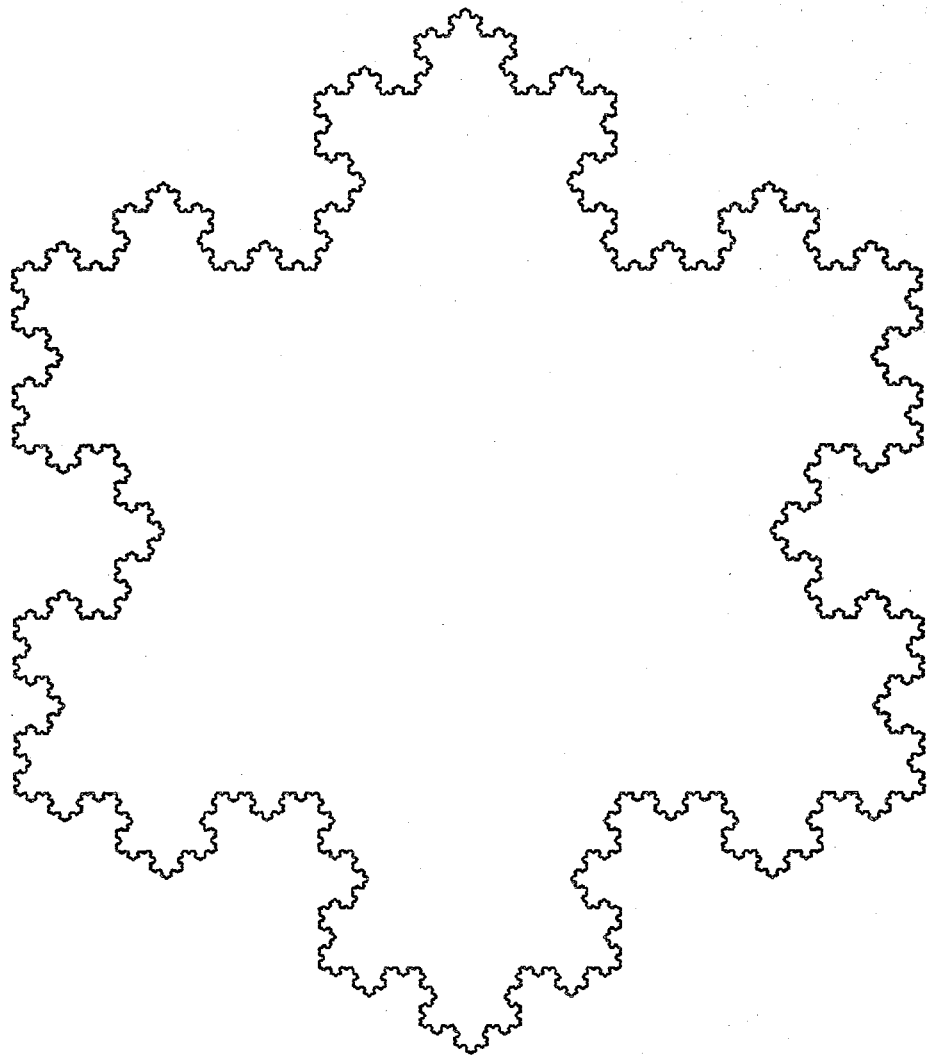

FIG. 2.1a Contour of triadic Koch island with $D = 1.26$.

from the Latin *fractus*, meaning "fragmented," and denotes objects that are (Mandelbrot 1989), "... rough and fragmented to the same degree at all scales."

An isoelevation contour in a topographic map, or the special case of the sea-level contour, *i.e.*, a coastline, illustrates the point, as Mandelbrot noted by the question (Mandelbrot 1967, 1977) "How long is the coastline of Britain?" expanding on a discussion by L. F. Richardson (published posthumously in 1961) on the length of various coastlines. A moment's reflection will reveal that the length of a cartographer's coastline will depend on the resolution (scale) at which the coastline is rendered.

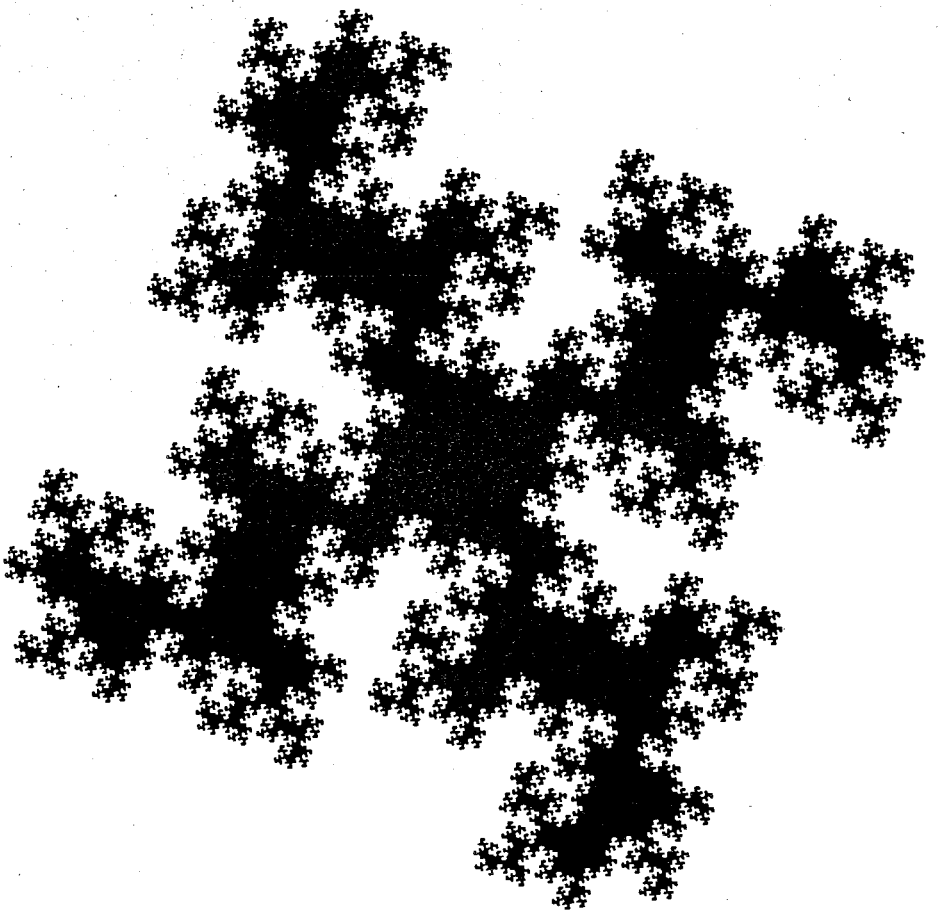

FIG. 2.1b A more complex Koch island with $D = 1.61$ (Mandelbrot 1977, Plate 51).

Following Richardson, one way the question may be addressed is by fixing the resolution to which the curve (or surface) is represented and then measuring the arc length (or surface area) with a commensurate yardstick, or step size, keeping track of the coastline length as a function of the step size. In particular, one can lay a ruler, open a pair of dividers, stretch a string, *etc.*, of length, say, λ, from a point on the curve and mark the point of its intersection with the curve at the other end. That point becomes the beginning of the next step, *etc.* A measure of the arc length, $L(\lambda)$, at this resolution, is then given by the product of the length of the string times the number of steps, $N(\lambda)$, required to traverse the coastline *i.e.*,

$$L(\lambda) \;=\; \lambda\, N(\lambda)\ . \tag{2.1}$$

If the coastline may be regarded as a fractal object that is "rough and fragmented to the same degree at all scales," then the fractional increase in the number

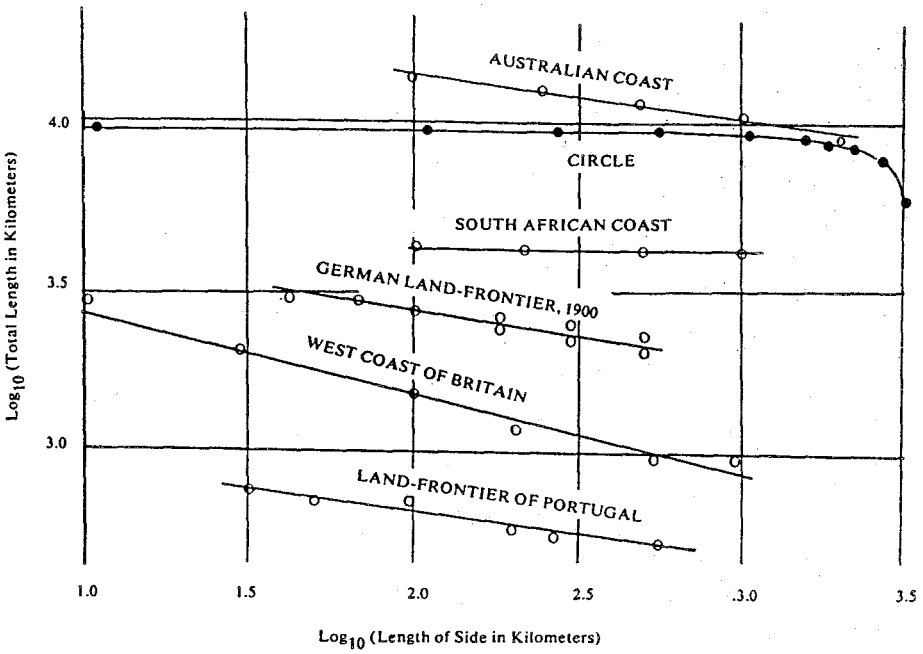

FIG. 2.2 Richardson (1961) coastline data (Mandelbrot 1977, Plate 32).

of steps required, per unit fractional increase in step size, will be a constant, *i.e.*,

$$\frac{\mathrm{d}N/N}{\mathrm{d}\lambda/\lambda} = -D \ , \tag{2.2}$$

and the number of λ-size steps required will follow a power-law relation,‡

$$N(\lambda) \propto \lambda^{-D} \ . \tag{2.3}$$

The (negative) exponent D is identified as the *fractal dimension* of the level set and can be seen to be the (negative) logarithmic derivative of the number of stretched-string steps with respect to λ, *i.e.* (Eq. 2.2),

$$D = -\frac{\mathrm{d}\log N}{\mathrm{d}\log \lambda} \ . \tag{2.4}$$

The corresponding measure of the length of the coastline can then be expressed as a function of the resolution (divider-point spacing, string-length, *etc.*) λ,

$$L(\lambda) = \lambda N(\lambda) \propto \lambda^{1-D} \ . \tag{2.5}$$

‡ See also discussion by G. Zaslavsky, elsewhere in this series, where it is shown that such behavior occurs on phase-space island boundaries, where geometric-scale self-similarity is encountered.

If the curve is a straight line, then $N(\lambda) \propto 1/\lambda$, $D = 1$, and $L(\lambda) \neq \text{fn}(\lambda)$, as one would like. For a complex coastline, however, we will have the benefit of stepping across "bays" and "peninsulas", with increasing step size λ, and will require a number of steps that decreases faster than $1/\lambda$, as λ increases. If the relation between $N(\lambda)$ and λ is a power law, then the level set may be regarded as a fractal, with a fractal dimension as indicated in Eq. 2.4.

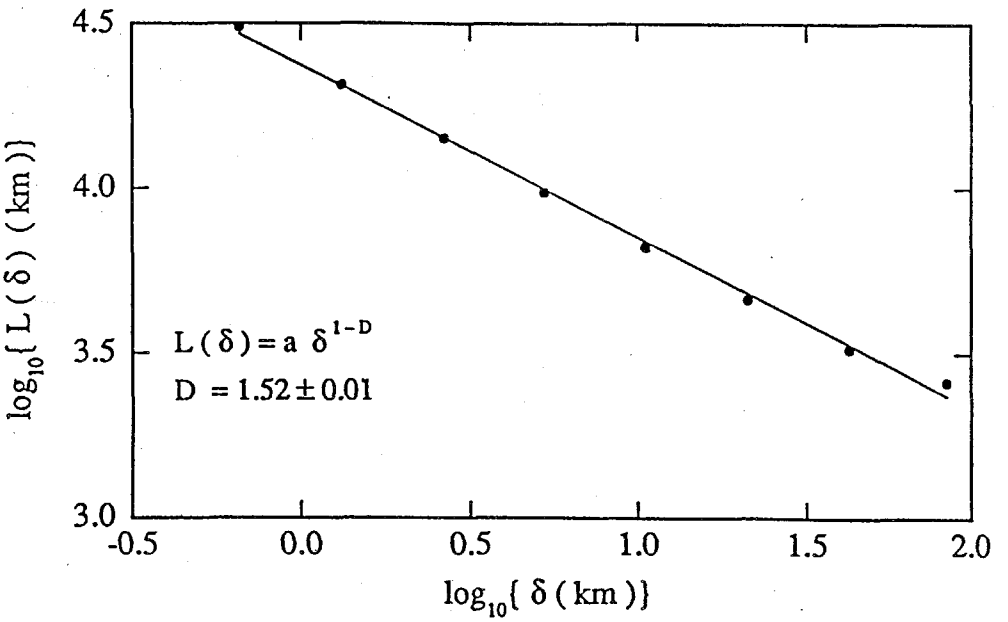

FIG. 2.3 Coastline data for Norway's fjords (Feder 1988, Fig. 2.2).

The western coastline of Britain was associated with an exponent for the coastline-*vs.*-resolution (*cf.* Eq. 2.5) of $1 - D \simeq 0.25$, in L. F. Richardson's (1961) data, corresponding to a fractal dimension of $D \simeq 1.25$. See Fig. 2.2, where Richardson's data on various coastlines are reproduced (from Mandelbrot 1977, Plate 32). A value of $D \simeq 1.5$ was assigned by Feder (1988) for Norway's fjords (*cf.* Fig. 2.3).

Generally speaking, the dimension of a fractal may be regarded as providing a measure of its geometrical complexity. A complex level set will offer the possibility of many jumps across "bays" and "peninsulas" with a count $N(\lambda)$ that decreases rapidly as λ increases, *i.e.*, will have a large D. The higher fractal dimension of the Koch island in Fig. 2.1b, than that of the triadic Koch Island depicted in Fig. 2.1a, as well as the higher D assigned to the coastline in Norway's fjords, than that for the West of Britain, indicates an overall geometrical complexity for the former that is higher than the latter. Such a complexity measure would be

important in our description of isosurfaces in turbulence. In the case of combustion on a stoichiometric surface, for example, a higher fractal dimension, D, could be expected to be generally associated with a higher burning rate per unit volume.

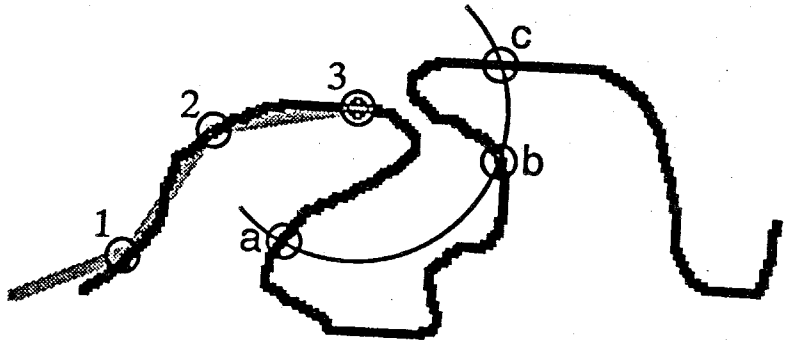

FIG. 2.4 Possible λ-string endpoints along a two-dimensional level set (Russ 1994, Fig. 2).

We pause, however, to note several difficulties with the "stretched-string" algorithm. In particular,

a. multiple end-point choices may exist for each step; the number of λ-steps, $N(\lambda)$, for a given level set, is not unique. See Fig. 2.4.

b. As λ increases, the stretched-string algorithm can result in a (negative) logarithmic derivative that exceeds 2, the dimension of the space the curve is embedded in and. for a curve embedded in a two-dimensional space, we would like the property, $D \leq 2$.

c. It is not clear how one completes the count as one goes around a closed curve; λ-steps are not likely to return to the starting point on a closed curve and for curves that exit the domain, an *ad hoc* decision must be made about how to count the exiting steps.

d. It is not clear how one deals with "islands" and "lakes" whose span is less than λ.

e. It is not clear how one extends the scheme to objects that live in three, or more, dimensions.

Some of these are noted by Mandelbrot (1977), who discusses several variations, but suggests that the basic conclusions are robust and transcend these difficulties, with the fractal dimension, D, rather insensitive to these choices. This has not been

the experience, however, in the application of these proposals to turbulence in the last decade-and-a-half, or so, at least at Caltech (Dimotakis 1996).

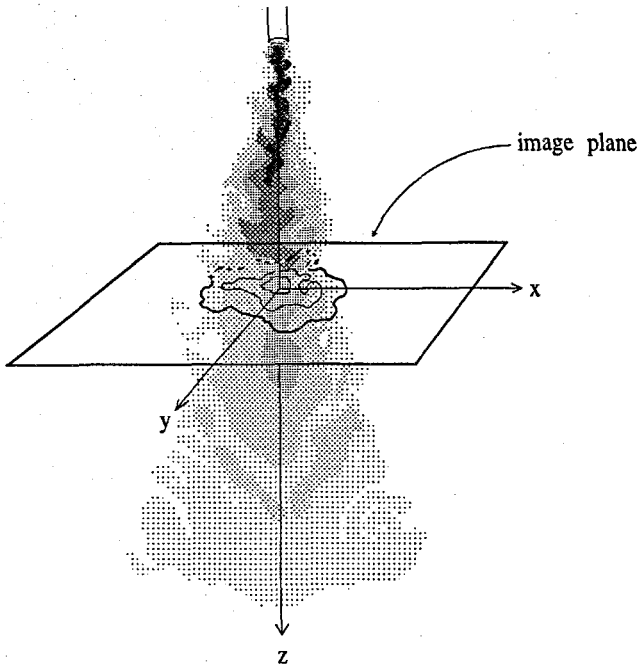

FIG. 2.5 Turbulent-jet far-field geometry in relation to imaged scalar-field (jet-fluid concentration) plane.

Fortunately, these difficulties can be overcome by an algorithm based on the (coverage) count, $N_d(\lambda)$, of successive sub-partitions of the embedding space into λ-size boxes — segments, tiles, parallelepipeds, *etc.* — in d-dimensions that are required to cover the level set, as a function of their size, λ (Catrakis & Dimotakis 1996a). For this purpose, the embedding space can be defined as the interior of the level-set bounding box. For a level set in two-dimensional space, for example, the bounding box can be defined as the smallest rectangle (or square, if need be) that contains the set (Tricot 1995). If such a two-dimensional box has an extent λ_x and λ_y along the x and y directions, respectively, then the bounding box size, $\delta_{\rm b}$, can be defined as the square root of its area,

$$\delta_{\rm b} \equiv A^{1/2} = \sqrt{\lambda_x \lambda_y} \,, \tag{2.6}$$

the geometric mean of the two sides. For a square bounding box, $\delta_{\rm b}$ is the length of its edge. In d-dimensions, the size of the bounding box can be defined as the $d^{\rm th}$

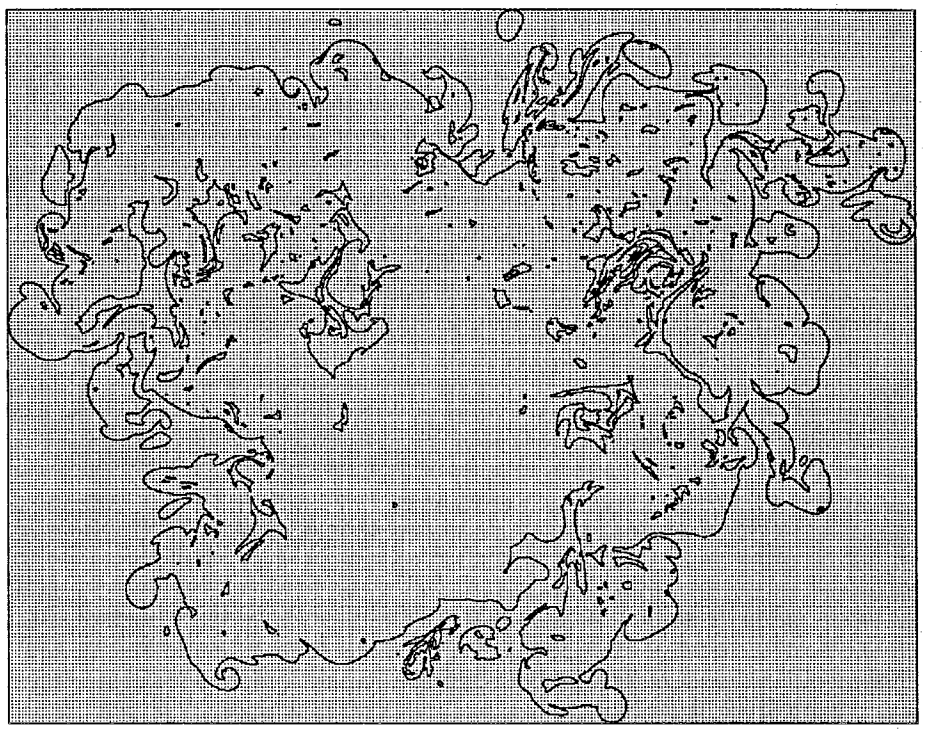

FIG. 2.6a Jet-fluid isoconcentration (level) set in the far field ($z/d_j = 275$) of a $Re = 4.5 \times 10^4$ turbulent jet (*cf.* Fig. 2.5). Shaded region indicates the level-set bounding box, of area $A = \lambda_x \lambda_y = \delta_b^2$; for $\lambda = \delta_b$, $N_2(\lambda) = 1$.

root of its d-dimensional volume, *i.e.*,

$$\delta_b \equiv V^{1/d} \ . \tag{2.7}$$

This can be illustrated on some isoscalar data derived from a slice in the far field of a turbulent jet (Catrakis 1996), along a plane perpendicular to the jet axis (*cf.* Fig. 2.5), at a jet Reynolds number of $Re = 4.5 \times 10^3$. The bounding box for an isoscalar (constant jet-fluid concentration) contour is shown as the shaded region in Fig. 2.6a. This shaded region may also be considered as the largest tile required to cover the level set, corresponding to a level-set coverage count of $N_2(\lambda) = 1$, for $\lambda = \delta_b$.

We now cut each direction of the bounding box in half, partitioning it into four equal tiles (Fig. 2.6b), corresponding to $\lambda = \delta_b/2$. The jet-fluid concentration level set contours visit all four regions covered by the $(\delta_b/2)$-size tiles and, therefore,

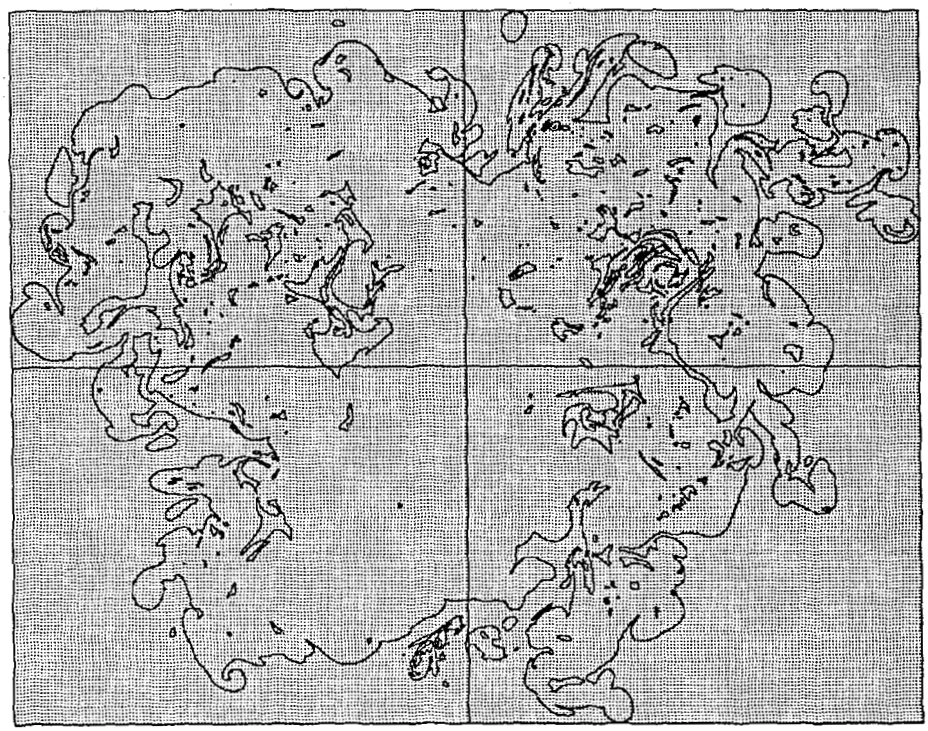

FIG. 2.6b Legend as in Fig. 2.6a. Bounding box partitioned into four tiles, all of which are required to cover the level set, *i.e.*, for $\lambda = \delta_b/2$, $N_2(\lambda) = 4$.

$N_2(\lambda) = 4$, for $\lambda = \delta_b/2$. If we were to seek a power-law relation, $N_2(\lambda) \propto \lambda^{-D}$ (Eq. 2.3), between the two-dimensional coverage count, $N_2(\lambda)$, and the tile size λ, we will have $D = 2$, at least in this large-tile-size range, since cutting the largest λ-tiles in half quadruples the two-dimensional coverage count, $N_2(\lambda)$. The resulting $D = 2$ value for these large tiles can be traced to the fact that *all* the boxes (tiles) required to cover the two-dimensional embedding space are also required to cover the level set that lives in it. That these fractal-dimension values are derived by counting the number of contiguous, non-overlapping tiles (boxes) required to cover the set (that also cover the embedding space exactly once), ensures that they are bounded by the dimension of the embedding space, *i.e.*,

$$D_d \leq d \, . \tag{2.8}$$

Further into the sequence, Fig. 2.6c depicts the same bounding box partitioned into a total of $N_{2,\mathrm{tot}} = 2^{10} = 1024$ tiles of size $\lambda = \delta_b/2^5$. Counting the number of tiles required to cover the jet-fluid concentration level set, we now find $N_2(\lambda) = 580$.

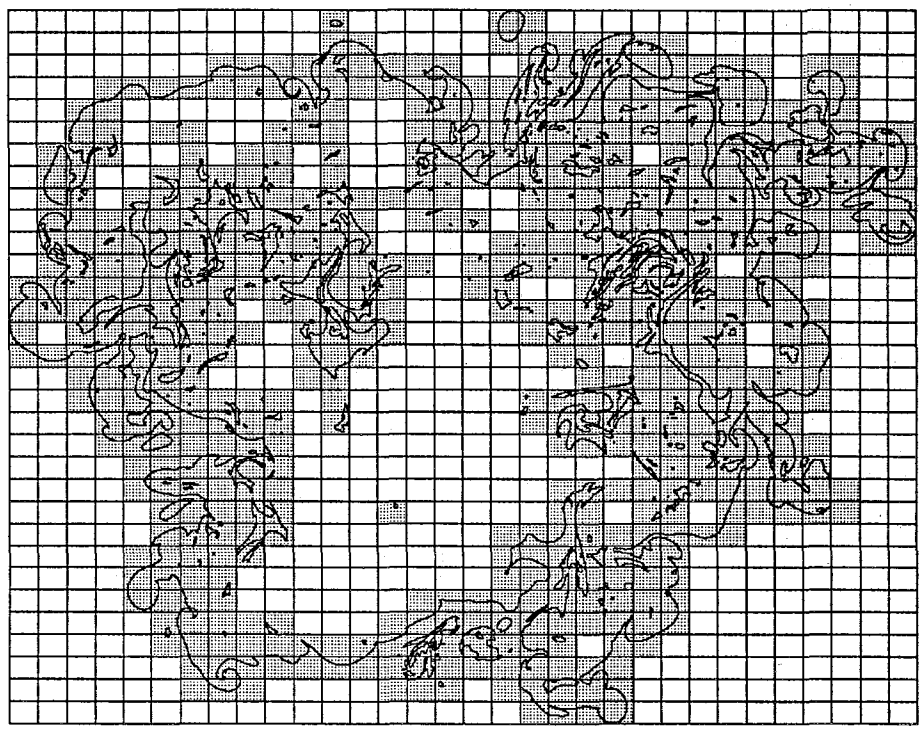

FIG. 2.6c Bounding box partitioned into a total of $N_{2,\mathrm{tot}}(\lambda) = 1024$ tiles of size $\lambda = \delta_\mathrm{b}/32$. Of these, $N_2(\lambda) = 580$ are required to cover the level set.

These are still rather large tiles, however, and we may prefer to go further into the binary embedding-space subpartition sequence, to smaller λ's yet, to estimate a fractal dimension from the coverage count at those scales.

For a size $\lambda = \delta_\mathrm{b}/2^7$, for which we have a total of $N_{2,\mathrm{tot}}(\lambda) = 2^{14} = 16{,}384$ tiles, we find that $N_2(\lambda) = 4363$ are required to cover the level set. These are the ones indicated in Fig. 2.6d. The next binary subpartition of the bounding box, in tiles of size $\lambda = \delta_\mathrm{b}/2^8$, yields a total of $N_{2,\mathrm{tot}}(\lambda) = 2^{16} = 65{,}536$ tiles and a coverage count of $N_2(\lambda) = 11{,}238$, as indicated in Fig. 2.6e. If a power-law describes the relation of the coverage count, $N_2(\lambda)$, to the tile size, λ, at this intermediate range of scales (tile sizes), the fractal dimension would be given by (Eq. 2.4),

$$D_2 \equiv -\frac{\mathrm{d}\log N_2(\lambda)}{\mathrm{d}\log\lambda} \simeq -\frac{\log N_2(\lambda_2) - \log N_2(\lambda_1)}{\log\lambda_2 - \log\lambda_1} = \frac{\log(11238/4363)}{\log(2)} = 1.36\,, \tag{2.9}$$

where the logarithmic derivative has been approximated here as a (first-order) finite-difference ratio. This is the slope of the straight line in the $\log N$ *vs.* $\log\lambda$ plot and,

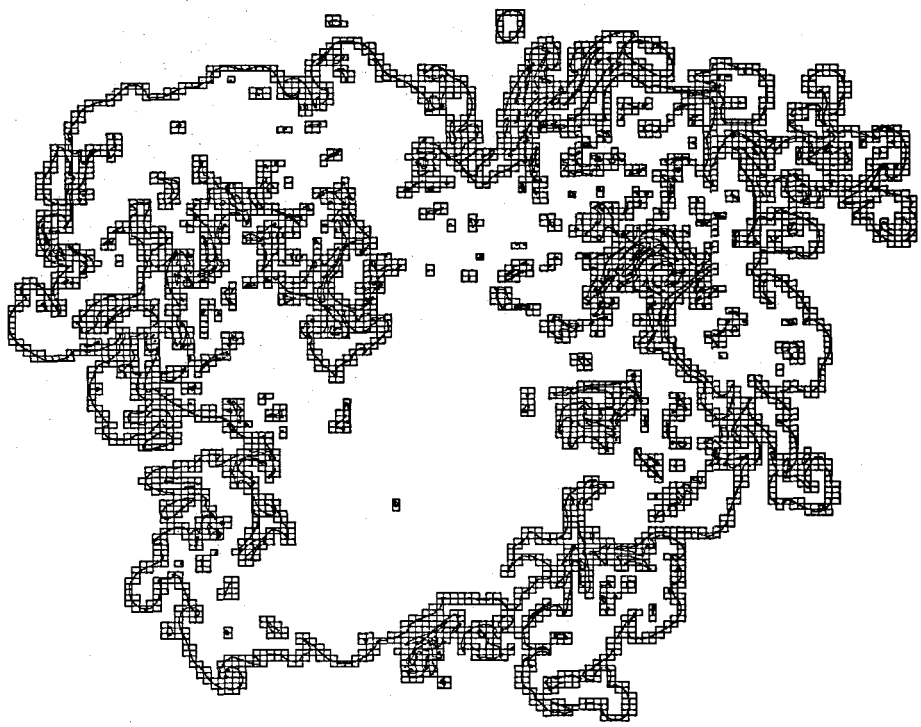

FIG. 2.6d Bounding box partitioned into a total of $N_{2,\mathrm{tot}} = 2^{14} = 16{,}384$ tiles of size $\lambda = \delta_\mathrm{b}/2^7$, with a coverage count, $N_2(\lambda) = 4363$. Only tiles that cover are indicated.

for a D that is constant and if the statistical fluctuations in the corresponding coverage counts are negligible, this estimate would be, of course, exact.

We open a parenthesis here to note that in cases where the level set may be regarded as extending to infinity in all directions, possessing, for example, a spatially-homogeneous stochastic geometry, coverage statistics may be derived by partitioning (tiling, in two-dimensions) the interior of a δ-size box that covers a selected/measured portion of the level set. In that case, the level set dimension may, but need not, approach the embedding dimension (*cf.* Eq. 2.8), as $\lambda \to \delta$.

Isoscalar surfaces, or contours, generated by turbulence are describable by a scalar-transport equation, as we've discussed (Eq. 1.16). In such a process, the effects of diffusivity, however small, will ensure differentiability of the level set and a finite arc length (rectifiable curves), in two dimensions, or a finite surface area, for isosurfaces in three dimensions. Strictly speaking, it is clear, in other words, that level sets generated by turbulence cannot be "rough and fragmented to the same

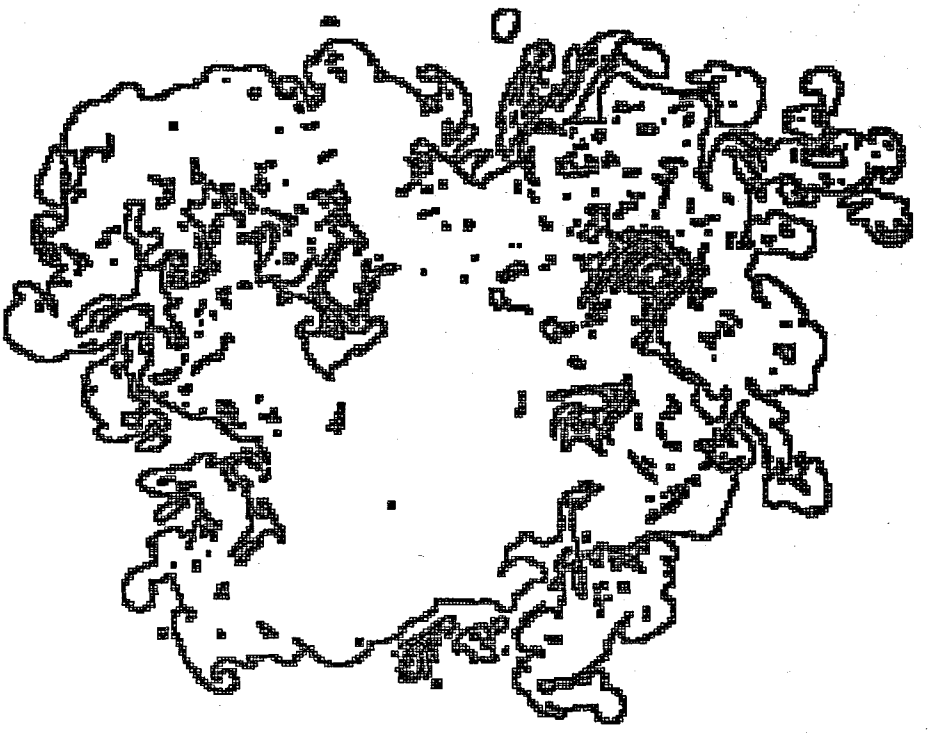

FIG. 2.6e Bounding box partitioned into a total of $N_{2,\mathrm{tot}}(\lambda) = 2^{16} = 65{,}536$ tiles of size $\lambda = \delta_\mathrm{b}/2^8$, with a coverage count, $N_2(\lambda) = 11238$. Only tiles that cover are indicated.

degree at all scales." For such level sets in two dimensions, as in our example, we expect that $D_2 \to 1$ as $\lambda \to 0$, *i.e.*, the level-set dimension should attain a value equal to the topological dimension value of a smooth curve, as guaranteed by scalar diffusion, and, in general (*cf.* Dimotakis 1991, Catrakis & Dimotakis 1996a, and Eq. 2.8 and related discussion),

$$\lim_{\lambda \to 0} D_d \;=\; d_\mathrm{t} \;, \tag{2.10}$$

where d_t is the topological dimension of the level set. This is also a property that one would also like a dimension to satisfy. For scalar data derived from turbulent flows, this limiting value for D may be expected to be approached for small λ, or, more precisely, for $\lambda \lesssim \max\{\lambda_\mathcal{D}, \lambda_\mathrm{res}\}$, where $\lambda_\mathcal{D}$ is the scalar species diffusion scale (Eq. 1.20) and λ_res is the resolution scale of the measurement (*e.g.*, the pixel size, λ_p, of a digital image, or the spatial extent of the measuring volume).

We should open a second parenthesis here to note that the limiting value indicated by Eq. 2.10 need not also be a lower bound. This may be illustrated by

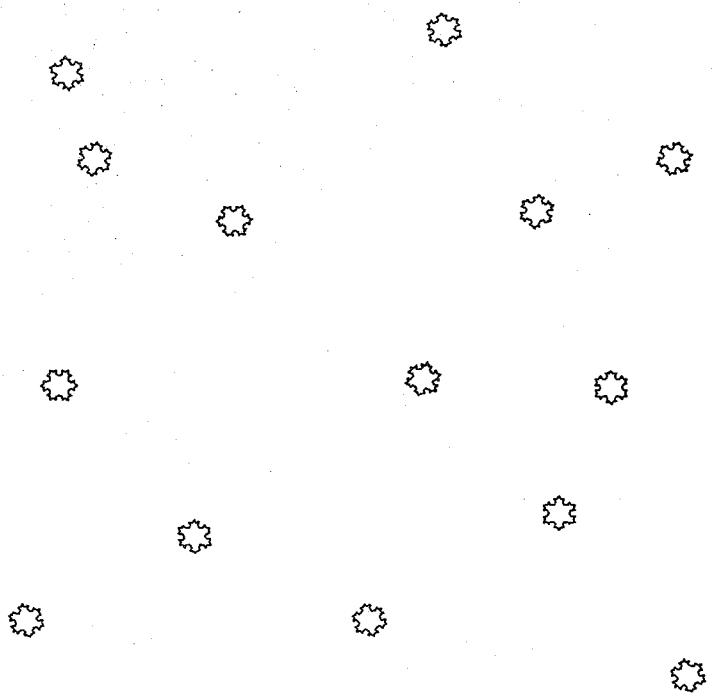

FIG. 2.7 Sparse archipelago of Poisson-distributed, randomly-oriented, uniform-size (triadic) Koch islands.

considering a level set comprised of a sparse cluster of small "islands" of, roughly, the same size, λ_0, such that $\lambda_0 \ll \delta_b$, sprinkled in the interior of a two-dimensional bounding box of size δ_b and separated by distances large compared to λ_0 (Fig. 2.7). To successive subdivisions of the bounding box, for a range of scales (tile sizes) $\lambda_0 \ll \lambda \ll \delta_b$, this sparse island archipelago will look like a collection of points, with a level-set dimension, D_2, that may be smaller than unity. For $\lambda < \lambda_0$, however, the islands will be covered by tiles, as is a coastline, yielding a level-set dimension that may be expected to be in the range, $1 < D_2 < 2$. Such multiscale sets can arise in the distribution of matter in clusters of galaxies, for example, as well as other natural phenomena.

To return, Mandelbrot's proposal that level sets generated by turbulence possess a coverage describable by a power-law relation must be interpreted as implying that there exists an intermediate range of scales of (tile) size λ, such that,

$$\lambda_D \lesssim \lambda_{\min} \ll \lambda \ll \lambda_{\max} \lesssim \delta_b \ , \tag{2.11}$$

in which the fractal dimension, D, assumes an intermediate value (*e.g.*, Eq. 2.9) that may be accepted as a constant over this λ-range. To quote Falconer (1990, p. xxi),

the underlying point of view is that, for naturally-generated complex geometrical objects, "... over certain ranges of scale they appear very much like fractals and at such scales may usefully be regarded as such." The required self-similarity in behavior, for fractal scaling, at least over some restricted range of scales, as indicated in Eq. 2.11, for example, was suggested by Vicsek (1992) as, "a property we can assume for all objects arising as a result of any physical process." In what follows, we will discuss these proposals in the context of turbulence, in particular, as well as the consequences as regards their capacity to describe natural phenomena, in general.

2.1 An overview of reports on fractals for turbulence

Welander, in 1955, discussed (what would now be termed) fractal properties of model objects like Koch islands, which he called "snow-flake curves". In a discussion focused on scalar transport in two-dimensional, liquid-phase, unsteady flow, he analyzed the representation of interfacial arc length, which he recognized could, in principle, increase to very high values. Welander suggested that methods of analysis, reminiscent of today's fractal-geometry tools, could be applied to the description of "snow-flake" curves, as well as scalar interfaces advected in turbulence. Figure 2.8 is reproduced from his paper, and depicts the deformation of a small (originally-square) dyed fluid region on the surface of a fluid, that he agitated and then set into rotation to maintain quasi-two-dimensional flow.

There probably exist other reports, as well, of discussions with similar proposals to apply fractal ideas. There can be no question, however, that it is Mandelbrot who must be credited for bringing the subject of fractals to attention, proposing that they can be expected to find application and that they constitute the natural formalism for the description of the geometrical properties of level sets generated in many natural phenomena. In the case of turbulence (Mandelbrot 1975a), he noted,

> "turbulent shapes ... almost cry out for proper geometrical description,"

and, in his book on fractals (Mandelbrot 1977, p. 146),

> "... we have already noted that sophisticated stochastic geometry is not used in any science, and includes the specific random surfaces and lines of turbulence. It is a pity. I believe that more imaginative stochastic geometry would be helpful in describing the truly disordered aspects of turbulence. Stochastic fractal geometry should be of particular interest."

FIG. 2.8 Observed deformation of a small, dyed square fluid region on the surface of an agitated fluid (Welander 1955, Fig. 3).

For isoscalar surfaces in three-dimensional homogeneous turbulence, he argued for a fractal dimension,

$$D_3 = 3 - 1/3 = 8/3 , \tag{2.12a}$$

if turbulence could be described as possessing "Kolmogorov-Gauss" scaling, a value he obtained by analyzing random, Gaussian fields with Kolmogorov variance (Mandelbrot 1975a, 1975b, and 1977), and a fractal dimension,

$$D_3 = 3 - 1/2 = 2.5 , \tag{2.12b}$$

for "Gauss-Burgers turbulence" (Mandelbrot 1977).

Mandelbrot also suggested that intermittency in turbulence is a direct consequence of the fractal nature of the geometry of regions in the flow where kinetic energy dissipation occurs, offering an alternative interpretation to the phenomenon than the latter theories proposed by Kolmogorov (1962) and, subsequently, others. See discussion in Monin & Yaglom (1975) as well as the more recent review by Frisch (1975, Ch. 8) of intermittency theories based on cascade, fractal, and multifractal models.

On this topic, comparing the contributions of this formalism to turbulence, *vs.* (low-order) dynamical systems, Frisch (1995, p. 205) notes,

> "Paradoxically, the multifractal character of fully developed turbulence is still a controversial matter, whereas attractors of chaotic dissipative dynamical systems are known, and sometimes proven rigorously, to be multifractal."

Intermittency and multifractal models deal with the *amplitude* distribution and support of the field of interest and are beyond the scope of the present discussion, which is focused on the stochastic geometrical properties of level sets of turbulence-generated scalar fields.

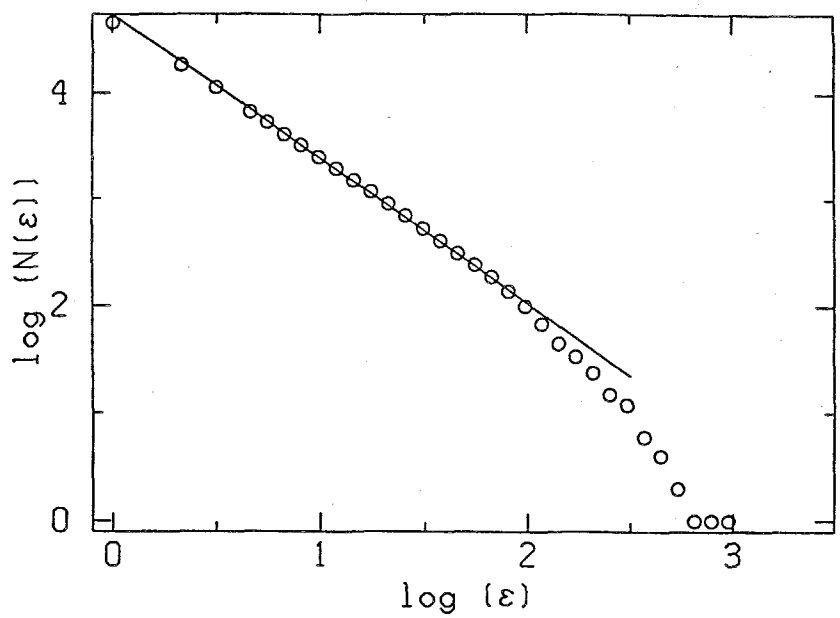

FIG. 2.9 "Log-log plot of the number of boxes $N(\epsilon)$ containing the boundary [in a longitudinal section] *vs.* the size of the box ϵ; from the straight line portion of the graph the fractal dimension is found to be 1.36" (square brackets ours). From Prasad & Sreenivasan (1989, Fig. 10).

Following Mandelbrot's proposals, experimental measurements investigating fractal behavior of level sets in turbulence were first reported by Sreenivasan & Meneveau (1986), for a variety of flows including shear layers, jets, wakes, and boundary layers. Sreenivasan & Meneveau accepted that level sets in turbulence, "can be expected to be fractal-like only in an intermediate range of scales ... bounded [from above] by scales comparable with or smaller than the large scale

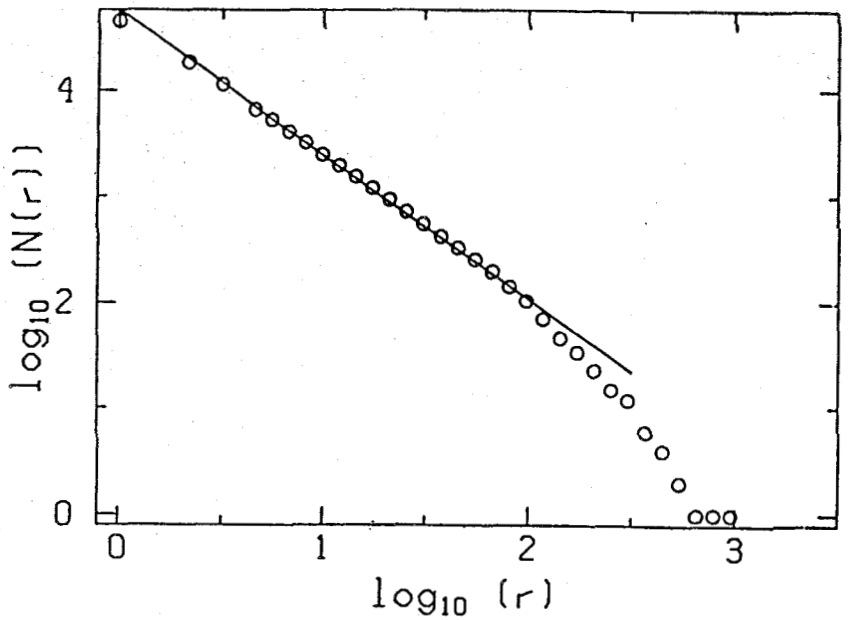

FIG. 2.10 "The log-log plot of the number of boxes $N(r)$ containing the boundary in an orthogonal section ($z/d_j = 21$) [in our notation] versus the size r of the box. As before, the slope of the straight region in the plot gives the fractal dimension of the boundary. The value of the dimension is the same as that calculated from longitudinal sections" (square brackets ours). From Prasad & Sreenivasan (1990a, Fig. 12).

of the flow ... and [from below] by the Kolmogorov scale."[♯] They reported a value of $D_1 = 0.32$, for one-dimensional (temporal) cuts of isoscalar data, and $D_2 = 1.33$, for two-dimensional measurements in a turbulent jet. Sreenivasan & Meneveau also accepted Mandelbrot's suggestion that, for isotropic level sets, a two-dimensional slice of a three-dimensional isosurface whose fractal dimension is given by D_3 would have a fractal dimension given by,

$$D_2 = D_3 - 1 \ , \tag{2.13}$$

and suggested that, therefore, three-dimensional isoscalar surfaces should be characterized by a fractal dimension, $D_3 = D_2 + 1 = 2.33$. In contrast to these findings, however, Sreenivasan & Meneveau pointed out, in the same paper, that long records (of the order of 500 large scales) of 1-D signals of the streamwise velocity in turbulent boundary layers do not appear fractal but, rather, exhibit statistics resembling

[♯] In the case of scalar fields, the lower bound would be associated with the (Batchelor 1959) diffusion scale. For water (high-Schmidt-number fluid), for example, this is substantially smaller than the (Kolmogorov) viscous scale (*cf.* Eq. 1.20).

those of random (Poisson) points on a line. On the whole, however, Sreenivasan & Meneveau concluded that "several aspects of turbulence can be described roughly by fractals."

Sreenivasan *et al.* (1989) reported a fractal dimension of $D_2 = 1.36$ for isoscalar jet data, with $D_2 = 1.35 \pm 0.05$ as a mean value for various turbulent shear flows, and offered arguments for a value of $D_3 = 7/3$ based on Reynolds-number similarity. Prasad & Sreenivasan (1989, 1990a) analyzed two-dimensional cuts of turbulent jets along the mean flow direction (*i.e.*, including the jet axis), as well as transverse to the jet axis (as in Fig. 2.5, above). Figure 2.9 reproduces their coverage data for a $Re = 4000$ jet, identified as corresponding to their streamwise cut ($8 \leq z/d_j \leq 24$, in our notation), from which the,

> "... value of D ... turns out to be 1.36. Orthogonal sections also yielded 1.36 within the experimental error, showing the independence of the result on the orientation of the intersecting plane."

The latter can be ascertained from their data, reproduced in Fig. 2.10 from their 1990a report, where they are identified as an example of coverage data derived from a transverse cut at $z/d_j = 21$ (in our notation), at the same Reynolds number. As can be seen by a comparison of the data in Figs. 2.9 and 2.10, the behavior is, indeed, very similar. Prasad & Sreenivasan (1990b) also analyzed three-dimensional data of the isoscalar surfaces in turbulent jets, reporting a dimension of $D_3 = 2.35 \pm 0.04$.

A lack of (constant-D) fractal scaling was later noted by Sreenivasan (1991), however, for isoscalar surfaces in the interior of the jet. Sreenivasan pointed out that, for level sets of concentration in turbulent jets at intermediate thresholds, "the log-log [coverage] plots are somewhat rounded," concluding that level sets "close to the mean concentration level ... are not good candidates for fractallike description" (Sreenivasan 1991, p. 553). Sreenivasan (1991, Fig. 6b) includes an illustration of this lack of fractal scaling, in the same paper.

A theoretical estimate for a dimension of $D_3 = 2.5$ was obtained by Constantin (1989, 1990), in accord with the Mandelbrot Gauss-Burgers turbulence model (Eq. 2.12b). An analysis of level-set geometry, based on the equations of motion, was put forth by Constantin *et al.* (1991), based on Constantin's 1989 work. Surface area estimates of a scalar isosurface portion in a fluid element advected with the flow were obtained using the co-area rule of geometric-measure theory.

A comparison with the experimental data is reproduced in Fig. 2.11.* Constantin *et al.* (1991) suggested a fractal dimension of $D_3 = 8/3$, for isoscalar surfaces in the jet interior, in accord with Mandelbrot's Kolmogorov-Gauss turbulence model (Eq. 2.12a), and $D_3 = 7/3$, for isoscalar surfaces near the jet boundary.

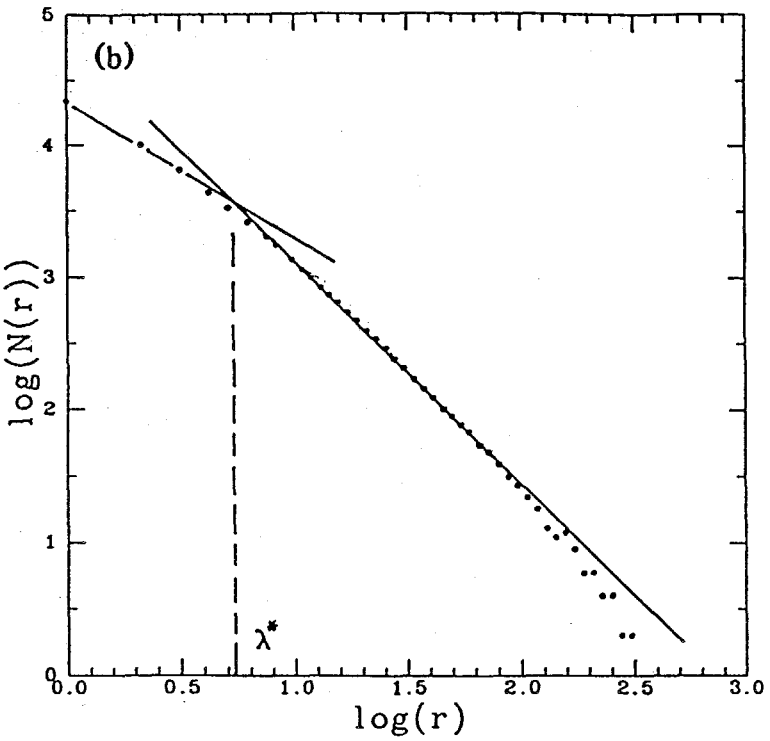

FIG. 2.11 Theory of Constantin *et al.* (1991) applied to experimental results for level sets of concentration in a turbulent jet.*

Procaccia *et al.* (1992), pointed out, however, that "the theory [of Constantin *et al.* (1991)] cannot exclude the possibility that the scaling exponent, D, depends on [the scale] r" (the scale λ, in our notation — inserts in square brackets ours). Procaccia *et al.* (1992) analyzed isosurfaces of vorticity in three-dimensional homogeneous turbulence, using the direct-numerical-simulation data of Vincent & Meneguzzi (1991), and concluded that, "... it is impossible to state with confidence that the [fractal] behavior [of the vorticity isosurfaces] is clear-cut."

Lane-Serff (1993) reported a threshold-dependent fractal dimension, for isoscalar contours estimated from images in liquid-phase jet and plume flows. A min-

* It would appear that the data found in agreement with the theory are the same as the ones that yielded the coverage data in Sreenivasan (1991, Fig. 6b), that led to the conclusion of a "rounded" coverage plot, *i.e.*, a lack of "fractallike description" (recall discussion above).

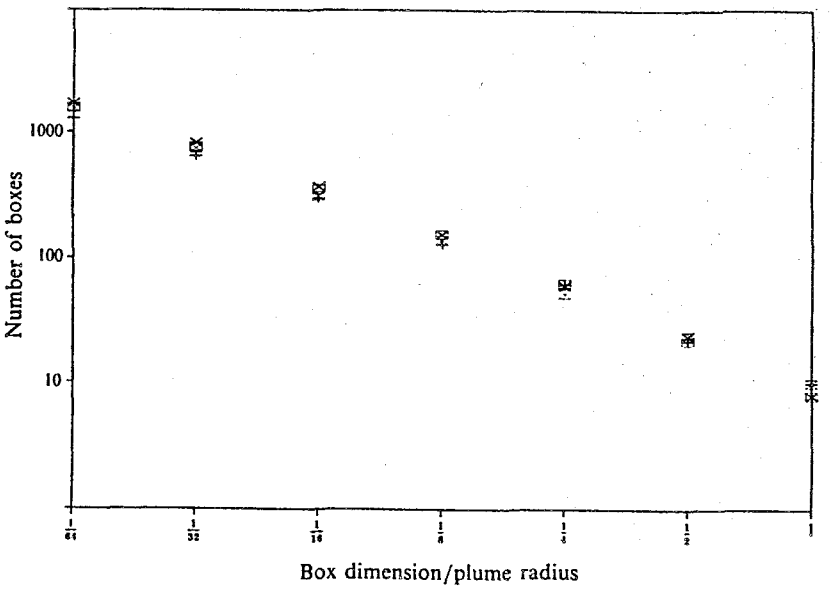

FIG. 2.12 Coverage counts *vs.* scale, normalized by local liquid-phase jet (plume) radius. Different symbols denote different image realizations. Systematic curvature in log-log plot noted by author (Lane-Serff 1993, Fig. 7).

imum value of $D_2 = 1.23$, with respect to the threshold choice, was estimated by fitting a least-squares straight line to the coverage data. Figure 7 of the Lane-Serff paper is reproduced here as Fig. 2.12. As the author noted, "The data are close to a straight line but there is a distinct curve." *i.e.*, curvature, in the log-log coverage plots. This was attributed, however, to "... the small range between integral and Kolmogorov scales at the Reynolds numbers of [the] experiments." Praskovsky *et al.* (1993) analyzed high-Reynolds-number turbulence level-set data of velocity, noting the absence of any wide range of scales characterized by a constant fractal dimension, but reported an average value of $D_1 \approx 0.4$.

The 1991 analysis by Constantin *et al.* was revisited and expanded by Constantin (1994a, 1994b) and Constantin & Procaccia (1994), with isosurface-area bounds obtained from the scalar transport equation, with Kolmogorov scaling for the advecting velocity field. In these analyses, as with the earlier discussion, it was assumed that level sets of the scalar fields were characterized by a constant fractal dimension. The 1994 update of this work identified the estimate of $D_3 = 8/3$ as a sharp estimate (rather than an upper bound), in the limit of $Sc \to \infty$.

Flohr & Olivari (1994) analyzed isoscalar surfaces in gas-phase turbulent jets and reported, "constant scaling behavior over a wide range [of scales]," with a

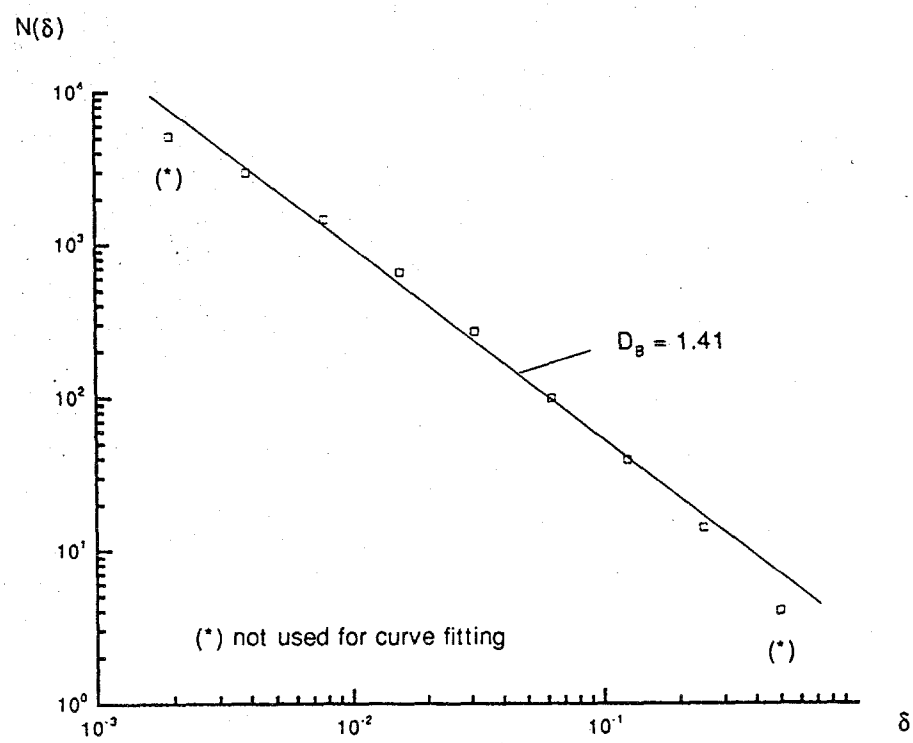

FIG. 2.13 Isoscalar (smoke concentration) box-counting statistics derived from a $Re \simeq 2000$ jet. Planar image normal to the jet axis at $z/d_j \simeq 15$ (Flohr & Olivari 1994, Fig. 7).

threshold-dependent fractal dimension exhibiting a maximum value.** For the outer isoscalar surfaces, they suggested that $D_2 = 1.30 \pm 0.05$. Their Fig. 7 is reproduced here as Fig. 2.13. Sreenivasan (1994) suggested that $D_3 = 2.35 \pm 0.05$ for outer isoscalar surfaces in turbulent jets, with fractal scaling, "over much of the interval between the integral scale and the Kolmogorov scale," and a fractal dimension of $D_3 = 2.67 \pm 0.05$ for the inner isoscalar surfaces, in a scaling range stated to be "smaller" than for outer isosurfaces. He characterized the degree of confidence of these conclusions as, "fairly certain." More recently, Baldyga & Bourne (1995) offered fractal and multifractal models of turbulent mixing, assuming constant-D behavior.

An analysis of the (temporal) evolution of a line element in grid-generated turbulence was reported by Villermaux & Gagne (1994). Their measurements of the wrinkling of a smoke filament, shed from a thin wire downstream of a grid in a wind tunnel, were interpreted in terms of a fitted power-law coverage dimension that increased (linearly) with the distance downstream from a thin wire. Invoking Kolmogorov scaling, they proposed that the slope of the fractal dimension *vs.*

** Recall that Lane-Serff (1993), however, reported data with a *minimum* value of the fractal dimension, with respect to scalar threshold.

(Lagrangian) time was proportional to $Re^{1/2}$, reporting good agreement with their data.

The reports mentioned above offered theoretical and experimental evidence in support of constant-D descriptions of level sets arising in turbulence. Over the same period, several others, however, arrived at the opposite conclusion, also based on both theoretical and experimental work. Namely, that a constant-D coverage description is not applicable to level-sets in turbulent flows and in other contexts. These latter reports will be briefly discussed below.

Takayasu (1982), argued on theoretical grounds that the dynamics of turbulent flow necessarily vary with scale. He suggested that descriptions of turbulent diffusion, in particular, may be expected to require coverage dimensions that are functions of scale and not constant, *i.e.*, in terms of the coverage, $N_d(\lambda)$,

$$D_d(\lambda) \;=\; -\frac{\mathrm{d}\log N_d(\lambda)}{\mathrm{d}\log \lambda} \tag{2.14}$$

of fluid-particle Lagrangian trajectories. Takayasu invoked Reynolds-number similarity to support his conjecture.† In his study of the geometry of the trajectory (as opposed to level set) of a one-dimensional random-walk particle as a function of step-size, λ, he employed a scale-dependent $D(\lambda)$, in our notation, and conjectured that such variable dimensions should be applicable to turbulent diffusion and other natural phenomena. He argued that, in random walks with a fixed step size, particle trajectories appear (inertially) correlated, when viewed at scales larger or smaller than the step size. G. I. Taylor (1921) had also considered a modified random walk as a model of turbulent diffusion, in which he allowed for particles with inertia, *i.e.*, a random walk with correlated steps. See discussion by McComb (1991), of G. I. Taylor's proposal. Takayasu used a real-space renormalization argument to derive an expression for the successive (spatial) coverage of a one-dimensional, random walk with finite step size. He initially used the term, "differential fractal dimension," later employing the term, "scale-dependent fractal dimension" (Takayasu 1992). In 1993, Borgas offered Lagrangian-statistic arguments for a scale-dependent $D(\lambda)$ for particle trajectories in turbulent flow and that, in particular, a power-law (constant-D) region should not be expected.

Regarding turbulence-generated level sets, Miller & Dimotakis (1991a) reported on high signal-to-noise-ratio measurements of the jet-fluid concentration in the far

† As noted above, the principle of Reynolds-number similarity had also been invoked by Sreenivasan *et al.* (1989), to argue for a (constant) fractal dimension of level sets.

field of liquid-phase turbulent jets, conducted at various Reynolds numbers, with level sets computed for a range of scalar thresholds. A constant D was not found, for either one-dimensional temporal data at a fixed point, one-dimensional spatial data, or two-dimensional space-time data. Instead, their coverage statistics indicated a variable, scale-dependent $D(\lambda)$, which they computed as the local slope (logarithmic derivative) of the coverage (Eq. 2.14). For a wide range of scalar thresholds straddling the local mean, the coverage dimension for one-dimensional temporal data varied smoothly from 0 to 1; for one-dimensional spatial data, from near 0 to near 1; and, for two-dimensional space-time data, from near 1 to near 2.

Sreenivasan (1991), in a review that followed shortly, commented on the Miller & Dimotakis experimental findings, suggesting they could be attributable to differences between temporal and spatial data.‡ Kerstein (1991) also commented on the Miller & Dimotakis, offering an alternate possible explanation for variable-D behavior.

A general discussion on constant-D behavior was offered by Dimotakis (1991), on the basis of dimensional analysis and similarity. He suggested that power-law expressions, like Eq. 2.3, on which fractal similarity (constant-D) is based, imply a relatively strong dependence of the level-set geometry on some characteristic scale, in contrast to accepted notions. In the case of turbulence, it was argued that such a scale was unlikely to apply to fully-developed turbulent flows.

Gluckman *et al.* (1993), in their experiments in thermal turbulence, reported that temperature isosurfaces do not display constant-D scaling, while species concentration isosurfaces show a limited range of "approximately-fractal" scaling. Recent experiments to investigate the geometry of scalar level sets were reported by Catrakis & Dimotakis (1996a), who obtained two-dimensional, high signal-to-noise ratio, spatial measurements of the concentration field in the far field of liquid-phase, turbulent jets, in a plane perpendicular to the jet axis. These investigations were conducted for a range of scalar thresholds and values of the Reynolds number below, near, and above the estimated mixing-transition Reynolds-number threshold of $Re \approx 10^4$ (*cf.* Sec. 1.1). The geometry of the jet-fluid concentration level sets were found to be described by a scale-dependent fractal dimension, $D_2(\lambda)$, increasing smoothly, with increasing scale, from unity, at small scales, to 2 at scales compara-

‡ Some previous reports of constant-D findings, based on one-dimensional data, such as those by Sreenivasan & Meneveau (1986), had also relied on temporal data. In addition to temporal data, variable-D behavior was also reported by Miller & Dimotakis (1991a) for (purely) spatial measurements.

As noted above, the reports summarized above, and others not listed here, fall in two categories. A set that is generally supportive of the (constant-D) fractal scaling proposals for turbulence-generated level sets and a set not supportive of these proposals. The reports that may be regarded as supportive, include experimental and theoretical analyses of level-set geometry derived from scalar, velocity, and vorticity fields in turbulence, extending the original proposals that fractal geometry may be applicable to isoscalar surfaces in turbulent flows.

Nevertheless, some of these generally supportive reports also cast some doubt on the notion of a power-law relation between the coverage count, $N(\lambda)$, versus the covering-box size, λ, *i.e.*, that a constant fractal dimension, D, exists over some significant range of scales. These doubts were either explicitly stated by the authors, or can be gleaned from the actual data presented and analyzed for the purpose, as suggested in the data and analysis reproduced in Figs. 2.9 and 2.10, as well the data in Fig. 2.11. The reader is invited to sight along the data and the fitted straight line in Figs. 2.9 and 2.10 to ascertain the systematic curvature in the coverage data. In particular, one can see a continuously-increasing slope, for most of the scale range, in the corresponding $\log N(\lambda)$ *vs.* $\log \lambda$ plots. Secondly, a part of the experimental evidence that was accepted as leading to this conclusion was derived from relatively low Reynolds number flows, *i.e.*, not fully-developed turbulence (*cf.* discussion in Sec. 1.1), for which, as was noted by some of the authors (*e.g.*, Lane-Serff 1993), the various similarity laws and, presumably, (constant-D) fractal similarity would not be expected to apply.

The reports that concluded that the fractal dimension must be treated as a scale-dependent variable, *i.e.*, that $D_d = D_d(\lambda)$, also included theoretical and experimental work. Interestingly, the need to extend the (power-law) fractal framework first appeared in a theoretical analysis of random-walk processes (Takayasu 1982), on which the conjecture that it should apply to other processes, such as turbulence, was made. To date, however, it has not proven possible to argue, theoretically, whether fully-developed (high-Re) turbulence is characterized by constant-D fractal geometry.

As noted above, the theoretical analyses that have dealt with the general issue have focused on fractal-dimension bounds and estimates, assuming constant-D fractal geometry. Recall, however, the negative statement by Dimotakis (1991), who argued that if co-dimension values, $d - D_d$, are in the range proposed, constant-D fractal behavior would require a strong dependence on some characteristic scale, whose existence is unlikely in fully-developed turbulence. The analysis, by Procac-

cia *et al.* (1992), of the isovorticity surfaces derived from the Vincent & Meneguzzi (1991) direct numerical simulations, was inconclusive on this question and, in any event, based on simulations at a (Taylor) Reynolds number that may not have been high enough to settle the issue either way. It was left to experiments to address the problem.

2.2 Other reports of scale-dependent geometry

Suzuki (1984) reported variable-D behavior for Japanese coastlines and discussed a scale-dependent Koch curve model. Suzuki used the term "transient fractal dimension" and "transient fractals" to describe scale-dependent geometrical properties. Mark & Aronson (1984) reported similar behavior in the analysis of topographic surfaces and used the term, "scale-dependent fractal dimension."

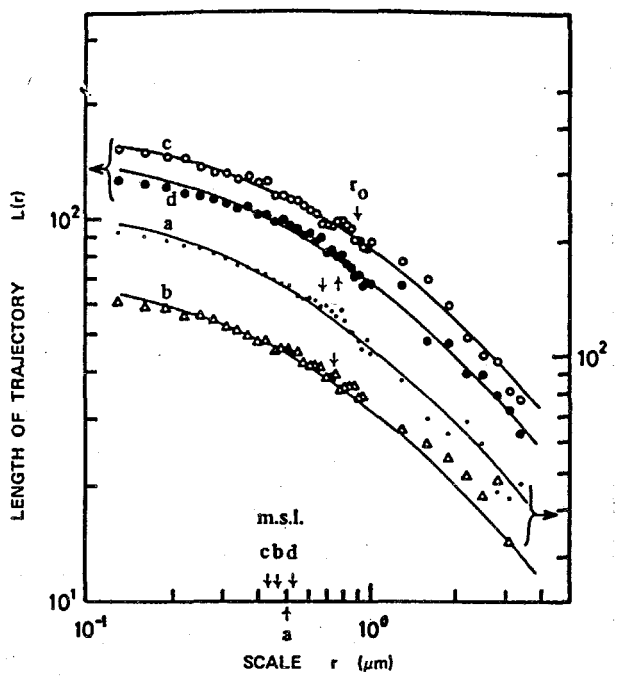

FIG. 2.14 Length of random-walk (Brownian-motion) trajectory of particles in solution, as a function of scale. (a) polystyrene latex; (b) bacteriophage T4; (c) T4 particles with host *E. coli B* cells; (d) as in (c) with measurements over a shorter time; m.s.l. denotes mean segment length (step size). From Matsuura *et al.* (1986, Fig. 1).

Matsuura *et al.* (1986) reported variable-D behavior in measurements of random walk (Brownian motion) trajectories of particles in solution, in accord with Takayasu's (1982) one-dimensional analysis, as shown in Fig. 2.14.

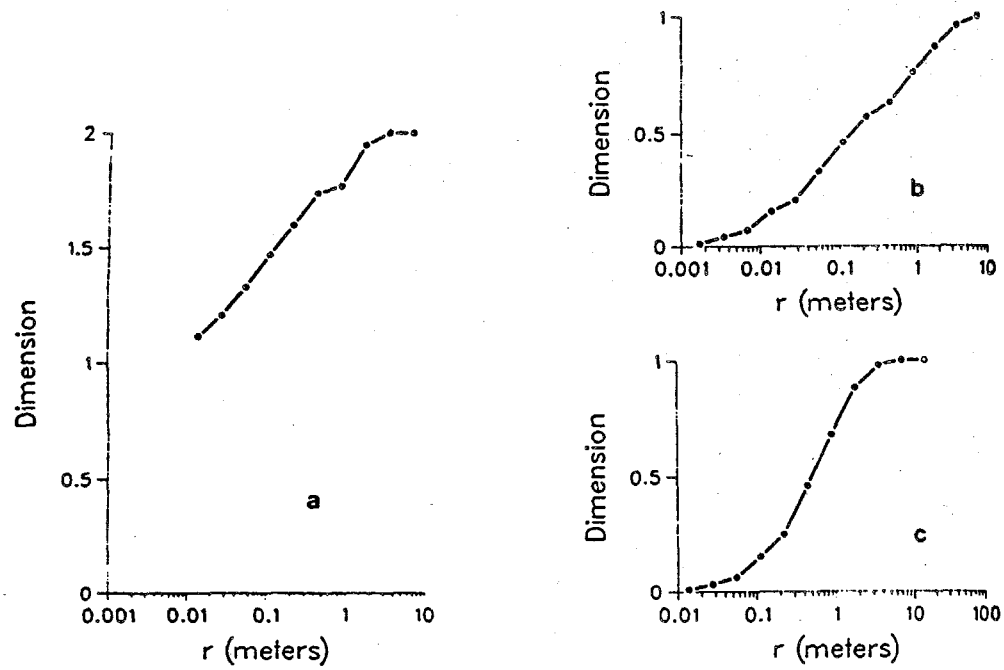

FIG. 2.15 SDF dimension of the fracture network of rocks. (a) 2-D survey of a 10 m × 10m section; (b) 1-D survey through the 2-D section of (a); (c) 1-D survey of a 80 m × 2m section of a drift wall (Chilès 1988, Fig. 6).

Chilés (1988) studied fractured rocks, finding a continuously-varying, "local similarity dimension," as a function of scale, in both 1-D and 2-D surveys, as shown in Fig. 2.15. Chilés suggested several models for such scale-dependent fractal behavior, including scale-dependent Cantor dust.

In his study of biological tissues using microscopic biometry, Rigaut (1991) also reported scale-dependent fractal behavior, as shown in Fig. 2.16. In particular, he found, in his words, a "drifting fractal dimension" with scale, and used the term "semi-fractals" as applicable to the analysis of the alveolar geometry of lungs of prematurely-born rabbits.

In characterizing the distribution of galaxies in the universe, Castagnoli & Provenzale (1991) suggested that, "... it is probably necessary to consider models whose scaling and fractal properties vary with the spatial scale." Brandt *et al.* (1991) reported in their analysis of solar granulation data, "... a smooth transition of the fractal dimension from small to large granules." More recently, Laherrère

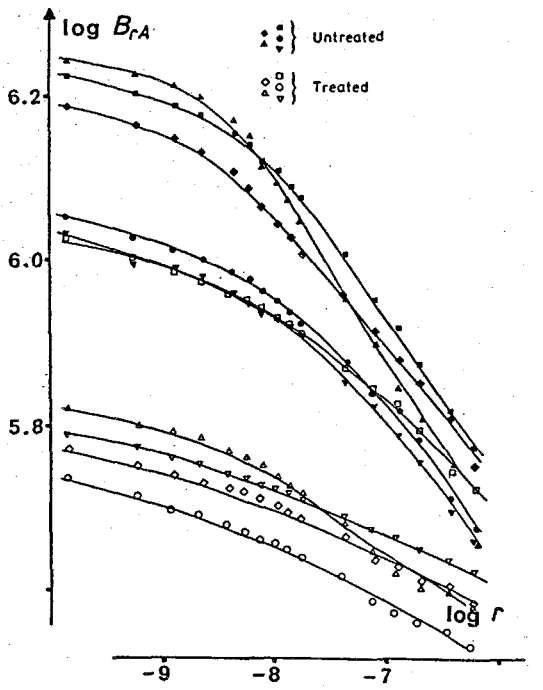

FIG. 2.16 The perimeter, B_{rA}, in a reference area, A, of the outline of microscopic sections of the pulmonary alveoles of prematurely born rabbits, as a function of scale, r. Untreated (underdeveloped) as well as treated (with surfactant at birth) alveoles were analyzed (Rigaut 1991, Fig. 14.1).

(1996) reported scale-dependent geometry in the distribution of town sizes and Andrle (1996) found similar behavior in the geometry of coastlines of fjord, volcanic, as well as tectonic origin.

2.3 Scale-dependent fractals

Before proceeding, we note that, in the original context of Mandelbrot, "scale-dependent fractal dimension" represents a contradiction in terms. In particular, if a fractal is to be regarded as, "rough and fragmented to the same degree at all scales," as Mandelbrot defined it, it must possess a constant (scale-independent) fractal dimension, as indicated in Eq. 2.2. In adopting the term "scale-dependent fractal dimension", employed by Mark & Aronson (1984), as well as by Takayasu (1992), and the proposed extension, we recognize that the requirement of scale-independent properties has been relaxed. However, the proposal is to retain the term "fractal", even though scale-dependent geometry is accepted, in deference to Mandelbrot's (1975a, 1975b) adoption of the latin root, *fractus* which (only) means "fragmented," with no implied requirement for scale self-similarity.

The proposed extension allows a more flexible description of the geometry of level sets and has a utility that extends beyond the descriptive, as will be demonstrated in the discussions that follow. In any event, constant-D fractal behavior is not excluded and may naturally be incorporated as a special case. The proposed extended framework is referred to as "scale-dependent-fractal" (SDF) geometry and retains the notion of quantifying complex geometries in terms of fractional dimensions, while allowing for scale-dependent geometric behavior, with the original, scale-invariant, fractal geometry of level sets referred to as "power-law-fractal" (PLF) geometry (Catrakis & Dimotakis 1996a).

As the chronology of the brief overview of the turbulence literature indicates, in this context, the earlier experimental work was, generally, supportive of the Mandelbrot (constant-D) PLF scaling proposals, with the experimental work indicating a need for a scale-dependent fractal (SDF) description appearing later, for the most part. Coming in the wake of the first set, the latter work had the benefit of the earlier experience and, in seeking an explanation for the discrepancy, explored additional questions that could influence the results. These will be discussed below.

3. Scale-dependent geometry of isoscalars in turbulent jets

Shortly after Mandelbrot's (1977) book, several investigations of fractal properties of level sets in turbulence were undertaken. Laser-induced-fluorescence images of turbulent jets (Dimotakis *et al.* 1983), such as the one reproduced in van Dyke's book (1982, p. 97), and others, were already available (*cf.* Figs. 1.3a,b). In the second edition of his book, Mandelbrot refers to Fig. 1.3a (1982, p. 52b) as evidence corroborating fractal proposals for turbulence. Our own attempts at the time, however, to perform a fractal analysis on the lower-Reynolds-number images (*e.g.*, Fig. 1.3a), that had the more easily identified scalar interfaces, did not yield constant fractal dimensions. The difficulties of the "stretched-string" algorithm that had been employed (recall Fig. 2.4 and related discussion), in conjunction with the limited ability to acquire and analyze enough data for reliable statistics, discouraged us from sharing these early results, which were regarded as inconclusive. A few other groups had made similar informal attempts, some using the same laser-induced photos of the turbulent jet, who reached the same conclusion. Later efforts at Caltech, based on linear-CCD images also failed to provide conclusive results (Dimotakis 1996).

The first reports by Sreenivasan and his group, and subsequently others, in support of Mandelbrot's fractal proposals for turbulent-flow-generated level sets, cited above, appeared shortly thereafter. However, in our opinion at least, some of the issues we were worried about had not been addressed.

To investigate the matter in a way that would settle some of these, an experiment was designed for the purpose: to produce data of adequate statistical confidence, have a large enough dynamic range of scales, permit a more reliable analysis of the data using coverage-based (rather than "stretched-string") algorithms, explore the effects of flow Reynolds number, investigate the dependence of the results on the scalar threshold chosen to define the level set. It was also designed to address the important issue of fixed-level crossings by a signal with a finite signal-to-noise ratio. The experiments were reported by Miller & Dimotakis (1991a) and are discussed below.

3.1 1-D temporal and spatial isoscalar behavior

The Miller & Dimotakis (1991a) experiments to investigate scalar level set behavior were carried in the facility schematically shown in Fig. 3.1. The discussion and figures in the brief account below are derived from their report. A water tank with glass windows on all four sides, with an interior volume of about $1.1\,\mathrm{m}^3$, acted as the (discharge) reservoir that provided the (unlabeled) fluid scalar entrained by the jet. To establish the flow, air was sonically metered to drive the jet fluid at constant velocity through a $d_\mathrm{j} = 2.54\,\mathrm{mm}$ (0.1 in) diameter nozzle at the base of the plenum, that was filled with water labeled with a fluorescent laser dye (disodium fluorescein), at a concentration less than 10^{-6} M.

For the single-point (one-dimensional) time-series measurements, an argon-ion laser beam was expanded, collimated, and aligned, crossing the jet centerline axis at right angles (radially) at the measuring station at $z/d_\mathrm{j} = 100$. The optics were designed to avoid spurious reflections and generated a small Gaussian waist at the focus formed on the jet centerline. The laser beam power was maintained at 1.0 W to avoid heating of the dyed fluid in the very small focal volume and to prevent saturation (photo bleaching). The much lower concentrations of dye at $z/d_\mathrm{j} = 100$ did not measurably attenuate or steer the beam. The resulting signal-to-noise ratio was 60 dB, as estimated on the basis of the scalar time series power spectrum (*cf.* Fig. 3.2).

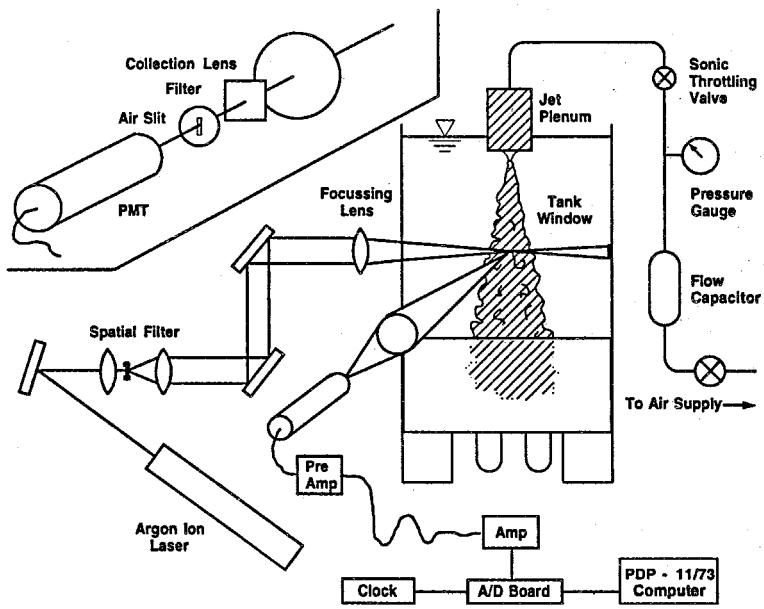

FIG. 3.1 Schematic of turbulent-jet apparatus used for 1-D temporal and spatial scalar measurements (*ibid.* Fig. 1).

The single-point time-series measurements were made utilizing a low f# lens to collect light from the very short segment centered at the waist of the focused laser beam at the measuring station, through an optical low-pass filter to eliminate the laser-frequency (green) light, onto a photomultiplier tube, yielding single-point jet-fluid concentration values *vs.* time. A slit spatial filter defined the length of the laser line segment sampled, with a width chosen such that the sampling volume was roughly cubic in shape, about 80 μm on a side.[♯] The signal chain incorporated a three-pole Butterworth filter, with a cutoff frequency set slightly under 10 kHz. The data were intentionally oversampled in time, by some margin (at a sampling frequency of 20 kHz), as can be seen by the frequency where the white noise floor crossed the concentration spectrum. The same sampling frequency was used in all the runs, permitting the reliable definition of a Wiener-filter kernel, as will be explained below.

The Reynolds number was varied in these experiments, with measurements in the range, $2.9 \times 10^3 \leq Re \leq 23 \times 10^3$. Special consideration was given to the treatment of noise. Specifically, power spectra of the data were computed, along with the optimal (least mean-square error) Wiener filter in each case (Wiener 1949, Press *et al.* 1986). The data were then convolved with the Wiener kernel to obtain

[♯] A slit, rather than a pinhole, was employed so that any small beam movements in the vertical direction did not alter the size of the measurement volume (and, by extension, the intensity of the signal).

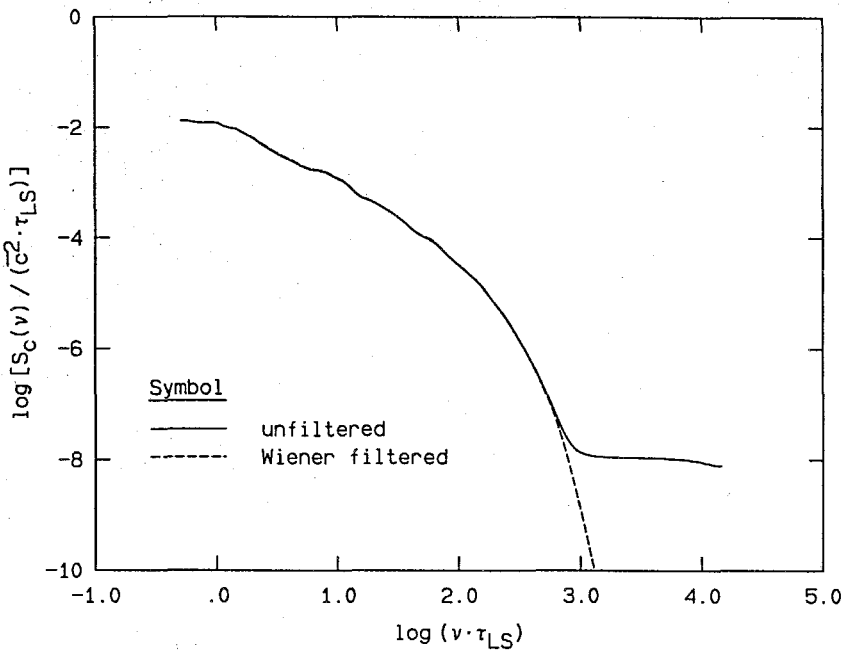

FIG. 3.2 Temporal power spectra of unfiltered and Wiener-filtered data (Miller & Dimotakis 1991a, Fig. 2).

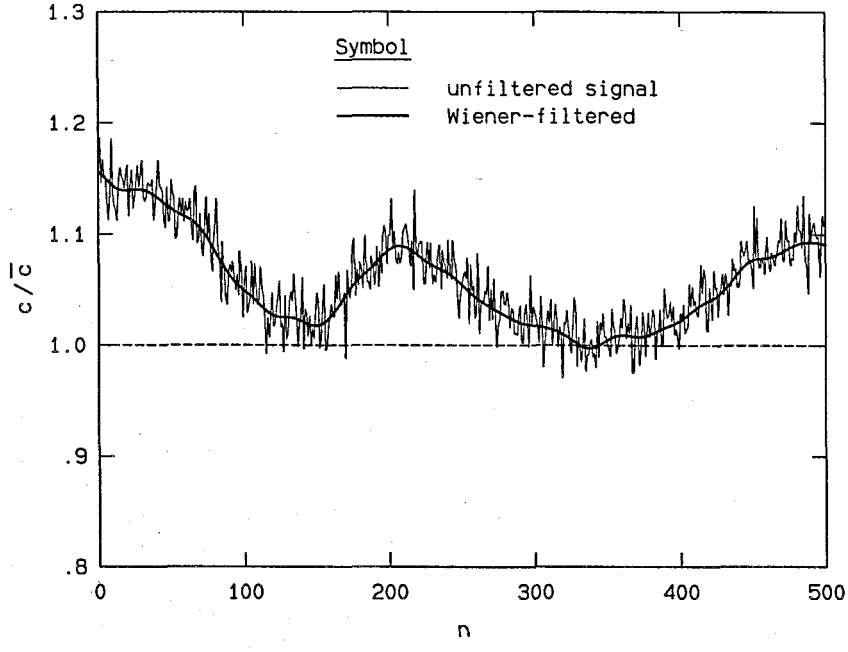

FIG. 3.3 Effect of noise on threshold transitions. Data recorded for $Re = 2.9 \times 10^3$ (*ibid.* Fig. 15). See Fig. 3.2, above.

the optimally-estimated signal, consistent with the detection noise level in each run.

The Wiener-filtered data were thresholded and transitions, *i.e.*, crossings at the selected scalar threshold value, were located. Figure 3.3 compares the level crossings, over a short time interval, of the raw (unfiltered) signal to those of the Wiener-filtered signal, at a scalar threshold equal to the local mean, $c = \bar{c}$. The choice of threshold is important and will be discussed below. As can be seen, the difference in both the number and spacing of level crossings between the two signals is very large. It should be recalled that it is the Wiener-filtered signal whose spectrum is concave downwards, as expected for a scalar time series, and is depicted as the dashed curve in Fig. 3.2.

The resulting level set, *i.e.*, the record of transition locations, was then processed using a 1-D box-counting algorithm. The algorithm determines the number, or coverage count, $N_1(\lambda)$, of contiguous, constant-length segments, or "tiles", required to cover the transition locations on a record, as a function of the tile size, λ. The fractal dimension, $D_1(\lambda)$ is then computed as the logarithmic derivative (Eq. 2.14) of the coverage count.

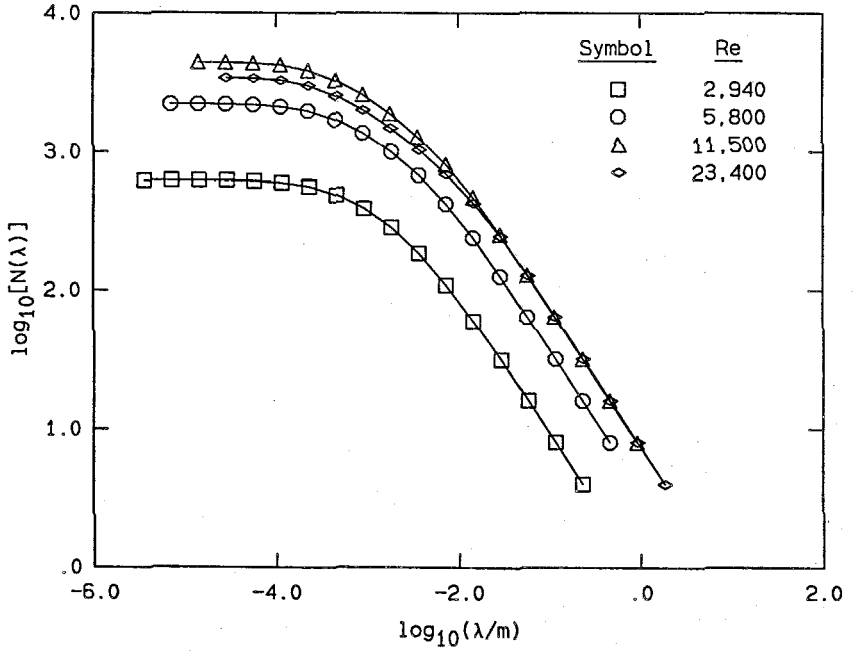

FIG. 3.4 Coverage, $N_1(\lambda)$, as a function of scale for 1-D temporal scalar measurements in a turbulent jet (*ibid.* Fig. 4).

The log-log plots of $N_1(\lambda)$ and plots of the resulting $D_1(\lambda)$ for the single-point, on-axis concentration measurements in the jet, using a threshold value equal to

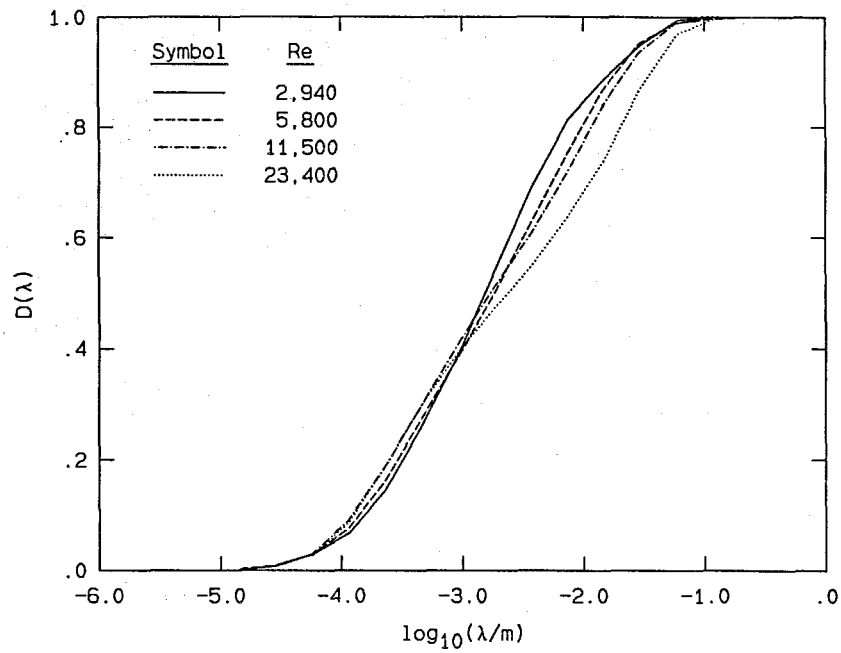

FIG. 3.5 Coverage dimension, $D_1(\lambda)$, as a function of scale, derived from the coverage data in Fig. 3.4 (*ibid.* Fig. 5).

the mean concentration, are shown in Figs. 3.4 and 3.5. The length scale, λ, was estimated by multiplying the time interval with the calculated mean (centerline) velocity and has been expressed in absolute length (meters). The local jet diameter at the measuring location was estimated as equal to $\delta(x) \simeq 0.1$ m, *i.e.*, $\log_{10}(\lambda/\mathrm{m}) = -1.0$ (*cf.* Fig. 3.5) corresponds to a scale $\lambda \approx \delta$.

If the level set possessed a constant fractal dimension, a horizontal portion of the curve would be observed in Fig. 3.5. As can be seen, no evidence of such a constant value is evident in the $D_1(\lambda)$ plots, other than the limiting values of 0 and 1 that can be argued for *a priori*. The observed continuous increase of $D_1(\lambda)$ occurs over a range of equivalent spatial scales from below the Kolmogorov scale, up to the outer large scales of the flow ($\log_{10} \lambda/\mathrm{m} \simeq 0.1$). The limiting value of 1 at the large tile sizes indicates that every tile of sufficient length covers (some) transitions. This is to be expected for scales on the order of the local jet diameter ($\delta(z) \simeq 11$ cm for the data in Fig. 3.5, or larger, since over such a distance (or corresponding time) a crossing of the mean concentration level is almost certain. Failure to reach an asymptotic value of unity would indicate that either the data record was of insufficient length to capture the largest scales of the flow, or that the processing algorithm stopped at a tile size shorter than the largest scales. All four curves

in Fig. 3.5 approach $D_1(\lambda) \simeq 0$, merging in the vicinity of the spatial resolution estimate, *i.e.*, $\lambda \simeq \lambda_{res} \simeq 80\,\mu$m, as noted above, for these measurements. The limiting behavior for $D_1(\lambda)$, for large and small λ, is consistent with what should be expected (Dimotakis 1991), as noted above (recall Eqs. 2.8 and 2.10, and related discussion).

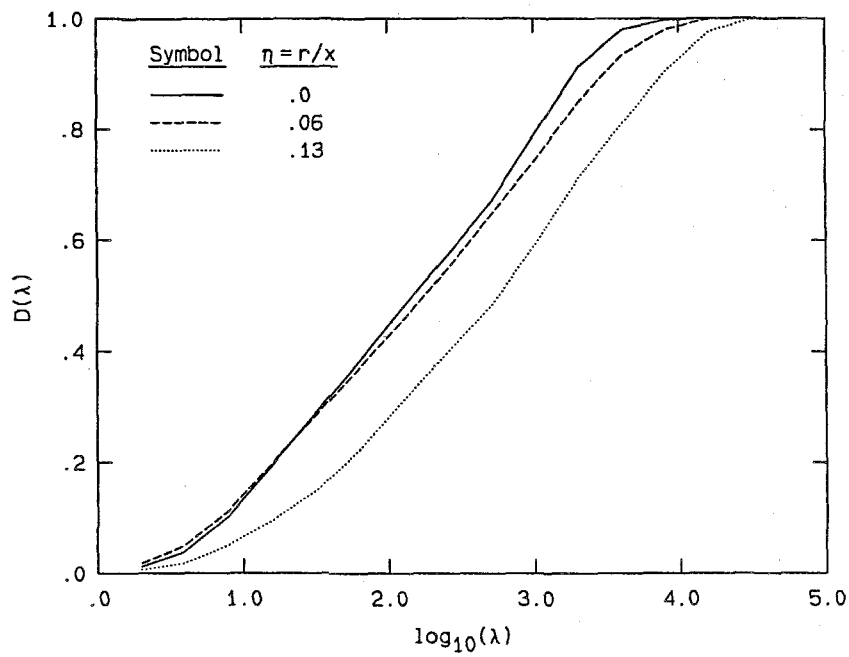

FIG. 3.6 Coverage dimension, $D_1(\lambda)$, derived from off-axis, 1-D temporal scalar measurements in a turbulent jet (*ibid.* Fig. 8).

Measurements were also made off the jet centerline, on the rays $\eta = r/z = 0.06$ and 0.13, at a Reynolds number of 8600. The results, from level sets derived for the threshold choice, $c = \bar{c} = \text{fn}(\eta)$, are shown in Fig. 3.6, along with the corresponding centerline curve, *i.e.*, $\eta = 0$. The similarity in the three results is noteworthy, despite the relatively large variation in the value of the threshold, $\bar{c}(\eta)$.

It had been suggested by Sreenivasan & Meneveau (1986), that if long records are used in the box-counting algorithm, they may mask local power-law fractal behavior. Miller & Dimotakis (1991a, Fig. 17 and related discussion) addressed this issue by processing a sequence of short records independently, and, aside from the impaired statistics, as expected from the shorter records, found a similar $D_1(\lambda)$ dependence on the scale, λ, as for the longer records.

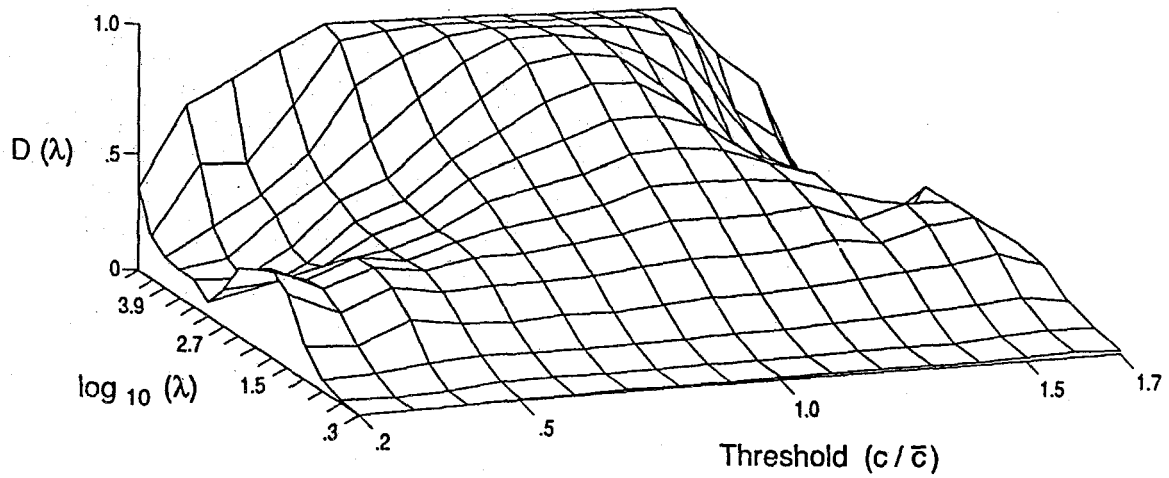

FIG. 3.7 Scalar-threshold effects on $D_1(\lambda)$ (*ibid.* Fig. 10).

Scalar-threshold effects were also addressed. A range of thresholds for the single-point data, both on-axis and off-axis at $\eta = 0.13$, were examined. The dependence of $D_1(\lambda)$ on the scalar-threshold is shown in Fig. 3.7. The continuous variation of the $D_1(\lambda)$ curves with λ can be seen to persist for a rather large range of threshold values on either side of the local mean concentration. As the threshold is either increased or decreased, two effects are observed. The sloping region shifts position, achieving the asymptotic value of 1 at progressively larger (time) scales, as would be expected for temporal data.* Secondly, a bump appears at smaller values of λ. While the linear scale may not make it clear, the off-axis data exhibit a similar bump at small scales as the on-axis data, when viewed at smaller values in logarithmic coordinates. This behavior reflects the stochastic character of the concentration signal (rather than the fluid dynamics of the turbulent jet), as indicated, by processing measurements of laser light scattered from a very dilute, constant-concentration fluorescent-dye solution.

To further understand the three-dimensional plots, the nature of the concentration signal must be considered. Possible scalar values are bounded by zero and some upper limit and the measured concentration time history exhibits many maxima and minima. Near the mean, relatively few of these extrema are encountered. On the other hand, for thresholds approaching the highest or lowest values detected, many such turning points are found, and they may dominate the statistics. Picture

* The probability of encountering a transition within a certain tile size (time interval) decreases for scalar thresholds away from the mean, increasing the tile size required to cover a threshold crossing with some certainty.

a local minimum in concentration, with a roughly parabolic dependence of $c(t)$ in its vicinity. Imagine then a threshold level that is slowly decreased toward the minimum value. Two threshold crossings are encountered, which, as the threshold is lowered, move closer together. These eventually (almost) join before the threshold drops below the minimum (recall that the signal is discretely sampled in time). Thus, near the turning points there can be a separation of scales; one length is associated with the typical distance between extrema, and the other is a much smaller scale associated with the spacing of crossings within pairs at each extrema.

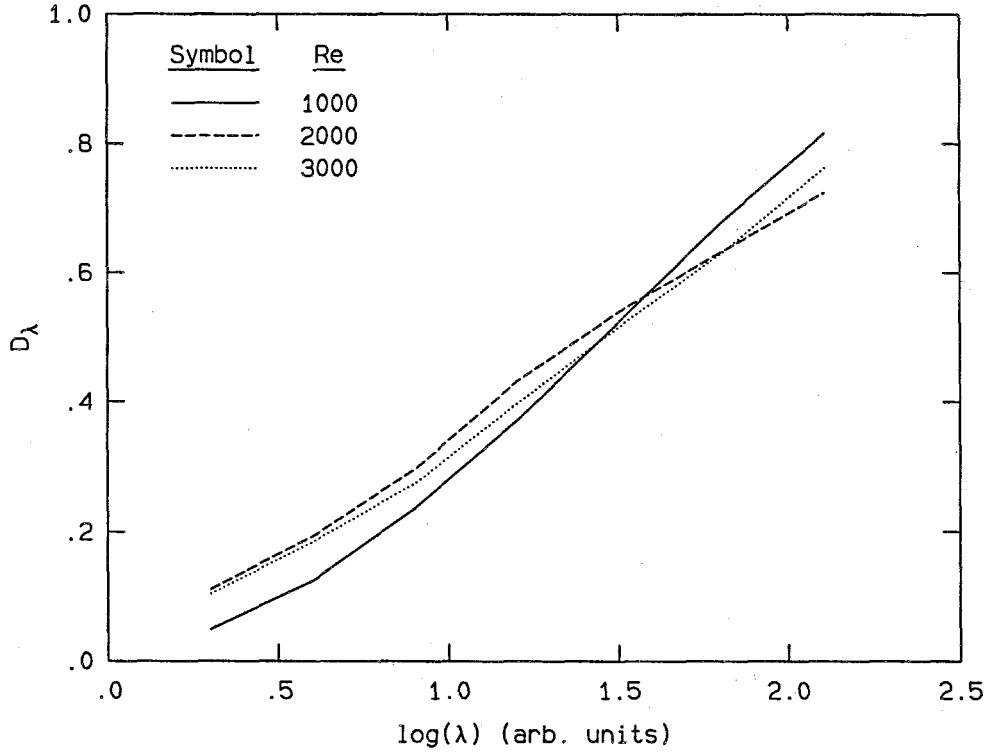

FIG. 3.8 Coverage dimension, $D_1(\lambda)$, derived from 1-D spatial scalar measurements in a turbulent jet (*ibid.* Fig. 6).

This scale separation manifests itself in the $D_1(\lambda)$ plots in two primary ways. One is the appearance of a bump at the smallest scales, traceable to the double crossings at each extremum. This bump is indicative of a characteristic length at that scale. The second is that the rise of $D_1(\lambda)$ to its asymptotic value of unity is shifted to larger scales as the threshold is increased, or decreased, from the local mean. This is ascribable to what could be called conservation of spacing. Pairs of crossings drop out as the threshold moves past their extrema, producing a larger length scale associated with the distance between crossings to either side of the pair. This is enhanced by crossings within a pair coming closer together as the

threshold approaches their extremum, causing the spaces between adjacent pairs to correspondingly increase. Both the bump at small scales and the shift in the rise are evident in all of the three-dimensional $D_1(\lambda)$ plots.

One-dimensional spatial measurements were also recorded (with different beam-expansion optics to produce a collimated beam; *cf.* Fig. 3.1), imaging a line element of the concentration field on a 512-pixel linear photodetector array. The line element spanned one tenth of the local jet diameter, at $z/d \simeq 300$, centered on the jet axis, at $Re \simeq 1.0\times10^3$, 2.0×10^3, and 3.0×10^3. The coverage dimension was computed for these data as a function of spatial scale, $D_1(\lambda)$, without invoking Taylor's hypothesis (Fig. 3.8). The behavior is similar to that of Fig. 3.5, even though, for these, smaller-dynamic-range data, the range of scales is insufficient to allow $D_1(\lambda)$ to attain the expected limiting values of 0 and 1 (*cf.* Eqs. 2.8, 2.10, and related discussion). In particular, no constant-D scale region is observed for these spatial data either.

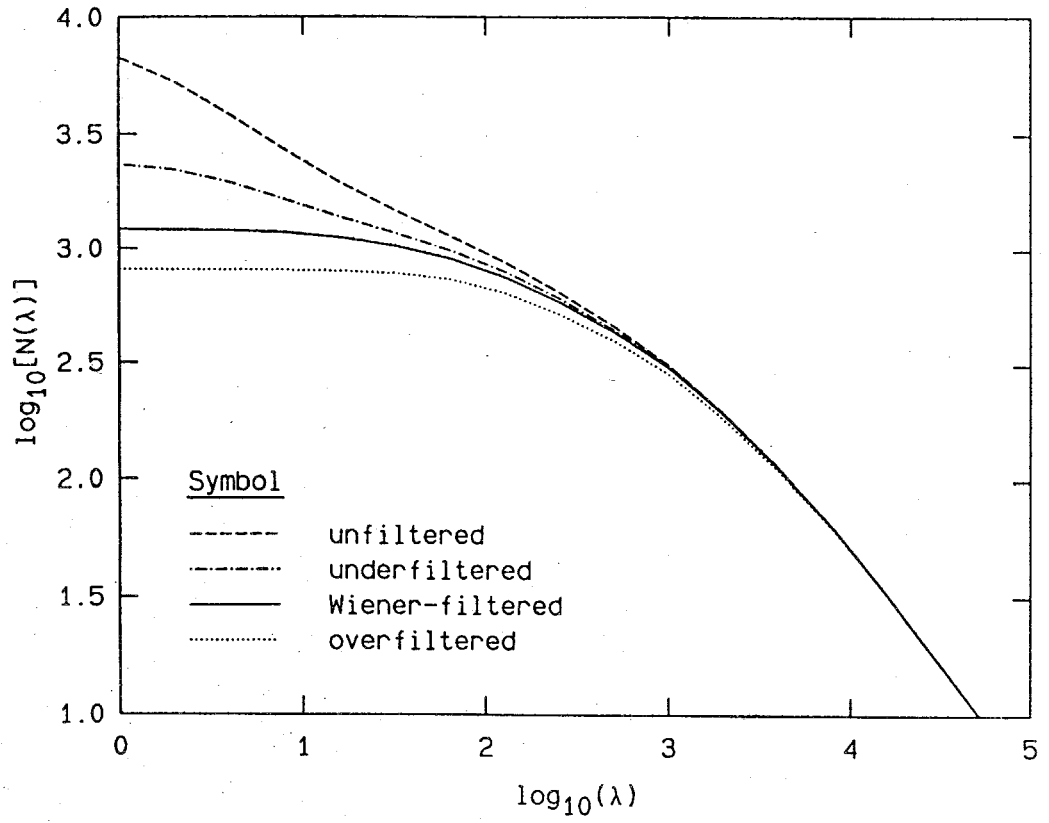

FIG. 3.9 Influence of noise on 1-D coverage statistics (*ibid.* Fig. 16).

Before ending this part of the discussion, we should cite the investigation of the effects of noise on the coverage statistics by Miller & Dimotakis (1991a). Briefly,

they computed the coverage of level crossings derived from the unfiltered data (*cf.* Figs. 3.2 and 3.3). The much-higher number of crossings computed from the unfiltered data dominated the coverage counts, for a surprisingly large scale range, which then reflected the behavior of the noise, rather than that of the scalar signal. In particular, a spurious region of near-constant coverage dimension was indicated by the noisy data, in contrast to the coverage statistics derived from the optimally-reconstructed scalar time trace, plotted in Fig. 3.4. This is illustrated in Fig. 3.9 (Miller & Dimotakis 1991a, Fig. 16). We will revisit the issue of noise in the context of level-set analysis of two-dimensional scalar data, below.

3.2 2-D spatial isoscalar behavior

Two-dimensional, spatial measurements of the jet-fluid concentration field in liquid-phase, turbulent jets were recently reported by Catrakis & Dimotakis (1996a). The experiments, which relied on laser-induced fluorescence digital-imaging, investigated transverse (jet-axis-normal) planar cuts in the far field ($z/d_j = 275$) of turbulent jets and included a coverage analysis of isoscalar geometry.

The experiments were conducted in the same facility used for the Miller & Dimotakis (1991a) experiments (*cf.* Fig. 3.1), employing a galvanometrically-driven mirror to (linearly) sweep a collimated laser beam that formed the illumination sheet (*cf.* Fig. 2.5). The sectional images were recorded on a cryogenically-cooled, (1024 × 1024)-pixel, CCD camera. The laser beam waist was estimated as $w_0 \lesssim 300\,\mu$m, with a Rayleigh range of ± 12.5 cm (on either side of the waist). The field of view spanned $\ell_0 \simeq 42$ cm, contained the full transverse spatial extent of the turbulent-jet fluid at the measuring station, and corresponded to a pixel resolution of $\lambda_p \simeq 420\,\mu$m. Consequently, the image-plane-normal resolution was smaller than the in-plane (pixel) resolution in the center, and comparable to it near the edges of the field of view.

At the downstream station in these experiments ($z/d_j = 275$), it was verified that the low jet-plenum dye (disodium fluorescein) concentration, $c_0 \simeq 2.0 \times 10^{-6}$ M, produced negligible laser attenuation across the field of view. The image calibration procedure employed ensured that the measured scalar-field values were referenced, in absolute value, to the (pure) jet-plenum concentration, c_0. Spatial power spectral measurements indicated a digital-image signal-to-noise ratio in excess of 50 dB, *i.e.*, in excess of 300:1.

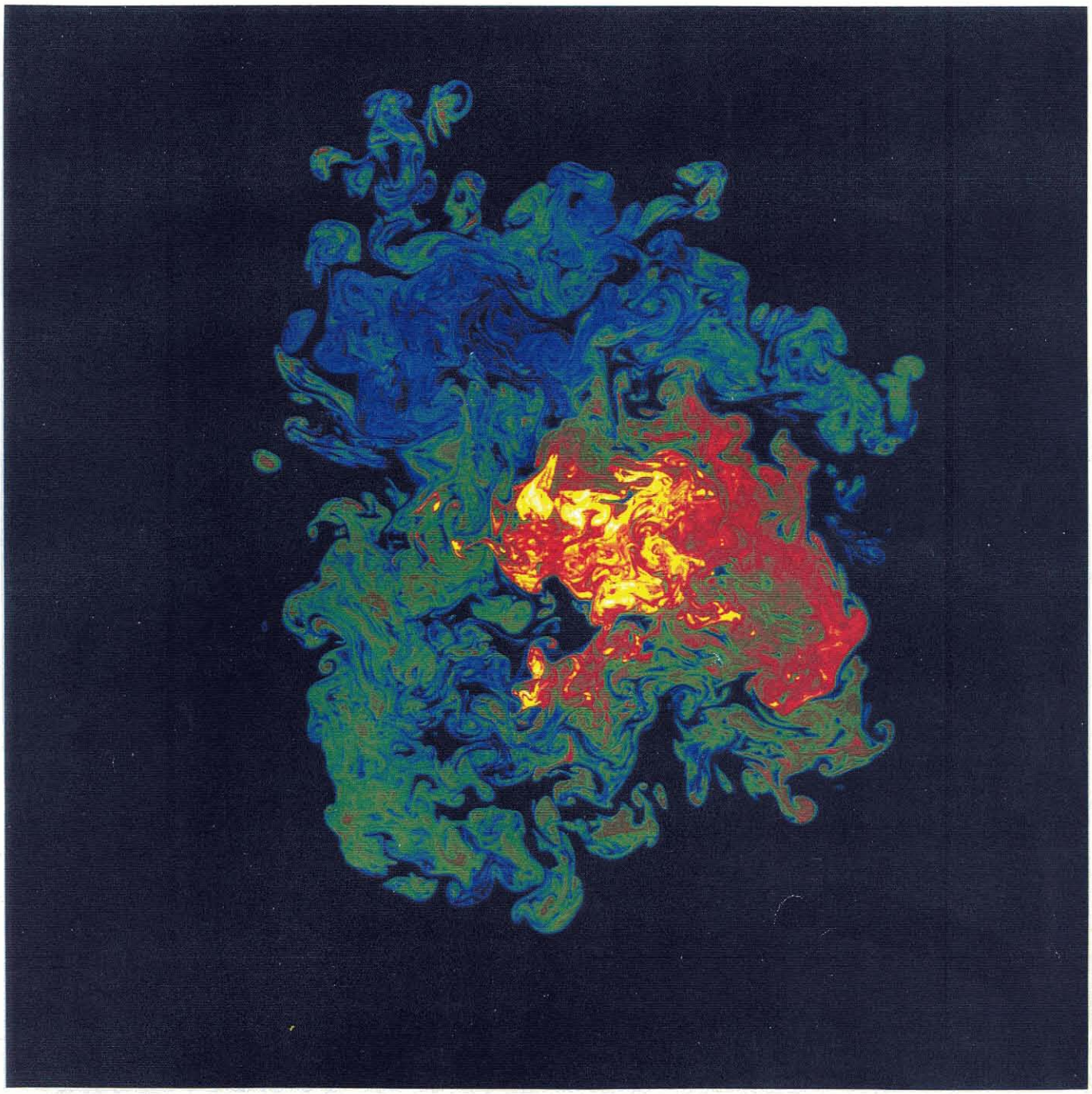

FIG. 3.10a Jet-fluid concentration in the far-field ($z/d_j = 275$) of a turbulent jet at $Re \simeq 4.5 \times 10^3$.

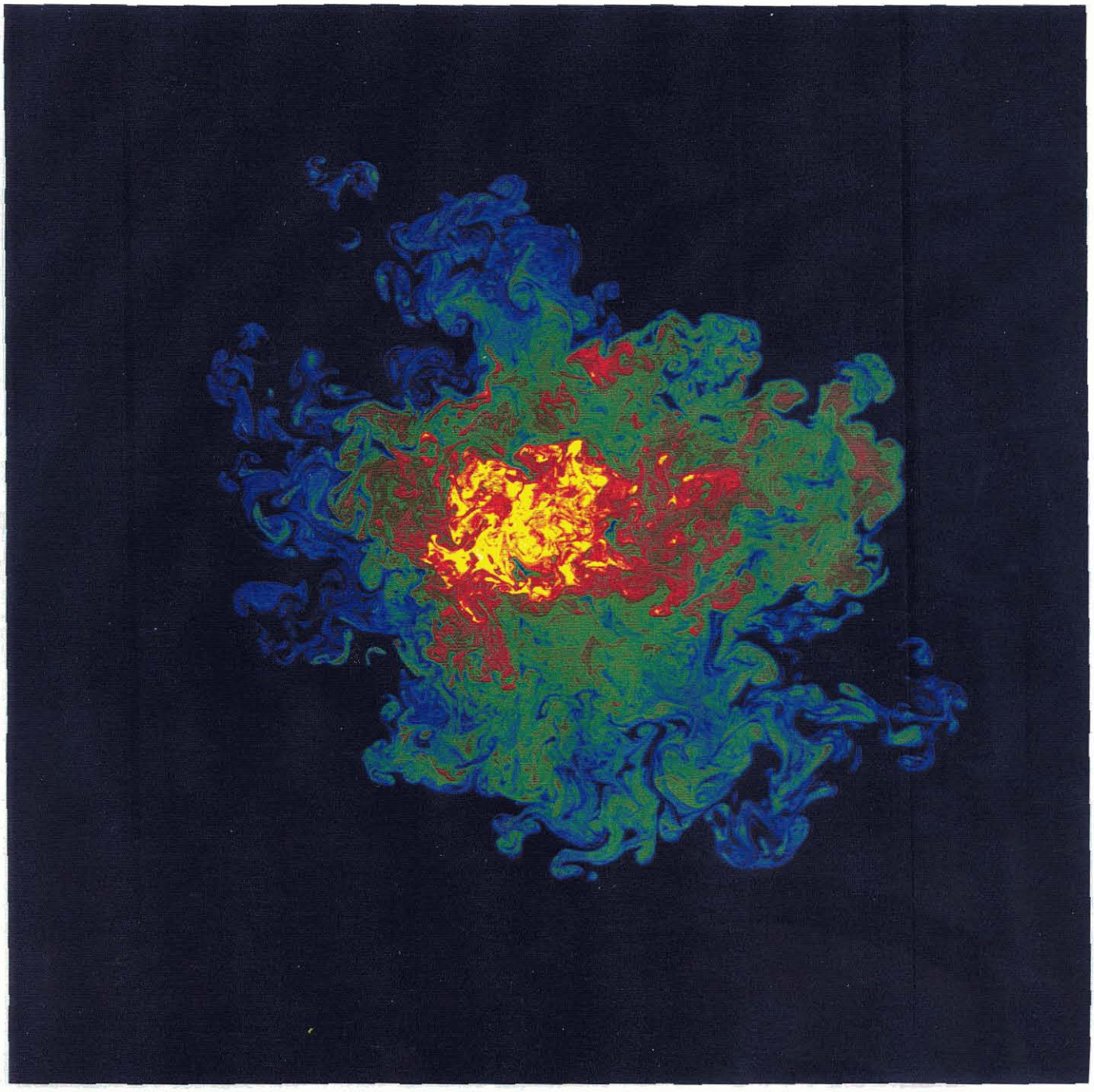

FIG. 3.10b Jet-fluid concentration in the far-field ($z/d_j = 275$) of a turbulent jet at $Re \simeq 9.0 \times 10^3$.

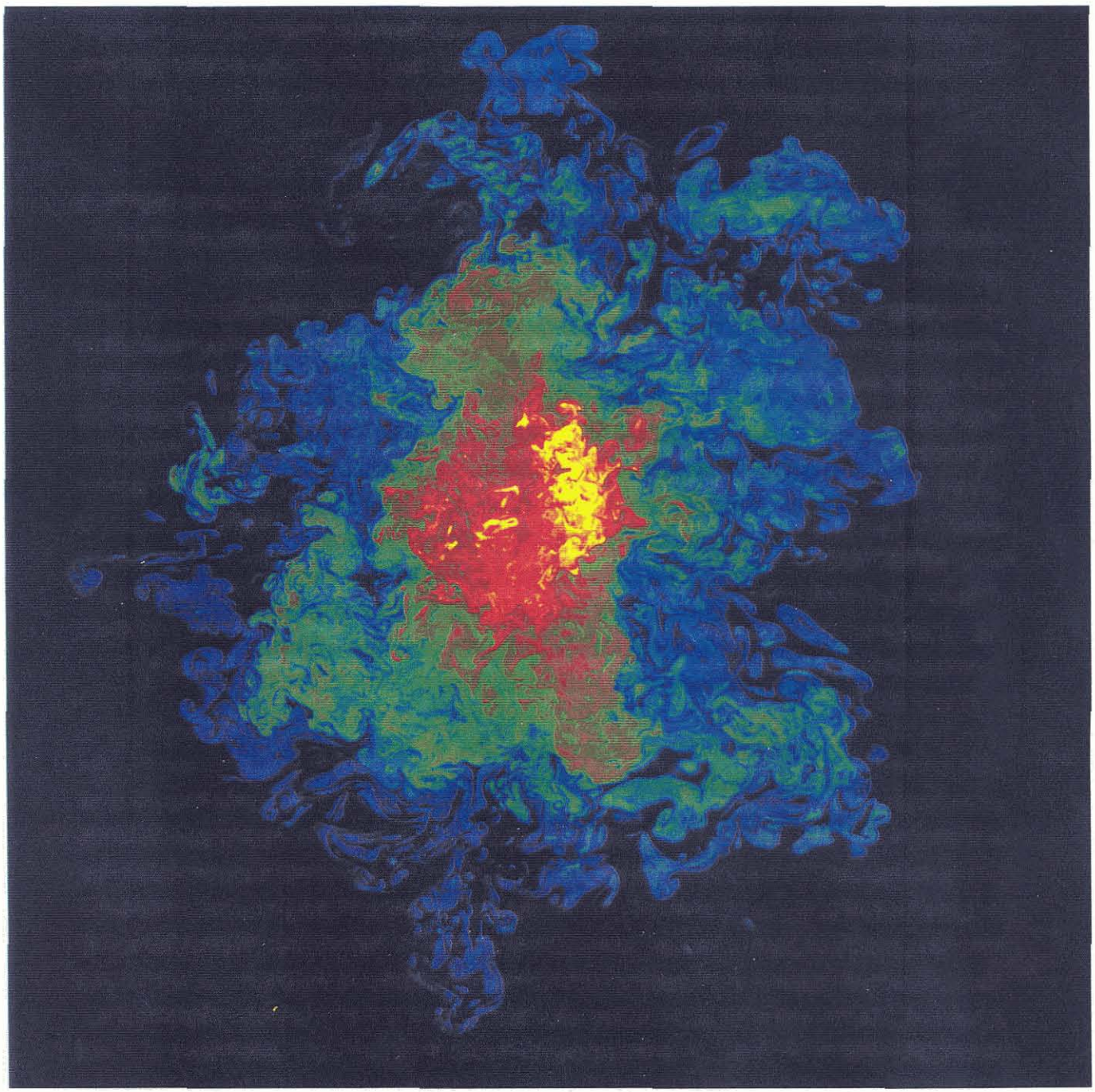

FIG. 3.10c Jet-fluid concentration in the far-field ($z/d_j = 275$) of a turbulent jet at $Re \simeq 18 \times 10^3$.

The jet far field was investigated for three Reynolds numbers: $Re = 4.5 \times 10^3$, 9.0×10^3, and 18×10^3. Images of individual realizations of jet slices, for each of the three Reynolds numbers, are depicted in Figs. 3.10a–c. In these figures, false-colors have been assigned to the scalar values, starting from black for zero jet-fluid concentration (unmixed reservoir fluid), through blue, for low-concentration fluid, on to green, red, and yellow for increasing concentration levels.

While the data in Figs. 3.10a–c are individual realizations and should be used with some caution in drawing general conclusions, they are representative and help illustrate some aspects of the Re-dependence of the geometry of the scalar field. In particular, the lowest Reynolds number flow ($Re \simeq 4.5 \times 10^3$) field data (Fig. 3.10a) indicate relatively high scalar gradients in the periphery (outer, low-speed region) of the jet. The false colors in the image data can be seen to transition from green and red, corresponding to moderately-high scalar concentrations, almost directly to black, corresponding to zero (negligible) scalar concentration, with very thin regions of intermediate scalar values (blue) in between. In contrast, the highest Reynolds number flow ($Re \simeq 18 \times 10^3$) image indicates a relatively large portion of the field occupied by low-scalar-concentration fluid (blue) with correspondingly lower scalar gradients (almost no direct transitions from red to black) in the periphery of the jet. The intermediate Reynolds number ($Re \simeq 9 \times 10^3$) flow slice also indicates lower scalar gradients in the periphery, with a low-concentration region (blue). However, a substantially smaller area is occupied by it than at $Re = 18 \times 10^3$.

At the intermediate Reynolds number, $Re \simeq 9.0 \times 10^3$ (*cf.* Fig. 3.10b), the scalar-diffusion (full-wavelength) scale, $\lambda_{\mathcal{D}}$, at the jet centerline conditions, is estimated to be approximately equal to the pixel size, λ_{p}, *i.e.*, underresolved by a factor of 2 (per Nyquist's criterion), but much larger than the pixel size in the outer region of the jet, where the level sets have been computed. Also, at this Reynolds number, the time for the passage of the scalar-diffusion scale is estimated to be a factor of 30 times larger than the exposure time of an individual pixel, on the jet axis, and larger yet in the outer regions of the jet. The images were acquired maintaining a constant product of the beam-scanning time, which scaled the time exposure per pixel, and the local flow velocity, over the Reynolds numbers investigated. These choices provided temporally- as well as spatially-resolved measurements of the scalar field, throughout the Reynolds number range, certainly in the intermediate-to-outer regions of the jet where level-set behavior was investigated.

Figures 3.11a–c, compiled from the individual realization data reproduced in Figs. 3.13a–c, provide another view into these differences. These are histograms

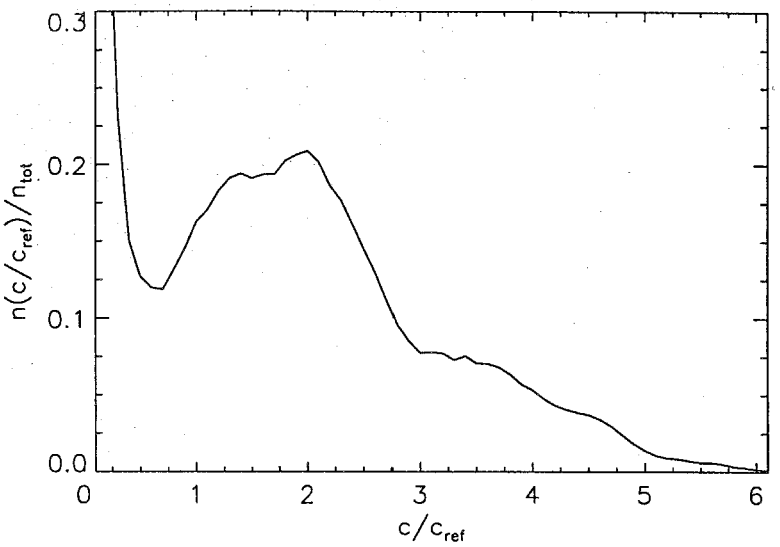

FIG. 3.11a Jet-fluid concentration histogram derived from individual $Re \simeq 4.5 \times 10^3$ jet slice data (Fig. 3.10a).

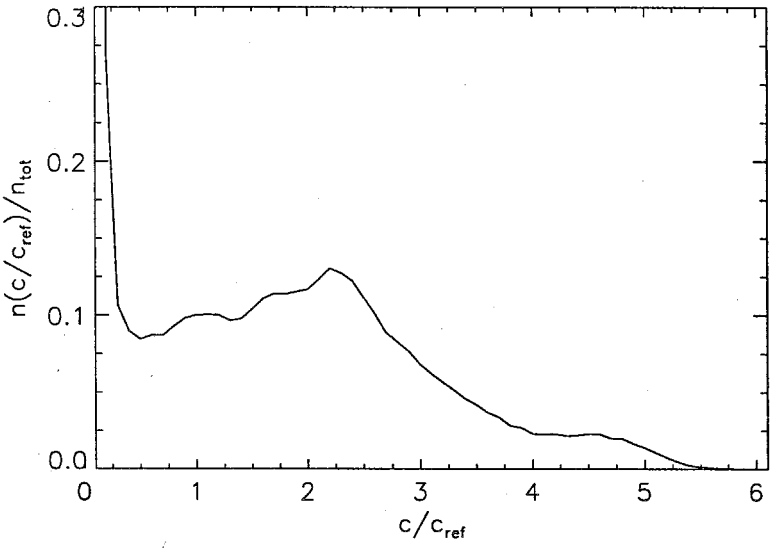

FIG. 3.11b Jet-fluid concentration histogram derived from individual $Re \simeq 9 \times 10^3$ jet slice data (Fig. 3.10b).

of the number of pixels found in the designated scalar range, normalized by the total number of pixels in each image, with scalar concentration values normalized by $c_{\rm ref} \simeq c_0/220$, for all the data. Again, it should be borne in mind that these represent the statistics of the three individual realizations. As can be seen, the most probable value (mode) of jet-fluid concentration, in the lowest Reynolds number data (Fig. 3.11a), is at $c/c_{\rm ref} \simeq 2$, in contrast to that for the highest Reynolds number data (Fig. 3.11c), for which the mode is at $c/c_{\rm ref} \simeq 1$, reflecting the qualitative

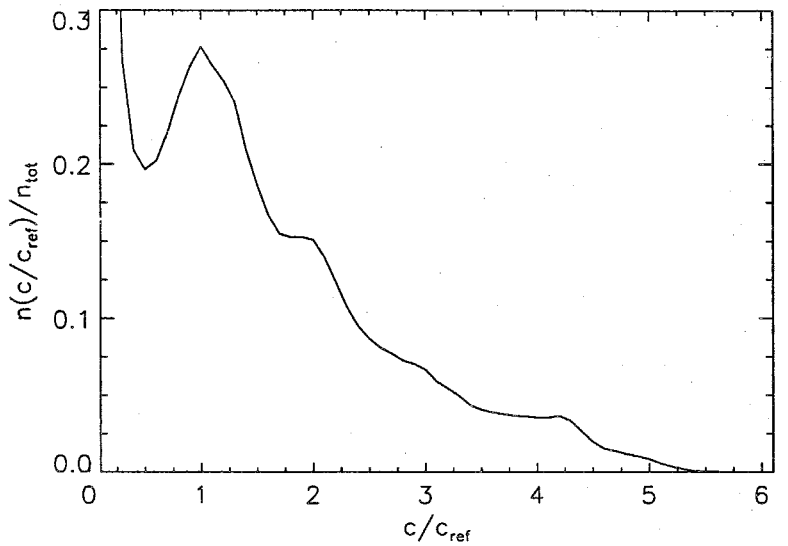

FIG. 3.11c Jet-fluid concentration histogram derived from individual $Re \simeq 18 \times 10^3$ jet slice data (Fig. 3.10c).

conclusion that was drawn on the basis of the false-color representation of the scalar values in Figs. 3.10.

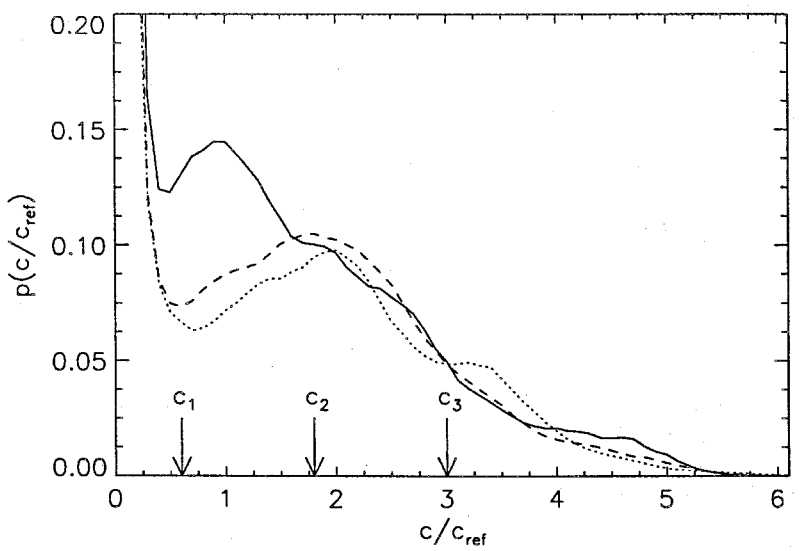

FIG. 3.12 Jet-fluid concentration pdf in the far-field ($z/d_j = 275$) of a turbulent jet. $Re \simeq 4.5 \times 10^3$: dotted line; $Re \simeq 9.0 \times 10^3$: dashed line; $Re \simeq 18 \times 10^3$: solid line. Three scalar-threshold values, c_1, c_2, and c_3, are also indicated.

An estimate of the scalar field (jet-fluid concentration) probability-density functions was made and are depicted in Fig. 3.12. Recall that these are spatially-normalized, representing the fraction of the area in each slice given to a range

of scalar values, *i.e.*,

$$p(c)\,\mathrm{d}c \;=\; \frac{|\mathrm{d}A(c)|}{A_0}\;, \tag{3.1}$$

where $\mathrm{d}A(c)$ is the (ensemble-averaged) image slice area over which the scalar values are between c and $c + \mathrm{d}c$ and A_0 is the total image slice area (*e.g.*, Kuznetsov & Sabel'nikov 1990, p. 27). The estimated pdf's indicate that scalar level-set measures may be expected to depend on both the threshold value employed to compute the level set, as well as the flow Reynolds number. Three scalar values are marked on the pdf abscissa: c_2, in the vicinity of the local c-maximum for the two lower-Re flows, c_1, in the vicinity of the local c-minimum — corresponding to the outer isosurface values — where (constant-D) fractal behavior has been reported (*cf.* Sreenivasan 1991), and a high-level, c_3, chosen such that $c_2 - c_1 = c_3 - c_2$, to investigate inner isosurface behavior.

Isoscalar contours (level sets) corresponding to the $c = c_2$ intermediate threshold, for the data depicted in Figs. Fig. 3.10a-c, for each of the three Reynolds numbers, are depicted in Figs. 3.13a-c, respectively, superimposed on the scalar-field data.

Several features can be deduced from these spatial pdf data, that also manifest themselves in the associated isoscalar behavior.

a. The scalar pdf values are very nearly matched for $c \gtrsim c_2$, within statistical confidence.

b. The data indicate a progressively increasing probability of encountering jet-fluid mixed to concentration levels $c < c_2$, with increasing Reynolds number.

c. As a consequence of the spatial normalization employed, the spatial extent of the jet, corresponding to low-concentration-level contours, may be expected to be Re-dependent.

d. The data indicate a qualitative change between the lower-Re scalar pdf's ($Re = 4.5 \times 10^3$, 9.0×10^3), which are characterized by a local maximum at $c \approx c_2$, and the $Re = 18 \times 10^3$ pdf, consistent with the expectation of a mixing transition at $Re \approx 10^4$ (recall discussion in Sec. 1.1).

e. The isoscalar contours appear to be more convoluted at *lower* Reynolds number, becoming less complex with increasing Reynolds number.

These observations will be discussed further below.

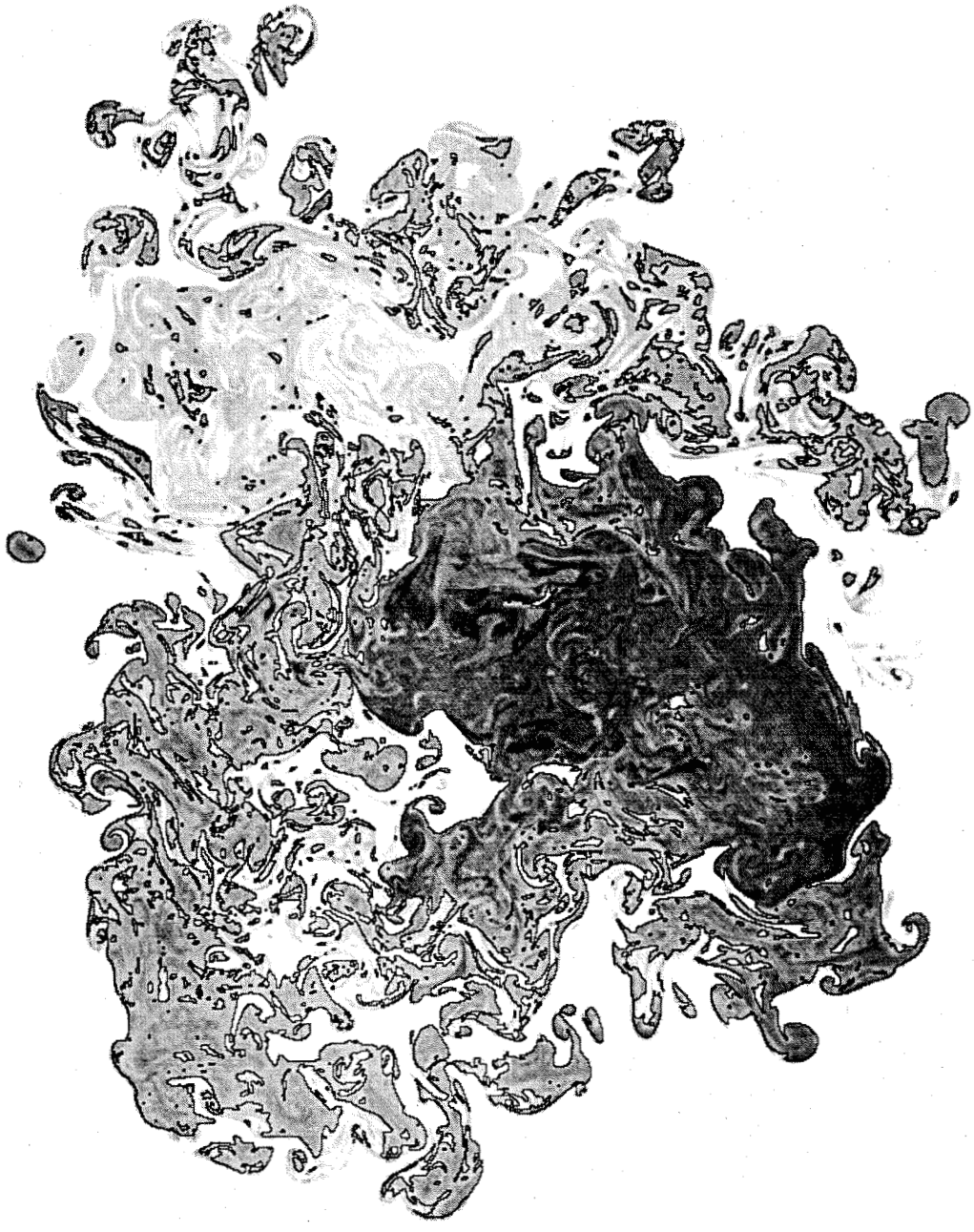

FIG. 3.13a Level set at $c = c_2$ of the jet-fluid concentration superimposed on scalar-image data in the far-field ($z/d_j = 275$) of a turbulent jet. $Re \simeq 4.5 \times 10^3$.

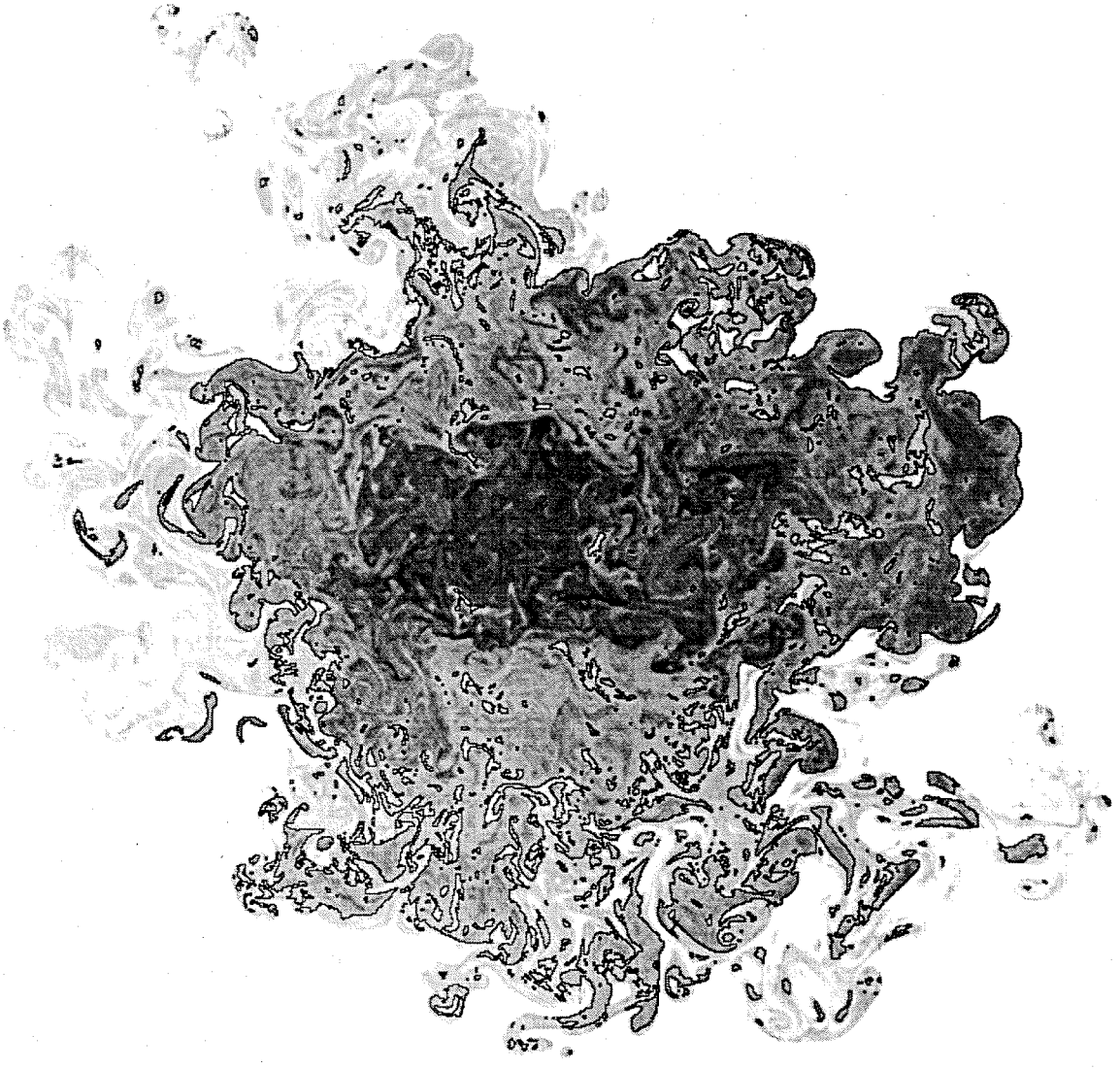

FIG. 3.13b Legend as in Fig. 3.13a: $Re \simeq 9.0 \times 10^3$.

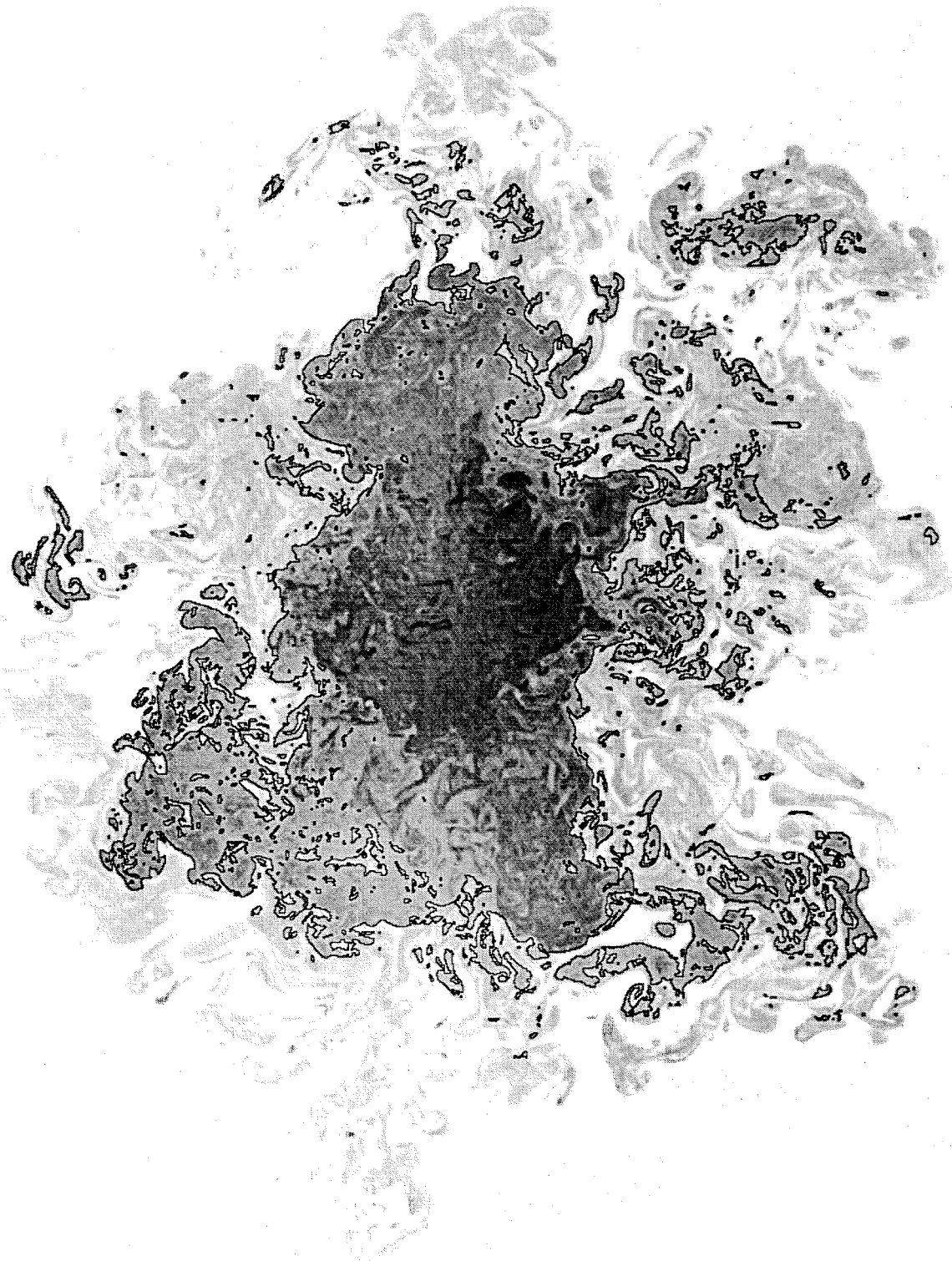

FIG. 3.13c Legend as in Fig. 3.13a: $Re \simeq 18 \times 10^3$.

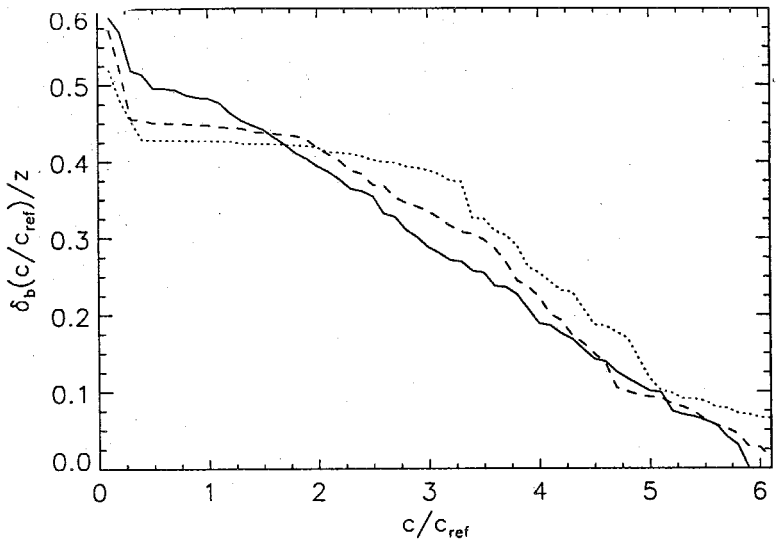

FIG. 3.14 Isoscalar bounding box size, $\delta_b(c; Re)$. $Re \simeq 4.5 \times 10^3$: dotted line; $Re \simeq 9.0 \times 10^3$: dashed line; $Re \simeq 18 \times 10^3$: solid line.

In what follows, the spatial scale of the coverage boxes (tiles), λ, is normalized by $\delta_b(c; Re)$, the ensemble-averaged, threshold- and Re-dependent, bounding-box size (*cf.* Eq. 2.6). It encloses the portion of the scalar field whose value exceeds the threshold, c (*e.g.*, Fig. 2.6a). The continuous dependence of δ_b on the threshold, c, is plotted in Fig. 3.14, for each of the three Reynolds numbers investigated. It is interesting that, at low Reynolds numbers, the data indicate a weak dependence of δ_b on threshold, for low threshold values, *i.e.*, diminished mixing that would have otherwise produced intermediate scalar values in the outskirts of the turbulent jet region.

The data suggest that, at high Reynolds numbers, δ_b approaches a straight line, *i.e.*,

$$\frac{\delta_b(c; Re)}{z} \rightarrow \beta_0 - \beta_1 \frac{d_j\, c}{z\, c_0} \ , \tag{3.2}$$

where $\beta_0 \simeq 0.6$ and $\beta_1 \simeq 0.08$.** This also indicates that the increased mixing in the outer regions of the jet has increased the transverse extent, or "reach", of the mixed (jet-plenum) fluid away from the jet axis. This can be directly discerned by comparing the mixed fluid region, for c-levels lower than c_2, for each of the three Reynolds numbers, in Figs. 3.13a–c. In particular, fluid mixed to $c < c_2$ (outside the c_2 level set) occupies an increasing area in the image with a substantial jump

** Equation 3.2 provides the correct scaling with z/d_j. It also appears in Catrakis & Dimotakis (1996a, Eq. 3.3), but as written there only applies to the particular downstream location, $z/d_j = 275$, of those experiments.

in going from $Re = 4.5 \times 10^3$ and 9.0×10^3, to $Re = 18 \times 10^3$, in accord with a mixing transition across this Re interval, as also noted earlier.

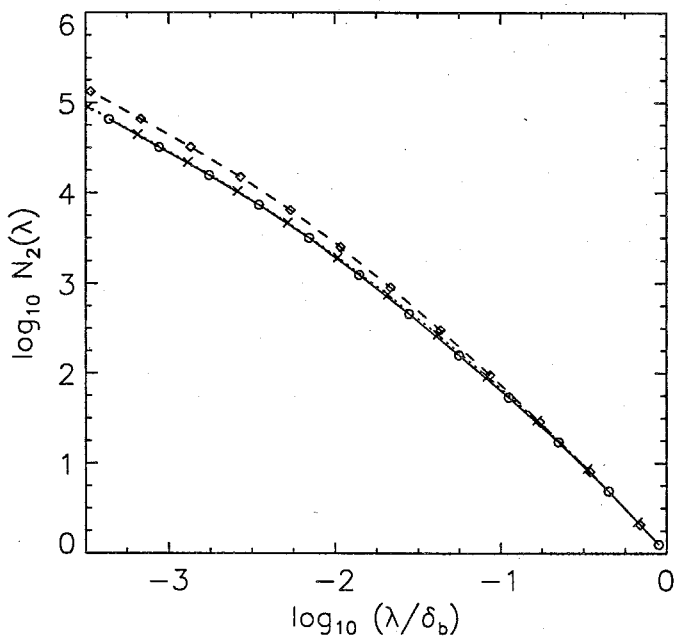

FIG. 3.15 Coverage, $N_2(\lambda)$, of isoscalar surfaces at $Re \simeq 9.0 \times 10^3$. $c = c_1$: dotted line, crosses; $c = c_2$: dashed line, diamonds; $c = c_3$: solid line, circles. Recall that $\delta_b = \delta_b(c; Re)$.

Figure 3.15 shows the ensemble-averaged, two-dimensional coverage count, $N_2(\lambda)$, of the level sets, for $Re \simeq 9.0 \times 10^3$. These are plotted for the three thresholds, c_1, c_2, and c_3, with lines of increasing solidity denoting increasing scalar threshold. The points are joined by straight-line segments and represent the coverage counts computed at the indicated λ-scales of the (binary) subpartitions of the bounding-box, in each case. Six images were ensemble averaged to estimate this statistic, permitting error bars (standard deviation of the mean count) to be estimated. They were smaller than the size of the symbols employed in the plot of Fig. 3.15. The coverage counts for the intermediate threshold, $c = c_2$, are seen to be larger than for $c = c_1$, or $c = c_3$, in accord with the scalar pdf behavior at this Reynolds number.

The coverage dimension, $D_2(\lambda)$, computed as a direct, second-order, (centered) finite difference of the $N_2(\lambda)$ data in Fig. 3.15, is shown in Fig. 3.16. The threshold dependence of the coverage dimension also reflects the scalar pdf behavior at this Reynolds number with $D_2(\lambda)$ largest, over most of the scale range, at the interme-

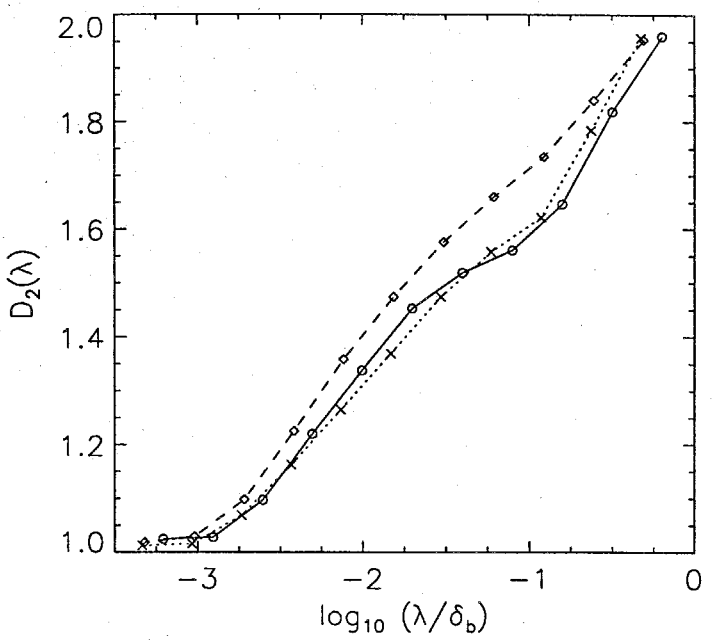

FIG. 3.16 Coverage dimension, $D_2(\lambda)$, of isoscalar surfaces at $Re \simeq 9.0 \times 10^3$ (*cf.* Fig. 3.15). Line/symbol legend as in Fig. 3.15.

diate threshold, c_2. It is seen that the dimension is a function of scale, increasing monotonically and continuously with scale, from near unity, at the smallest scales, to 2, at the largest scales, *i.e.*,

$$\frac{\mathrm{d}D_2(\lambda)}{\mathrm{d}\lambda} > 0 \ , \quad \text{with,} \quad 1 < D_2(\lambda) < 2 \ . \tag{3.3}$$

The bounds are the topological dimension, $d_t = 1$, and the embedding dimension, $d = 2$, as expected for a nondecreasing coverage dimension with scale (recall Eqs. 2.8 and 2.10, and related discussion).

Figure 3.17 shows the Re-dependence of the coverage dimension, derived from the coverage data for the c_2 level sets. These data are in substantial agreement with the Miller & Dimotakis (1991a) 1-D temporal on-axis (Fig. 3.5) and off-axis (Fig. 3.6) coverage data as well as with their 1-D spatial (Fig. 3.8) data. In particular, the 2-D spatial data do not support the proposal of constant-D fractal scaling. They also indicate that the coverage dimension decreases, in the range of moderate-to-large scales, as Re increases, as also indicated by the Miller & Dimotakis (1991a) coverage-dimension data (reproduced in Fig. 3.5, above). This is interesting in that it suggests that the complexity of the level sets, as measured here by $D_2(\lambda)$, *decreases* (*cf.* Figs. 2.1a and 2.1b) with increasing Reynolds number at intermediate scales.

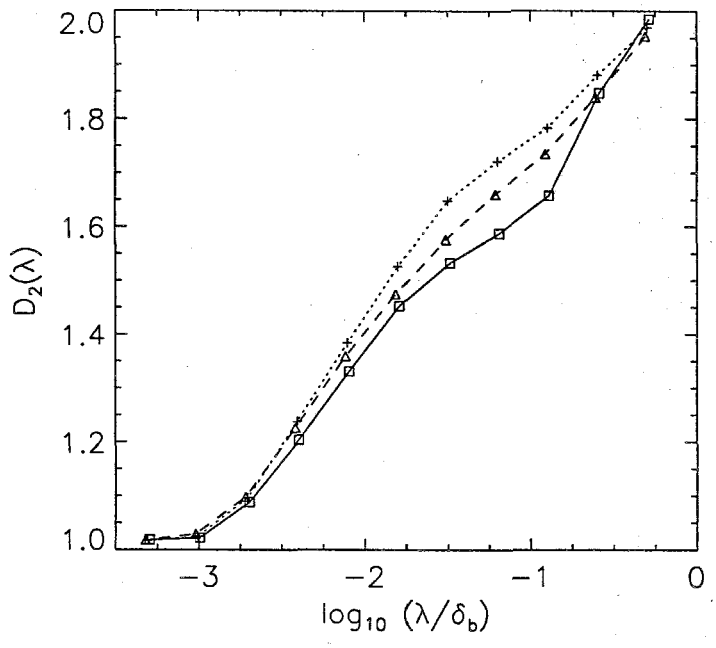

FIG. 3.17 Reynolds-number dependence of coverage dimension, $D_2(\lambda)$, at the intermediate scalar threshold, c_2. $Re \simeq 4.5 \times 10^3$: dotted line, crosses; $Re \simeq 9.0 \times 10^3$: dashed line, triangles; $Re \simeq 18 \times 10^3$: solid line, squares.

While the quantitative results depend on scalar threshold, the qualitative behavior is relatively insensitive to this choice. As noted above (Sec. 2.1), it has been argued (Sreenivasan 1991) that constant-D scaling should be applicable to jet-fluid isoscalars in the outer regions of the turbulent jet. Such scalar level sets correspond to lower thresholds (*e.g.*, $c = c_1$) one of which is depicted in Fig. 3.18. A compilation of the coverage dimension for the (outer) c_1 level sets, is plotted in Fig. 3.19. No constant-D scaling range is indicated by the data for these outer contours either. Notably, the dependence of $D_2(\lambda; c = c_1)$ on Reynolds number is relatively weak and does not reflect the jump in behavior seen in the scalar pdf, for example, between the lower and higher Reynolds numbers; coverage statistics capture different measures than scalar pdf's, for example.

It is interesting to study the Reynolds-number dependence of the (normalized) isoscalar coverage length, *i.e.*,

$$\frac{L(\lambda)}{\delta_b} \equiv \frac{\lambda}{\delta_b} N_2(\lambda) \ . \tag{3.4}$$

This notion is derived from the posthumous publication of Richardson's (1961) proposal, that provides a measure of the length of coastlines (recall Figs. 2.2 and 2.3 and related discussion) and brought to general attention by Mandelbrot (1967,

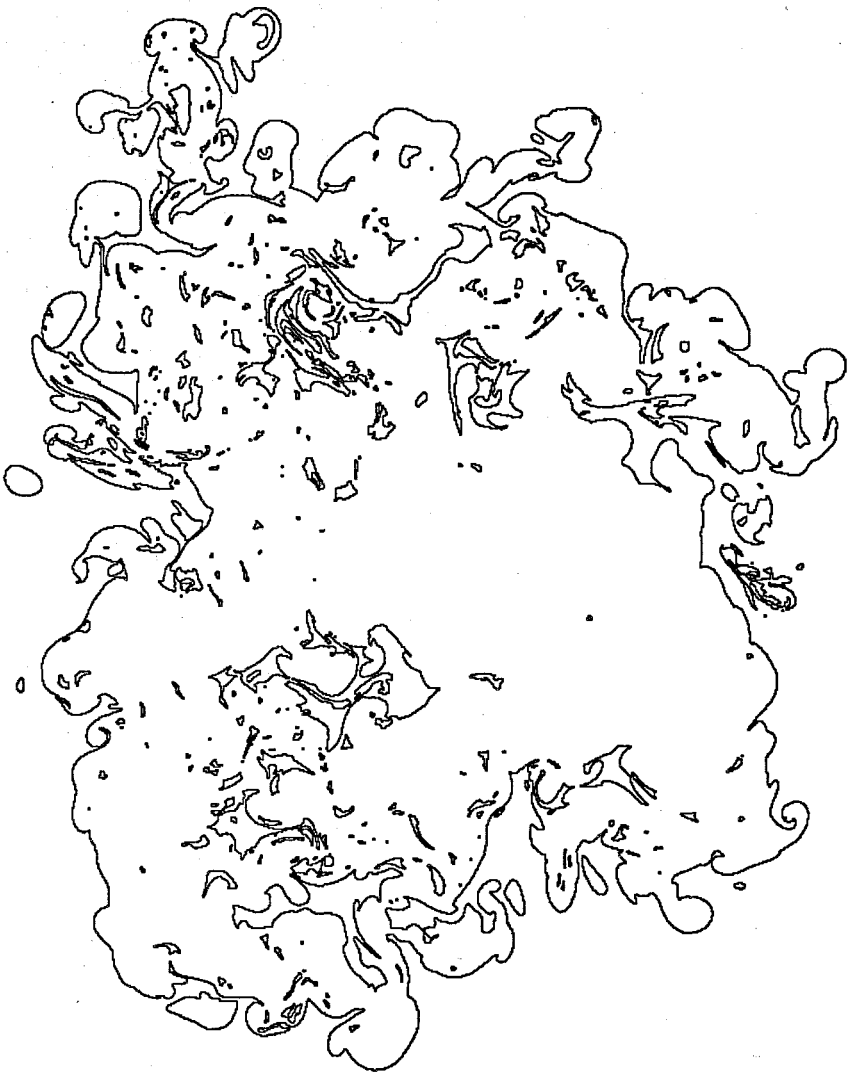

FIG. 3.18 Level set for $c = c_1$, derived from $Re = 9.0 \times 10^3$ image data.

1977). In Richardson's analysis, the count $N_2(\lambda)$ was estimated by the number, $N(\lambda)$, of λ-steps in the "stretched-string" algorithm (recall Eqs. 2.1 and 2.5 and related discussion). In the case of the turbulent-jet level-set contours, it was derived from the coverage counts depicted in Fig. 3.15, as was also done in the Feder (1988) analysis of the Norwegian fjords (Fig. 2.3). The results for the c_2 level sets are

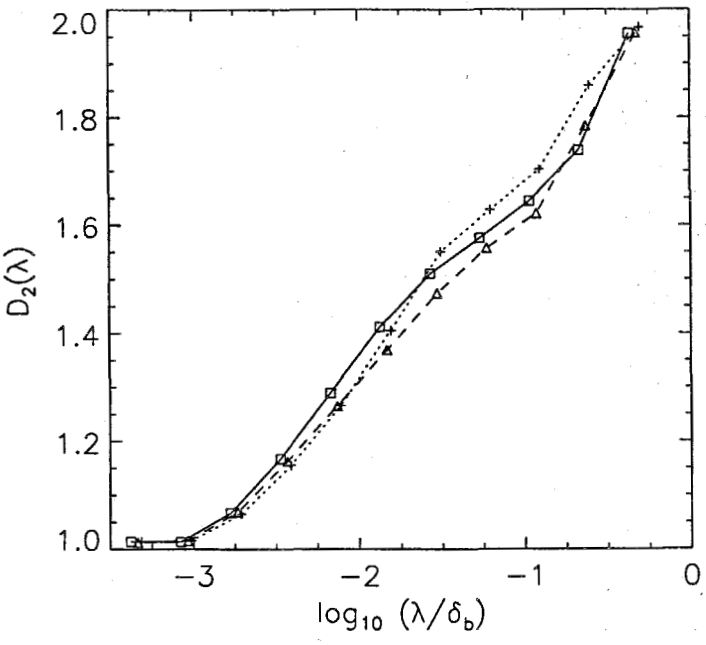

FIG. 3.19 Reynolds-number dependence of coverage dimension, $D_2(\lambda)$, at the lower threshold, c_1 (outer contours). Legend as in Fig. 3.17.

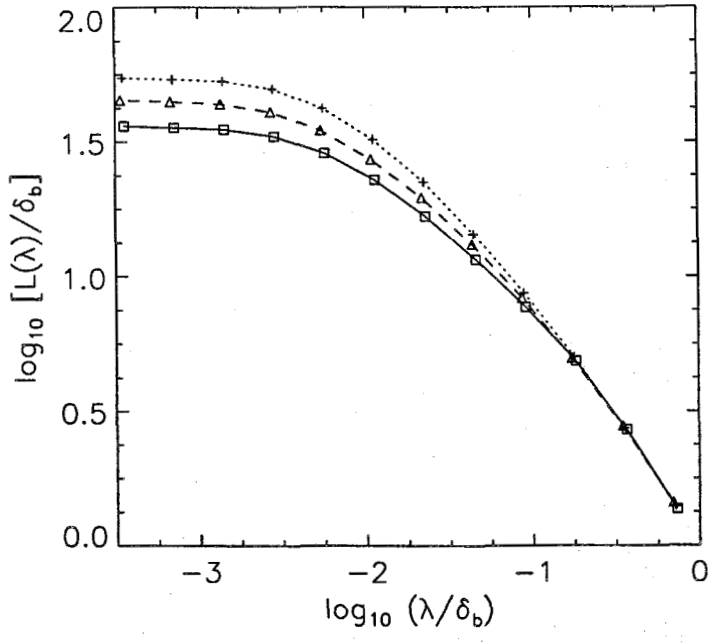

FIG. 3.20 Normalized coverage length, $L(\lambda)/\delta_b = \lambda N_2(\lambda)/\delta_b$, derived from coverage data used to compute the Re-dependent $D_2(\lambda)$, at c_2 (*cf.* Fig. 3.17).

depicted in Fig. 3.20. Note that the limit,

$$f_2(\lambda \to 0) \;=\; \varsigma_2 \;=\; \frac{L(\lambda \to 0)}{\delta_b^2} \;, \tag{3.5}$$

represents the (coverage) arc-length per unit area within the bounding box. At this intermediate threshold, the coverage-length data indicate a *decreasing* level-set length-to-area ratio, with increasing Reynolds number. This is an important result and also seen in the $D_2(\lambda)$ behavior. It can be attributed to increased *mixing* (and homogenization) of the scalar field, relative to *stirring*, for this turbulent-jet flow, with increasing Reynolds number. This is also apparent in the streamwise slices of the scalar-field depicted in Figs. 1.3a,b and is in accord with previous, high-resolution point measurements, on the jet axis, that indicate a decrease in scalar fluctuations (increased mixing) with increasing Reynolds number (Miller & Dimotakis 1991b, Fig. 4). We'll discuss other manifestations of this behavior below. The small-scale limit of the coverage length, as normalized by the perimeter of the bounding box, yields $L(\lambda \to 0)/(4\delta_b) \approx 11$. In other words, the turbulent convection-diffusion process generates scalar level sets approximately an order of magnitude longer (by this measure) than the bounding-box perimeter.

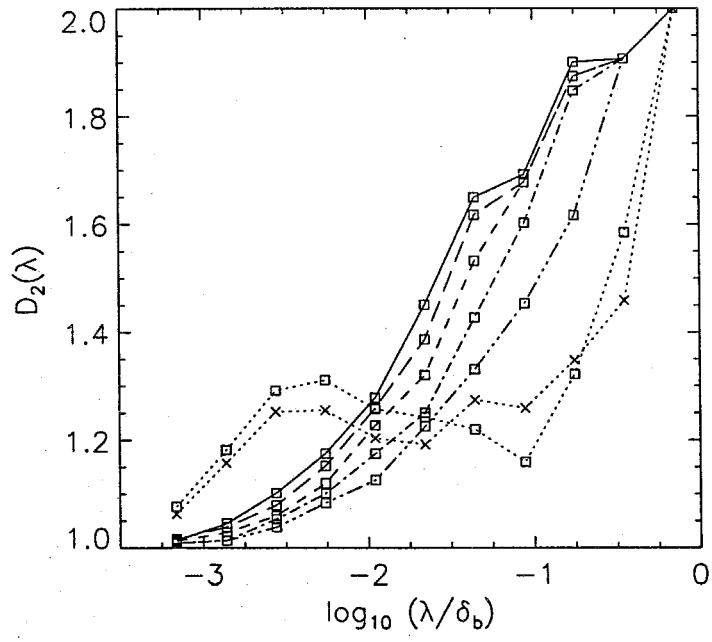

FIG. 3.21 $D_2(\lambda)$, computed for level sets at low thresholds. $c/c_{\rm ref} = c_1/c_{\rm ref} = 0.6$ (solid line), 0.5 (long-dash line), 0.4 (short-dash line), 0.3 (dot-dash line), 0.2 (triple-dot-dash line), 0.1 (dotted line, squares), and 0.104 (dotted line, crosses).

The effects of noise on the two-dimensional level set coverage statistics were also investigated (Catrakis 1996, Appendix B). In particular, it was found that for threshold levels substantially lower than c_1 (*cf.* Fig. 3.12), the level sets extended progressively beyond the main body of the mixed fluid, *i.e.*, in regions of low (local) signal-to-noise ratio. The c_1-level set for a $Re = 9.0\times10^3$ run is depicted in Fig. 3.18, for reference (substantially free of noise).

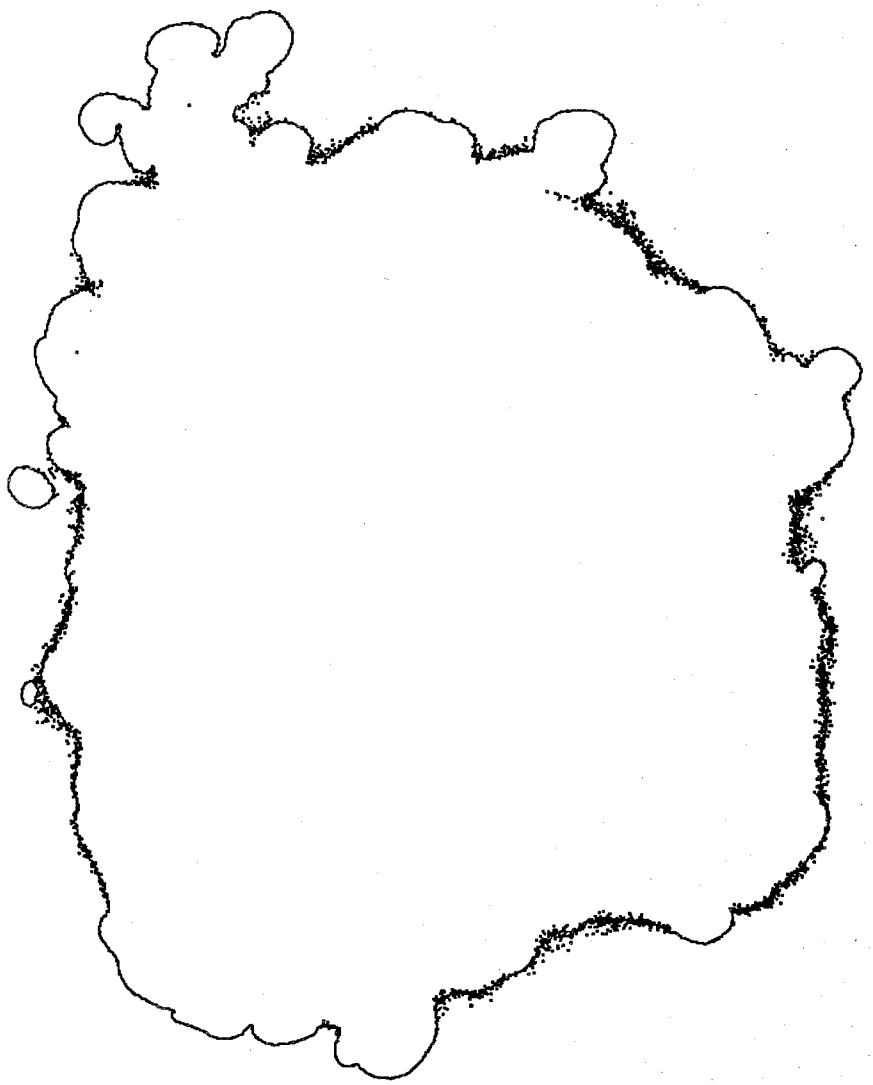

FIG. 3.22 Level set for $c = 0.104\,c_{\rm ref} \approx c_1/6$, yielding near-constant-D behavior (due to noise). Isoscalar derived from same image data used in Fig. 3.18.

A progression of level sets, for very low threshold values, $c \leq c_1$ (*cf.* Fig. 3.12), was processed to extract the corresponding coverage dimension, $D_2(\lambda; c)$. This is

depicted in Fig. 3.21. As can be seen, as the threshold is lowered below c_1, $D_2(\lambda; c)$ evolves, passing through a near-constant coverage-dimension regime, which was encountered at $c/c_{\text{ref}} = 0.104 \approx c_1/6$. The effective coverage dimension, at this threshold, can be seen to be very nearly constant, with $D_2 \approx 1.25 \pm 0.05$, in a scale range, $-2.5 \lesssim \log_{10}(\lambda/\delta_b) \lesssim -1.0$.

Considering the interest in constant-D fractal scaling, it is illustrative to examine the level set that begets this result. It is reproduced in Fig. 3.22. As can be seen, the level set of the measured image field, at this very low threshold, in addition to the evident imprint of the low-level isoscalar contour, has a significant contribution stemming from the noise "dust" in the image. As was noted by Miller & Dimotakis (1991a), level sets derived from low signal-to-noise data can be dominated by the characteristics of noise and yield coverage behavior more reflective of it, rather than the geometry of the (scalar) field under investigation.

4. Consequences of scale-dependent geometry

The preceding overview of the experimental results on level-set behavior in turbulent jets, as well as those stemming from reports in both fluid-mechanics and other contexts (Secs. 2.1 and 2.2) necessitate a generalization of the framework of coverage dimensions that allows scale-dependent level-set behavior. This is a natural extension of the constant-D framework that is dictated by phenomena whose dynamics are not scale invariant. In general, scale-dependent objects may be regarded as possessing a higher level of complexity than constant-D sets. The notion was addressed by Mikhailov & Loskutov (1991), for example, who discussed a three-level hierarchy of complexity, in which Level 1 can be assigned to Euclidean objects (circles, squares), Level 2 objects are (constant-D) fractals, with Level 3 reserved for more complex objects yet, with a scale-dependent structural complexity.

Revisiting the Koch island archipelago (Fig. 2.7) illustrates the point. At larger scales, the coverage statistics would be dominated by the Poisson-distributed statistics of positions of the Koch islands. On the other hand, in the limit of scales smaller than the Koch island extent, the fractal character of the individual islands will prevail. Coverage statistics that span the two scaling regimes will yield a coverage dimension, $D(\lambda)$, that reflects the two-scale character of this set, transitioning from the constant (triadic) Koch-island coverage dimension, at small scales, to a variable-D scale regime, at larger scales, reflecting the Poisson-distributed positions, as we'll discuss below.

For both turbulent-flow level sets, as well as other geometrical structures, such as the Koch island archipelago, the level-set geometry statistics can be captured, in a uniform manner, by the proposed scale-dependent-fractal (SDF) framework. This was presented by Catrakis & Dimotakis (1996a, Sec. 5) and is described below.

4.1 SDF framework

Scale-dependent-fractal (SDF) objects exhibit a variable coverage dimension (Eq. 2.14),

$$D_d(\lambda) \;=\; -\,\frac{\mathrm{d}\log N_d(\lambda)}{\mathrm{d}\log\lambda}\;. \tag{4.1}$$

Objects exhibiting scale-invariant (Eq. 2.2), constant-D, or power-law-fractal (PLF) behavior, over some range of scales, can then be regarded as a special case. The geometry of an object will be considered as SDF if,

$$\frac{\mathrm{d}D_d(\lambda)}{\mathrm{d}\lambda} \;\neq\; 0\;, \tag{4.2}$$

while it will be PLF (constant-D), in a range of scales, if,

$$\frac{\mathrm{d}D_d(\lambda)}{\mathrm{d}\lambda} \;=\; 0\;, \tag{4.3}$$

in that scale range.

The SDF dimension, $D_d(\lambda)$, can be expected to tend to the topological dimension, d_t, at the smallest scales, and to the embedding dimension, d, at the largest scales, *i.e.*,

$$D_d(\lambda) \;\longrightarrow\; \begin{cases} d_t, & \text{as } \lambda \to 0\,; \\ d, & \text{as } \lambda \to \delta\,, \end{cases} \tag{4.4}$$

where δ is the largest characteristic scale of the set (*cf.* Dimotakis 1991 and discussion in Sec. 2, above). For data confined in a bounding box, the SDF dimension will approach the embedding dimension at the scale $\delta = \delta_b$ (the bounding-box size).†

The SDF geometric-coverage law that follows from Eq. 4.1 is given, in differential form, by

$$\frac{\mathrm{d}N_d(\lambda)}{N_d(\lambda)} \;=\; -\,D_d(\lambda)\,\frac{\mathrm{d}\lambda}{\lambda}\;. \tag{4.5}$$

† If $D_d(\lambda)$ is monotonic with scale, the limiting values in equation (4.4) will also be the bounding values. As noted above, non-monotonicity of the SDF dimension is possible, however, for cluster-like structures, for example. Scale-local clustering may lead to SDF dimension values that are below the topological dimension, in a range of scales.

Notably (*cf.* Eq. 2.3),

$$\text{if} \quad D_d(\lambda) \neq \text{const.} , \qquad \text{then} \quad N_d(\lambda) \not\propto \lambda^{-D_d(\lambda)} . \tag{4.6}$$

Integrating the differential coverage relation (Eq. 4.5) from some reference scale, λ_1, we obtain (*cf.* Takayasu 1982, 1992)

$$\frac{N_d(\lambda)}{N_d(\lambda_1)} = \exp\left\{ -\int_{\lambda_1}^{\lambda} D_d(\lambda') \frac{\mathrm{d}\lambda'}{\lambda'} \right\} \tag{4.7}$$

and, if the set possesses a bounding scale, δ_b, we also have, since $N_d(\delta_\mathrm{b}) = 1$,

$$N_d(\lambda) = \exp\left\{ \int_{\lambda}^{\delta_\mathrm{b}} D_d(\lambda') \frac{\mathrm{d}\lambda'}{\lambda'} \right\} . \tag{4.8}$$

In contrast to PLFs, SDF coverage is, in general, a nonlocal function of scale, with geometric structure across the whole range of scales potentially contributing to the coverage at any one scale.

A useful coverage measure is the coverage fraction, $F_d(\lambda)$, or (embedding space) volume-fill fraction, of the set at a scale λ, defined as (*cf.* Dimotakis 1991),

$$F_d(\lambda) \equiv \frac{N_d(\lambda)}{N_{d,\mathrm{tot}}(\lambda)} = \left(\frac{\lambda}{\delta_\mathrm{b}}\right)^d N_d(\lambda) , \tag{4.9}$$

where, for a finite domain, $N_{d,\mathrm{tot}}(\lambda)$ is the total number of d-dimensional partitioning boxes of the δ_b-bounding box.‡ The coverage fraction can be identified as the geometric probability that a randomly placed λ-box, interior to the bounding δ_b-box, contains part of the set. The coverage fraction, as opposed to the SDF dimension, must be a nondecreasing function of scale (*cf.* Eq. 4.2), *i.e.*,

$$\frac{\mathrm{d}F_d(\lambda)}{\mathrm{d}\lambda} \geq 0 , \tag{4.10}$$

at all scales. The logarithmic derivative of $F_d(\lambda)$ follows from Eqs. 4.1 and 4.9,

$$\frac{\mathrm{d}\log F_d(\lambda)}{\mathrm{d}\log\lambda} = d - D_d(\lambda) , \tag{4.11}$$

---

‡ These relations can be extended to spatially-unbounded sets, in which case the δ_b-bounding box size is selected to exceed the scale sizes of interest and $N_{d,\mathrm{tot}}(\lambda) = (\delta_\mathrm{b}/\lambda)^d$.

which is the SDF codimension. The limiting behavior of the coverage fraction is (*cf.* Eq. 4.4),

$$F_d(\lambda) \begin{cases} \sim \lambda^{d-d_t} , & \text{as } \lambda \to 0 ; \\ \to 1 , & \text{as } \lambda \to \delta_b . \end{cases} \tag{4.12}$$

Integrating Eq. 4.11 from a coverage scale, λ, to the largest scale, δ_b, the SDF relation for the coverage fraction becomes (*cf.* Eq. 4.7),

$$F_d(\lambda) = \exp\left\{ -\int_{\lambda}^{\delta_b} \left[d - D_d(\lambda') \right] \frac{d\lambda'}{\lambda'} \right\} , \tag{4.13}$$

since $F_d(\delta_b) = 1$ (*cf.* Eq. 4.12). The extent to which a SDF set fills space, therefore, varies with scale and, potentially, depends on the geometric behavior at all scales.[♯]

The above SDF statistics can be connected to the distribution of (various measures of) scales of the set $\mathcal{S}$. The coverage fraction, $F_d(\lambda)$, can be identified as the geometric probability that a (randomly-placed) λ-box covers part of $\mathcal{S}$, as noted above (Eq. 4.9). It can also be interpreted as a cumulative distribution function of a measure of spatial scales, in the following sense. For a scale increment, $\Delta\lambda$, the coverage fraction can be written as,

$$F_d(\lambda + \Delta\lambda) \equiv F_d(\lambda) + \int_{F_d(\lambda)}^{F_d(\lambda+\Delta\lambda)} dF_d(\lambda') . \tag{4.14}$$

The differential coverage fraction, in this integral, can be associated with a probability density function of a measure of scales, $f_d(\lambda)$, where

$$f_d(\lambda) \equiv \frac{dF_d(\lambda)}{d\lambda} . \tag{4.15}$$

In this expression, $f_d(\lambda)$ is the probability density function of the *largest-empty-box* (LEB) scale, λ, *i.e.*, the size of the largest box that is empty, *i.e.*, covers no part of $\mathcal{S}$, as discussed below.

Consider a λ-box and a $(\Delta\lambda/2)$-wide strip, around the λ-box, as illustrated in Fig. 4.1. The identification of $f_d(\lambda)$, in (4.15), with the largest-empty-box scales can be established by considering the probabilities of the following three events:

$$\begin{aligned} \mathcal{A} &\equiv \{ (\lambda + \Delta\lambda)\text{-box covers part of } \mathcal{S} \} \\ \mathcal{B} &\equiv \{ \lambda\text{-box covers part of } \mathcal{S} \} \\ \mathcal{C} &\equiv \{ (\Delta\lambda/2)\text{-wide strip, around } \lambda\text{-box covers part of } \mathcal{S} \} . \end{aligned}$$

[♯] For PLF sets, for which $d - D_d(\lambda) = d - D_d = \text{const.}$, Eq. 4.13 recovers, $F_d(\lambda) \propto \lambda^{d-D_d}$.

The geometric probabilities of events $\mathcal{A}$, $\mathcal{B}$, and $\mathcal{C}$ are related as follows,

$$\mathcal{P}\{\mathcal{A}\} = \mathcal{P}\{\mathcal{B} \cup \mathcal{C}\} \equiv \mathcal{P}\{\mathcal{B}\} + \mathcal{P}\{\mathcal{C} \cap \overline{\mathcal{B}}\} \ . \tag{4.16}$$

Since,

$$F_d(\lambda + \Delta\lambda) = \mathcal{P}\{\mathcal{A}\} \qquad \text{and} \qquad F_d(\lambda) = \mathcal{P}\{\mathcal{B}\} \ , \tag{4.17}$$

we have (*cf.* Eq. 4.14),

$$\int_{F_d(\lambda)}^{F_d(\lambda+\Delta\lambda)} \mathrm{d}F_d(\lambda') = \mathcal{P}\{\mathcal{C} \cap \overline{\mathcal{B}}\} \ , \tag{4.18}$$

i.e., the probability that the $(\Delta\lambda/2)$-wide strip, around a λ-box, covers part of $\mathcal{S}$ *and* that the λ-box is empty.

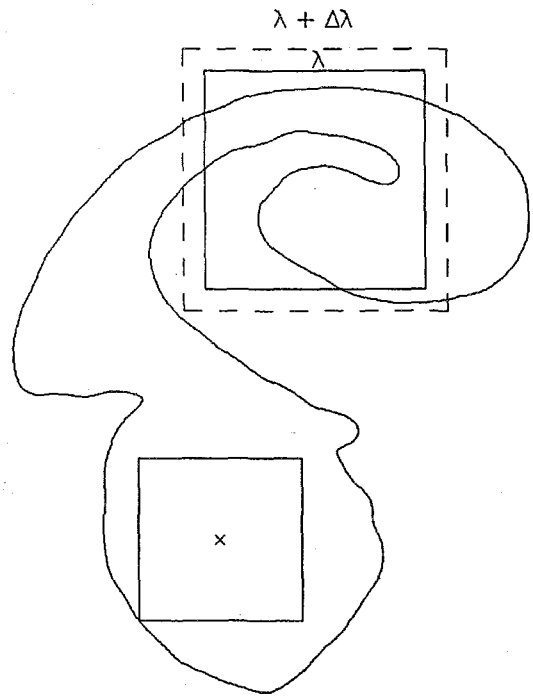

FIG. 4.1 Illustration of a λ-box and a $(\lambda + \Delta\lambda)$-box, for relating geometric probabilities of coverage. An example of a LEB is also depicted.

This relation allows the connection between the coverage statistics and the distribution of this (multidimensional) measure of spatial scales, λ. In this context, this scale is identified as the size of the LEB containing a randomly-located point, P, but no part of $\mathcal{S}$, *i.e.*, is empty. Equivalently, the scale λ is a measure of (twice) the distance from a point P to the nearest element of $\mathcal{S}$.

From Eq. 4.15, we see that $f_d(\lambda)$ satisfies the required normalization condition over the range of spatial scales, *i.e.* (*cf.* Eq. 4.12),

$$\int_0^\infty f_d(\lambda)\,\mathrm{d}\lambda \;=\; F_d(\infty) \;-\; F_d(0) \;=\; 1 \;, \tag{4.19}$$

Integrating Eq. 4.15, we have,

$$F_d(\lambda) \;=\; \int_0^\lambda f_d(\lambda')\,\mathrm{d}\lambda' \;. \tag{4.20}$$

This allows a direct connection between the SDF dimension, $D_d(\lambda)$, and the distribution of LEB scales, $f_d(\lambda)$, *i.e.*,

$$D_d(\lambda) \;=\; d \;-\; \frac{\lambda\, f_d(\lambda)}{\int_0^\lambda f_d(\lambda')\,\mathrm{d}\lambda'} \;. \tag{4.21}$$

This can be inverted to yield the LEB scale pdf from the SDF dimension, *i.e.* (*cf.* Eqs. 4.13 and 4.15),

$$\begin{aligned} f_d(\lambda) \;&=\; \frac{d - D_d(\lambda)}{\lambda}\, F_d(\lambda) \\ &=\; \frac{d - D_d(\lambda)}{\lambda}\, \exp\left\{ -\int_\lambda^\infty [d \;-\; D_d(\lambda')]\, \frac{\mathrm{d}\lambda'}{\lambda'} \right\} \end{aligned} \tag{4.22}$$

Equations 4.21 and 4.22 may be regarded as a SDF transform pair in d-dimensional space.

From these relations, we can derive the small-scale behavior of $f_d(\lambda)$. In particular (*cf.* Eqs. 4.12 and 4.15),

$$f_d(\lambda) \;\sim\; \lambda^{d-d_t-1} \;\rightarrow\; \begin{cases} \varsigma_d\,, & \text{as } \lambda \rightarrow 0\,, \text{ for } d_t = d-1\;; \\ 0\,, & \text{as } \lambda \rightarrow 0\,, \text{ for } d_t < d-1\;, \end{cases} \tag{4.23}$$

In this expression, ς_d is a constant we will discuss below. The case $d_t = d-1$ is an important special case and applies, for example, to isoscalar surfaces, as created and described by the scalar convection-diffusion equation (Eq. 1.16). The case $d_t < d-1$ corresponds to points in 2-D, space-curves in 3-D, *etc.* The large-scale behavior of $f_d(\lambda)$ is given by (*cf.* Eq. 4.12),

$$f_d(\lambda) \;\rightarrow\; 0\,, \text{ as } \lambda \;\rightarrow\; \infty\;, \tag{4.24}$$

unconditionally.

4.2 One-dimensional scale distribution

Exploratory investigations of the mean spacing, l_m, of zero-crossings of 1-D velocity signals in turbulence were reported and discussed by Liepmann (1949). Measurements of the corresponding spacing pdf have been approximated by Poisson statistics in turbulent boundary layers by Sreenivasan *et al.* (1983), and Kailasnath & Sreenivasan (1993).

Lognormal spacings were also reported by Sreenivasan *et al.* (1983), for some of their data, for level crossings in 1-D in various turbulent flows, including level-crossings of 1-D velocity measurements in turbulent boundary layers. One-dimensional records of the streamwise velocity in turbulent boundary layers were found by Sreenivasan & Meneveau (1986) to have level sets qualitatively resembling Poisson spacings and exhibited a (nonconstant-D) coverage behavior that the authors attributed to the random point spacings they found were described by (near-) Poisson statistics. In a subsequent discussion, however, Sreenivasan (1991) reported constant fractal dimensions from such signals. In what follows, we will discuss the relation between level-set spacings and coverage statistics.

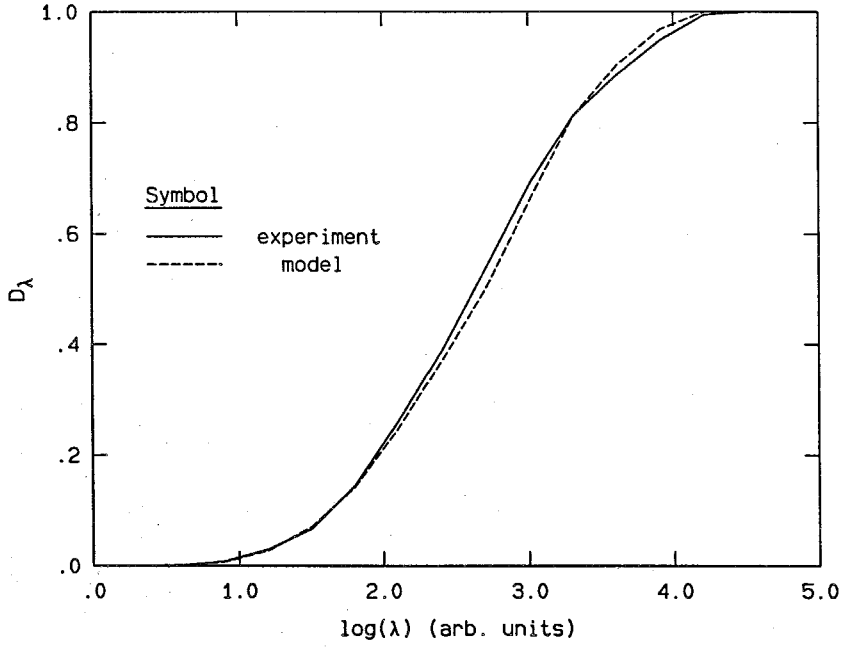

FIG. 4.2 Comparison of $D_1(\lambda)$, derived from 1-D scalar measurements in turbulent jets ($Re = 5800$), with a model based on a lognormal pdf of spacing scales (Miller & Dimotakis 1991a, Fig. 9).

In an effort to model the coverage behavior of level sets of their 1-D measurements of concentration in turbulent jets, Miller & Dimotakis (1991a) noted that random, lognormally-spaced points are characterized with a SDF dimension that can provide a good (two-parameter) fit to $D_1(\lambda)$, as experimentally determined from their turbulent-jet data. Pdf's of the measured crossing spacings independently showed that the lognormal distribution is a good approximation. Figure 4.2, from their paper, includes the result for a Reynolds number of 5800. Level sets of 1-D scalar signals derived from plumes dispersing in the atmospheric surface layer (Yee *et al.* 1995) were also found to be described by lognormal statistics.

The preceding discussion suggests that there may exist a relation between the spacing statistics of 1-D signals and the associated coverage dimension. It also points to an apparent contradiction stemming from reports of constant fractal dimensions derived from the analysis of data reported to be well-described by Poisson, or lognormal, statistics.

The connection between the spacing statistics in 1-D level sets and the coverage dimension can be established (Catrakis & Dimotakis 1996b). Based on the relation of $F_1(\lambda)$ and the probability, $p_{1,e}(l)$, of an empty l-interval on the 1-D level-set record, the general result,

$$D_1(\lambda) \;=\; 1 \;-\; \frac{\lambda \displaystyle\int_\lambda^\infty p_1(l)\,\mathrm{d}l}{\displaystyle\int_0^\lambda \int_{\lambda'}^\infty p_1(l)\,\mathrm{d}l\,\mathrm{d}\lambda'}\;, \tag{4.25}$$

follows. This can be inverted (analytically) to obtain $p_1(l)$, given $D_1(\lambda)$. By way of example, for a Poisson distribution,

$$p_1(l) \;=\; \frac{e^{-l/l_\mathrm{m}}}{l_\mathrm{m}}\;, \qquad \text{and} \qquad D_1(\lambda) \;=\; 1 \;-\; \frac{\lambda/l_\mathrm{m}}{e^{\lambda/l_\mathrm{m}}-1}\;. \tag{4.26}$$

Expressions for lognormal and (truncated) power-law spacings pdf's were also derived. Significantly, while constant-D fractal scaling generally implies power-law spacing statistics, the converse is not true. The nonlocal relation (Eq. 4.25) between $D_1(\lambda)$ and $p_1(\lambda)$ may result in a scale-dependent $D_1(\lambda)$, even if $p_1(\lambda)$ is power-law for a substantial range of scales.

The spacing pdf, $p_1(l)$, can also be connected to the one-dimensional largest-empty-box (LEB) size pdf, $f_1(\lambda)$, and is given by (*cf.* Eq. 4.15),

$$f_1(\lambda) \;=\; \frac{1}{l_\mathrm{m}} \int_\lambda^\infty p_1(l)\,\mathrm{d}l \;=\; \frac{\mathrm{d}F_1(\lambda)}{\mathrm{d}\lambda}\;.$$

The generalization to two (and higher) dimensions can be made in terms of the LEB size pdf, $f_d(\lambda)$, as was discussed in the previous section. The notion of "spacings", as used here, is restricted to one-dimensional data.

An account of this analysis was reported by Catrakis & Dimotakis (1996b) and is also discussed elsewhere in this NATO/ASI series (Catrakis & Dimotakis 1996c).

4.3 Two-dimensional scale distribution

Using the analytical results discussed in Sec. 4.1, the pdf of the LEB scale distribution, $f_2(\lambda)$, was computed from the two-dimensional scalar data, discussed in Sec. 3.2, at $Re \simeq 9.0 \times 10^3$, for the same three scalar thresholds: c_1, c_2, and c_3. This is depicted in Fig. 4.3, with lines of increasing solidity denoting increasing threshold, as before (recall that the intermediate threshold, c_2, corresponds to the peak of the scalar pdf). This is a normalized pdf over the range of scales. For a given threshold, $f_2(\lambda)$ is seen to be larger at smaller scales, approaching a constant value at the smallest scales,

$$\lim_{\lambda \to 0} \{f_d(\lambda)\} \;=\; \varsigma_d(c; Re) \;, \tag{4.27}$$

as expected for level sets consisting of lines (curves) in a plane, *i.e.*, for geometric sets with $d_t = d - 1$ (recall Eq. 4.23 and related discussion).

The data indicate a higher probability density of LEB scales, at small scales, for the c_2 threshold corresponding to the neighborhood of the peak of the scalar pdf. The small-scale limit, $f_2(\lambda \to 0) = \varsigma_2(c; Re)$, is a measure of the surface-to-volume ratio (perimeter-to-area ratio in 2-D) of the isosurface. The highest surface-to-volume ratio is observed at the c_2 threshold.

The Re dependence of the LEB scale pdf, $f_2(\lambda)$, is shown in Fig. 4.4. A systematic trend with increasing Re is evident. Specifically, the small-scale limit of the LEB scale pdf *decreases* with increasing Re, *i.e.*, the surface-to-volume (perimeter-to-area) ratio is decreasing with increasing Re. This, perhaps, surprising result can be seen in the SDF dimension behavior (*cf.* Fig. 3.17) — from which it is derived (Eq. 4.22) — with $D_2(\lambda)$ decreasing with increasing Re. It is also in accord with the conspicuous Re-dependence of the coverage length, $L(\lambda)$ (*cf.* Fig. 3.20 and related discussion), which is derived directly from the coverage counts (Eq. 3.4).

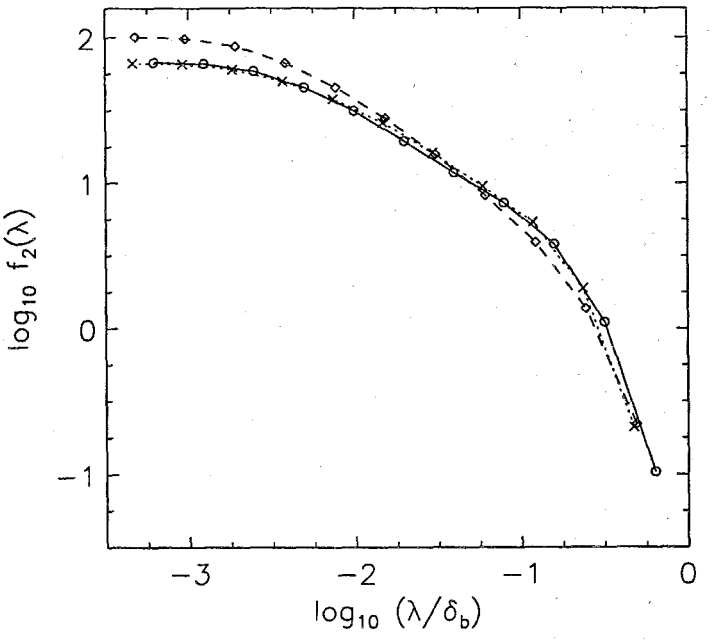

FIG. 4.3 Pdf of LEB scales, $f_2(\lambda)$, for isoscalar surfaces at $Re \simeq 9.0 \times 10^3$. $c = c_1$: dotted line, crosses; $c = c_2$: dashed line, diamonds; $c = c_3$: solid line, circles. Recall (Fig. 3.14) that $\delta_b = \delta_b(c; Re)$.

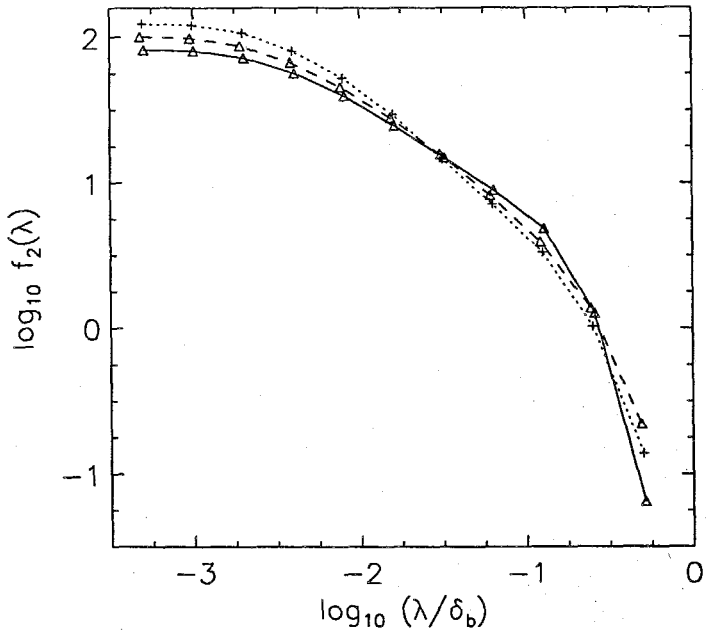

FIG. 4.4 Re dependence of LEB scale pdf, $f_2(\lambda)$, at the intermediate threshold, c_2. Lines of increasing solidity denote increasing Re.

The scale dependence on Reynolds number is better illustrated in terms of the pdf, $\tilde{f}_2(\log\lambda)$, of $\log\lambda$. This is depicted in Fig. 4.5. These data indicate that

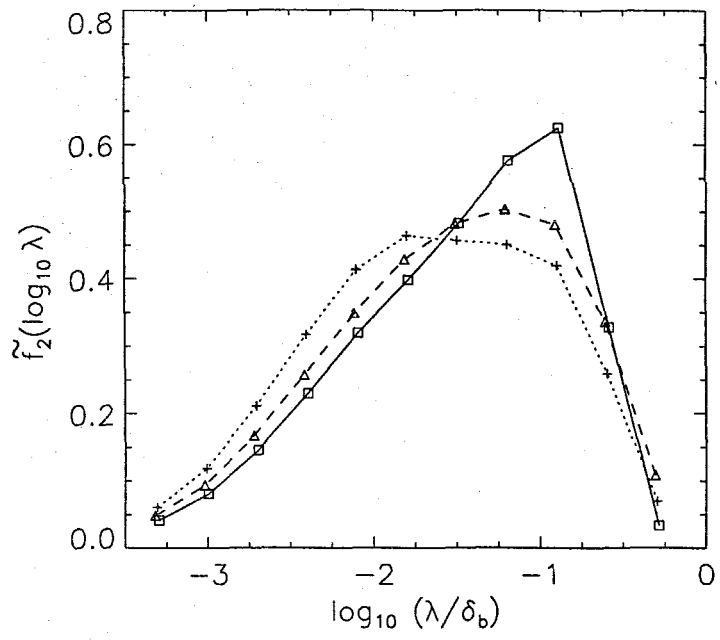

FIG. 4.5 Re dependence of pdf of the logarithm of LEB scales, $\tilde{f}_2(\log\lambda)$, for $c = c_2$. Lines of increasing solidity denote increasing Re.

small-scale regions of the flow are more likely to be visited by the isosurfaces; a lower probability of finding a largest-empty-box region of that size, as the Reynolds number is increased. Additionally, the expectation value of the LEB scale (as well as the most probable) is *increasing* with increasing Reynolds number, *i.e.*, the mean distance from a point in the interior of the bounding box to the c_2 isosurface is *increasing* with increasing Reynolds number.

These observations, taken collectively, indicate enhanced molecular *mixing*, that is responsible for (local) scalar-field homogenization, relative to *stirring* (recall discussion in Sec. 1.2), that is responsible for isoscalar surface-area generation, with increasing Reynolds number. This occurs at thresholds corresponding to isoscalar surfaces (contours) mostly to be found in the intermediate-radius (high-shear) regions of the jet. This can be gleaned directly, in retrospect, from the level-set contours in Figs. 3.13a,b,c. An examination of these three images confirms this (possibly counterintuitive) conclusion, *i.e.*, that the geometric complexity of the c_2 isocontour is decreasing, as the Reynolds number increases.

4.4 Two-dimensional size distribution

Level sets of jet-fluid concentration consist of multiple, disjoint, closed, isoscalar contours of varying size and shape. These isoscalar contours may be viewed as either "islands", or "lakes", depending on whether the neighboring interior isosurfaces are at a higher, or lower, threshold, respectively (Fig. 3.18). The largest island in each image realization may be regarded as the "continent".

The pdf of the island/lake sizes, $p_A(A^{1/2}/\delta_b)$, with size defined as the square-root of the area enclosed by the contour, $A^{1/2}$, is depicted in Fig. 4.6. The lake/island data were compiled from all the 2-D slice data recorded at a Reynolds number of 9.0×10^3 and computed for level-set contours at the intermediate threshold, c_2. See Fig. 3.13b and Catrakis & Dimotakis (1996c, Fig. 5) for examples of individual realizations. Several hundred islands and lakes are found in each such image, with several thousand included in the statistics in Fig. 4.6. A Gaussian fit of the data (in these coordinates) is included in Fig. 4.6. The quality of the fit indicates that a lognormal distribution provides a good description of isoscalar island/lake sizes, at the inner scales (Catrakis & Dimotakis 1996b).

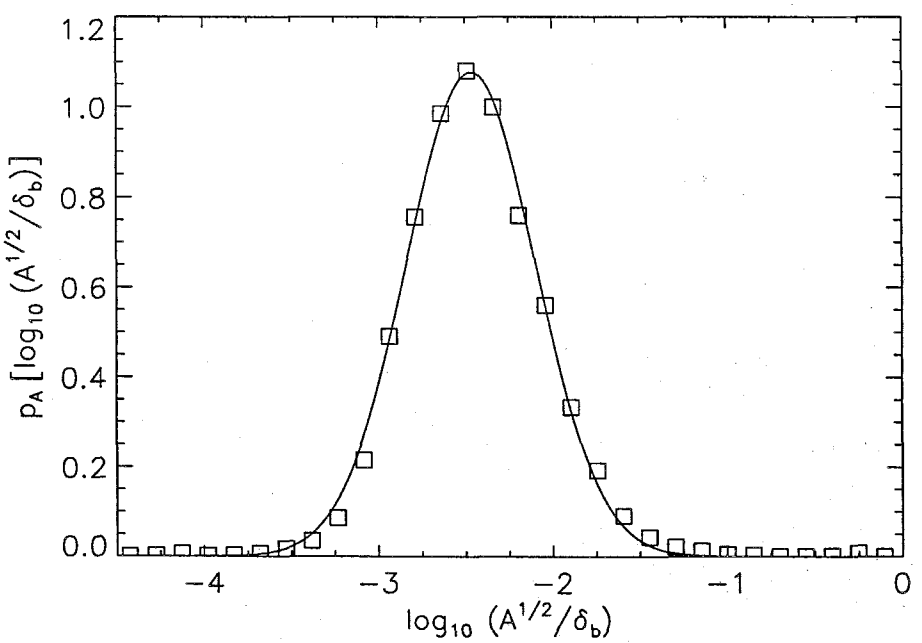

FIG. 4.6 Probability density function of size, $A^{1/2}$, of isoscalar islands/lakes ($Re = 9.0 \times 10^3$). Solid curve: Gaussian fit (in these coordinates).

This result is in accord with measurements of the (horizontal) size of clouds and radar-echo regions, for which a lognormal distribution was found in a variety of atmospheric conditions (Lopez 1977). Also consistent are the previously-cited findings of lognormal distributions of level-crossing (spacing) scales derived from 1-D scalar measurements in liquid-phase turbulent jets (Miller & Dimotakis 1991a) and in plumes in the atmospheric surface layer (Yee *et al.* 1995).

Arguments for lognormal statistics have been put forth by Kolmogorov (1941b, 1962), Oboukhov (1962), Lopez (1977), Bernal (1988), and others, as applicable to stochastic fragmentation (or growth/amalgamation) processes, such as may be expected to occur in turbulence and mixing.

5. Three-dimensional scalar data

Before concluding, we should recall that turbulence — and the fields it generates — lives in three-dimensional space, $\mathbf{x} = (x, y, z)$, and, by being unsteady, generates scalar and other fields that are four dimensional (three space dimensions, plus time), *e.g.*, concentration fields, $c = c(\mathbf{x}, t) = c(x, y, z, t)$. The advent of high framing-rate digital-image techniques, in conjunction with laser-induced fluorescence diagnostics, offer the promise of recording three- and four-dimensional, quantitative information of turbulent flows. Reports to date have documented imaging of small portions of turbulent flows at the inner scales (*e.g.*, Prasad & Sreenivasan 1990b; Dahm *et al.* 1991; Merkel *et al.* 1996), as well as investigations of large-scale structure by whole-field imaging (*e.g.*, Yoda *et al.* 1994).

Preliminary experiments to investigate the geometry of outer scalar isosurfaces from 3-D whole-field measurements are also in progress in our laboratory. This work represents a collaborative effort with J. Janesick, A. Collins, and T. Elliott of JPL; and D. Lang and D. Laidlaw of Caltech. In these experiments, three-dimensional space-time measurements (2-D space, plus time) of the jet-fluid concentration were obtained at the same far-field station ($z/d_j = 275$) of a liquid-phase turbulent jet by imaging the laser-induced fluorescence in the plane perpendicular to the jet axis and recording successive images as a function of time. Figure 5.1 shows a schematic of the flow geometry and associated imaging, as well as of the 3-D (fixed-z) slice space-time data, *i.e.*, $c(x, y, t; z = 275 d_j)$. The jet Reynolds number was $Re \simeq 9.0 \times 10^3$. For the data presented here, the framing rate was, approximately, 1-frame/s, with 1024^2 pixels/frame.

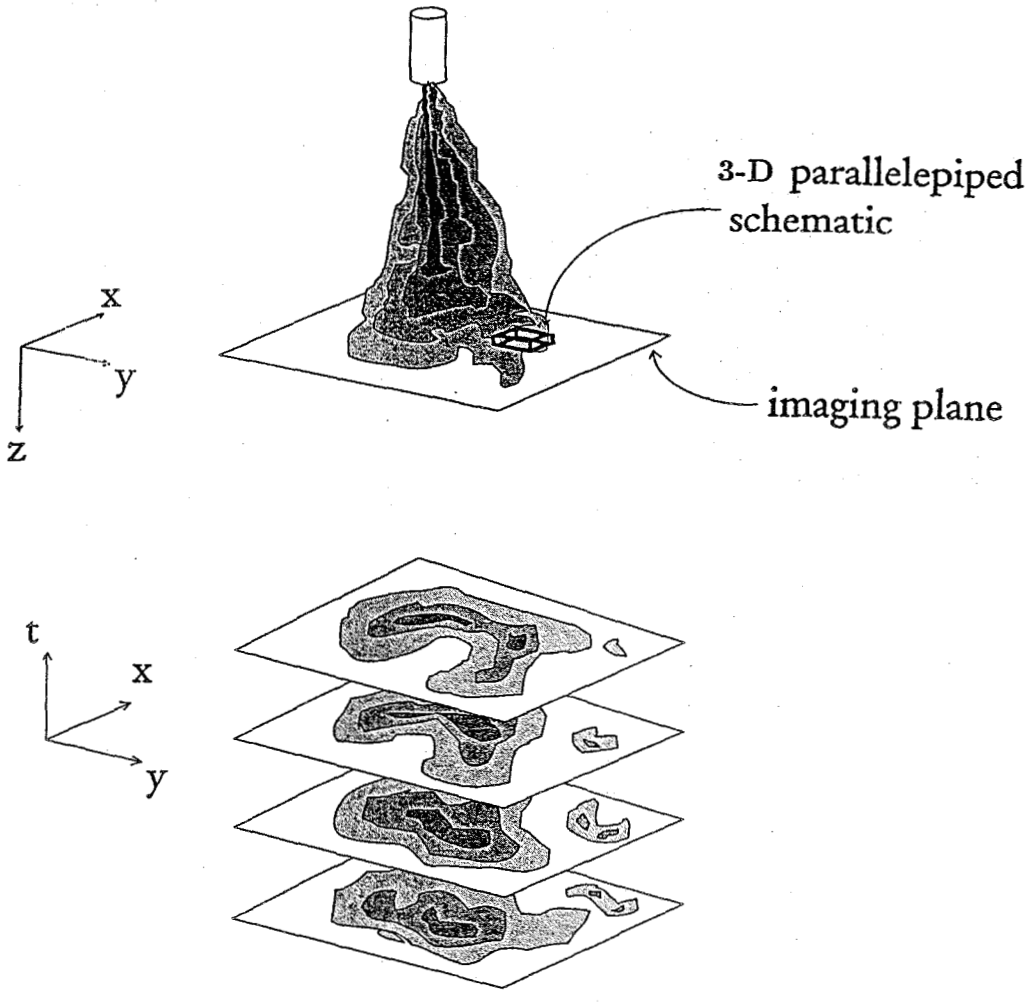

FIG. 5.1 Schematic of flow geometry, associated imaging, and space-time data for 3-D (2-D in space, plus time) scalar-field measurements in a turbulent jet.

The successive-frame image data (30 frames total) were normalized and calibrated, pixel by pixel, using an ensemble-average of 8 background-noise images and 8 uniform-concentration images, using the same procedure as with the data in Figs. 3.10a–c. The signal-to-noise ratio of the data was also approximately 300:1, as estimated from the $\approx 50\,\mathrm{dB}$ amplitude range in the scalar power spectra. The total image-data were then comprised of $1024 \times 1024 \times 30 = 30\,\mathrm{Mpixels}$ of 12-bit data.

A $256 \times 256 \times 25$ portion of the image data was selected, near the outer boundary of the jet, to form the 3-D space-time images. In that region, the fluid velocity can be substantially lower than in the interior. Additionally, the successive, 256×256, subframe regions that were processed were selected as exhibiting a low rate of change from one temporal slice to the next. While, even for that portion, the scalar field

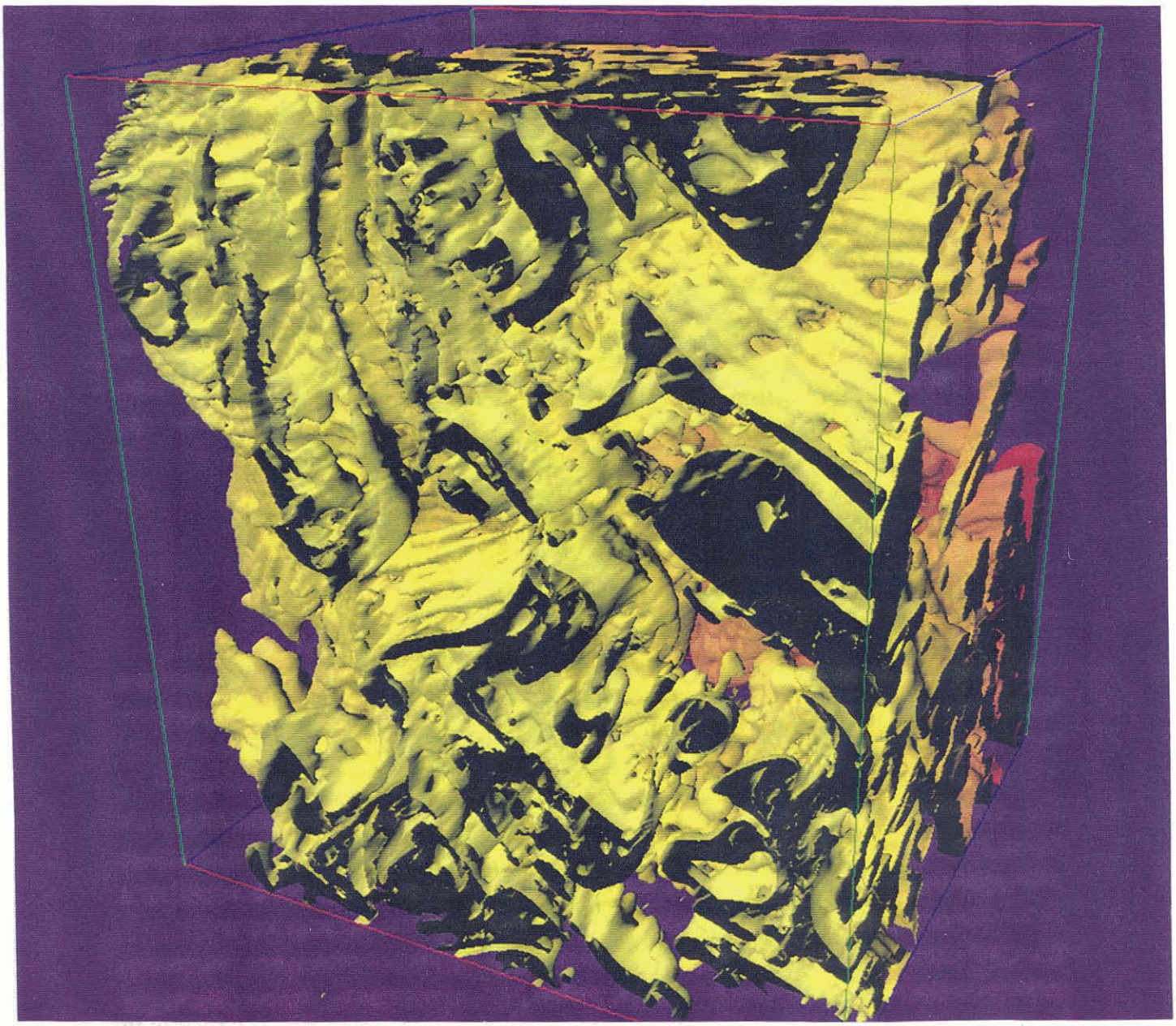

FIG. 5.2 3-D rendering of an outer (low scalar threshold) isosurface portion, derived from (2+1)-D space-time measurements of the jet-fluid concentration in the far field of a turbulent jet.

must be regarded as temporally undersampled, in the strict sense, the resulting space-time image can be used to visualize the structure of the (outer) isosurfaces.

A 3-D rendering of an outer (low scalar threshold) isosurface portion, in this three-dimensional space-time volume, computed by D. Laidlaw of the Caltech Computer Science Department, is depicted in Fig. 5.2. In the computer visualization, a light source was positioned in this space-time volume and illuminated the, approximately, three million polygonal facets that were required to render the isosurface. Color codes time, with red marking early time (rear) and yellow late time (front).

The selected scalar isosurface is seen to have a complex geometry, indicating the existence of both sheet-like ("lasagna") structures, with evidence of developing Kelvin-Helmholz instabilities (top right), isoscalar surfaces wrapped around tube-like ("spaghetti") structures (top left), as well as composite topologies, not readily classifiable, near the bottom. The three-dimensional geometrical structure of such isosurfaces can be analyzed by the natural extensions of the framework that was used for the 1-D and 2-D data discussed above.

6. Summary and conclusions

Proposals and experimental evidence, from both numerical simulations and laboratory experiments, regarding the behavior of level sets in turbulent flows have been discussed. A few important conclusions can be drawn from this overview.

Isoscalar surfaces in turbulent flows, at least in liquid-phase turbulent jets, where sufficient experimental evidence is available, appear to have a geometry that is more complex than (constant-D) fractal. Their description requires an extension of the original, scale-invariant, fractal framework that can be cast in terms of a variable (scale-dependent) coverage dimension, $D_d(\lambda)$. We have accepted the terms, scale-dependent-fractal (SDF) set and scale-dependent-fractal dimension, the latter originally employed by Mark & Aronson (1984), to accommodate the description of sets exhibiting such behavior.

Sets exhibiting constant-D behavior have been termed "power-law-fractal" (PLF) sets and may be regarded as a special case. It is found that while constant-D scaling, generally, implies power-law, point-spacing statistics, in one-dimension, for example, the converse is not true. Power-law spacing statistics, over a significant (but finite) range of scales, may not produce constant-D fractal scaling.

The extended, scale-dependent framework allows level-set coverage statistics to be related to other quantities of interest. In addition to the pdf of point-spacings (in 1-D), it can be related to the scale-dependent surface-to-volume (perimeter-to-area in 2-D) ratio, as well as the distribution of sizes of empty-space regions, *i.e.*, in the case of level sets, the distribution of the length-scale of regions not visited by the isosurface. This latter statistic yields a measure of the distance from a random point in the domain to the set. This framework allows level-set geometry, in general, and scalar mixing, in particular, to be studied in terms of quantitative measures that are useful in many contexts.

The application of this SDF framework to the study of turbulent-jet mixing indicates that the geometric measures of the scalar (jet-fluid concentration) level-set field depend on both scalar threshold and flow Reynolds number. There is every reason to believe that this conclusion may be expected to apply to other turbulent flows as well and that no universal behavior need exist.

As regards mixing, the quantitative isoscalar analysis facilitated by the new tools indicate increased mixing with increasing Reynolds number, in liquid-phase turbulent jets, at least for the range of Reynolds numbers for which reliable data are available. This results in a progressively less-complex level-set geometry, at least in liquid-phase turbulent jets, with increasing Reynolds number. This, perhaps surprising, result is discernible in the scalar and isoscalar image data directly, in retrospect, and can be attributed to the increasingly effective homogenization of the scalar field and the attendant simpler isoscalar geometry with increasing Reynolds number.

By a number of measures, liquid-phase turbulent-jet flows exhibit a mixing transition, at a Reynolds number in the vicinity of 10^4, as has been documented to also occur in many other flows. Turbulent flows at Reynolds numbers below this value should, probably, not be regarded as fully-developed.

In liquid-phase turbulent jets, the spacings in one-dimensional records, as well as the size distribution of individual "islands" and "lakes" in two-dimensional isoscalar slices, where size is defined as the square root of the area of the individual islands and lakes, are found to be well described by lognormal statistics in the small-scale range. The scale-dependent coverage dimension derived from such sets is also in accord with lognormal statistics, in the small-scale range. Such statistics may be expected to apply to other flows, as well.

The technology that has yielded the preliminary three-dimensional data in turbulent flows, by us and others, along with data from the computational world, hold the promise of quantitative analysis of the full dimensionality of turbulence and its dynamics, across the whole range of scales, for the first time. If, as we have argued, a minimum Reynolds number is required for turbulence to attain its fully-developed character, perhaps the laboratory will be able to help us sooner than numerical simulations. Even in the laboratory, however, it is also on the computer we must rely to acquire, store, and analyze the demanding volume and rate of the new multi-dimensional experimental data.

In conclusion, recent data and a new geometric framework have provided additional information and tools that have helped probe the complex geometric signatures of turbulence. While the insight, thus far, derived from the new vantage point has been primarily descriptive, one may hope that it will also add to the experimental and theoretical means by which the dynamics of turbulence can be analyzed. It is too early to say whether these new tools will result in substantive progress in our quest to understand the behavior of turbulence, qualitatively and quantitatively. An important part of the complex natural world we live in, turbulence has intrigued observers from the earliest instances of recorded thought and has, for the most part, defied an adequate description. Perhaps because, as Heracleitos remarked many years ago,

Η φὺσις κρὺπτεσθαι φιλεῖ,

or, "Nature likes to conceal itself," or, to be more precise, "... likes to conceal *herself*." The word *nature* is feminine and there can be no doubt that, in the eyes of the ancient Greeks, nature was a woman.

Acknowledgements

The work on fractals and their relation to mixing, described in this overview, has benefited from research performed at Caltech over the last 15 years, or so. The informal, unpublished, early efforts had contributions by R. Miake-Lye, D. Dowling, and G. Losi. The development of high signal-to-noise, temporal and spatial imaging, data-acquisition technology, on which this work has heavily relied, has had the benefit of many and valuable contributions by D. Lang. This tutorial has benefited from discussions with P. Miller, originally at Caltech and presently at

the Lawrence Livermore National Laboratories, as well as with C. Bond, M. Cross, A. Leonard, D. Meiron, D. Pullin, and P. Saffman, at Caltech, and P. Constantin of the University of Chicago, I. Procaccia of the Weizmann Institute in Israel, and K. Sreenivasan of Yale University.

The preliminary 3-D space-time measurements discussed in Sec. 5 have not been published previously. They were recorded using the "Cassini camera", a digital-imaging system developed by D. Lang, P. Dimotakis, and P. Svitek at Caltech, with assistance and advice by J. Janesick, S. A. Collins, and T. Elliott, of Caltech's Jet Propulsion Laboratory. It is based on a 1024×1024 CCD focal-plane array developed by the above JPL team for the upcoming Cassini space mission. The camera is capable of higher framing rates and is presently being used to acquire additional and better-resolved space-time data. The resulting 3-D visualization image was computed by D. Laidlaw of Caltech.

The work at Caltech described here is part of a larger effort to investigate turbulent mixing and chemical reactions in free-shear flows, initially supported by AFOSR and GRI and, more recently, under AFOSR Grants F49620–92–J–0290 and F49620–94–1–0353. Finally, the authors would like to thank H. Chate, J.-M. Chomaz, E. Villermaux, and the organizers of this NATO/ASI summer school for the invitation, their gracious hospitality, and financial support that made our participation possible.

References

ANDRLE, R. 1996 "Complexity and Scale in Geomorphology: Statistical Self-Similarity vs. Characteristic Scales," *Math. Geol.* **28**(3), 275–293.

AREF, H. 1984 "Stirring by chaotic advection," *J. Fluid Mech.* **143**, 1–21.

BALDYGA, J. & BOURNE, J. R. 1995 "Interpretation of turbulent mixing using fractals and multifractals," *Chem. Eng. Sci.* **50**(3), 381–400.

BATCHELOR, G. K. 1953 *The Theory of Homogeneous Turbulence* (Cambridge U.P., London).

BATCHELOR, G. K. 1959 "Small-scale variation of convected quantities like temperature in turbulent fluid. Part 1. General discussion and the case of small conductivity," *J. Fluid Mech.* **5**, 113–133.

BERNAL, L. P. 1988 "The statistics of the organized vortical structure in turbulent mixing layers," *Phys. Fluids* **31**(9), 2533–2543.

BERNAL, L. P., BREIDENTHAL, R. E., BROWN, G. L., KONRAD, J. H. & ROSHKO, A. 1979 "On the Development of Three-Dimensional Small Scales in Turbulent Mixing Layers," 2^{nd} *Int. Symposium on Turb. Shear Flows* (Springer-Verlag, New York, 1980), 305–313.

BETCHOV, R. & SZEWCZYK, A. 1963 "Stability of a shear layer between parallel streams," *Phys. Fluids* **6**, 1391–96.

BLASIUS, H. 1908 "Grenzschichten in Flüssigkeiten mit Kleiner Reibung," *Z. Math. u. Phys.* **56**, 1–37.

BORGAS, M. S. 1993 "The multifractal lagrangian nature of turbulence," *Phil. Trans. Roy. Soc. Lond.* A **342**, 379–411.

BRANDT, P. N., GREIMEL, R., GUENTHER, E. & MATTIG, W. 1991 "Turbulence, Fractals, and the Solar Granulation," in *Applying Fractals in Astronomy* (Eds., A. Heck, J. M. Perdang, Springer, Berlin), 77–96.

BREIDENTHAL, R. E. 1981 "Structure in Turbulent Mixing Layers and Wakes Using a Chemical Reaction," *J. Fluid Mech.* **109**, 1–24.

BROWN, G. L. & ROSHKO, A. 1974 "On Density Effects and Large Structure in Turbulent Mixing Layers," *J. Fluid Mech.* **64**, 775–816.

BURKE, S. P. & SCHUMANN, T. E. W. 1928 "Diffusion Flames," *Ind. Eng. Chem.* **20**(10), 998.

CARRIER, G. F., FENDELL, F. E. & MARBLE, F. E. 1975 "The Effect of Strain Rate on Diffusion Flames," *SIAM J. Appl. Math.* **28**(2), 463–500.

CASTAGNOLI, C. & PROVENZALE, A. 1991 "From small-scale fractality to large-scale homogeneity: a family of cascading models for the distribution of galaxies," *Astro. and Astrophysics* **246**, 634–643.

CATRAKIS, H. J. 1996 *Mixing and the Geometry of Isosurfaces in Turbulent Jets*, Ph.D. thesis, California Institute of Technology.

CATRAKIS, H. J. & DIMOTAKIS, P. E. 1996a "Mixing in turbulent jets: scalar measures and isosurface geometry," *J. Fluid Mech.* **317**, 369–406.

CATRAKIS, H. J. & DIMOTAKIS, P. E. 1996b "Scale Distributions and Fractal Dimensions in Turbulence," *Phys. Rev. Lett.* **77**(18), 3795–3798.

CATRAKIS, H. J. & DIMOTAKIS, P. E. 1996c "Scale-dependent-fractal geometry," NATO Advanced Studies Institute series, *Mixing: Chaos and Turbulence* Cargèse (Corsica, France), 7–20 July 1996.

CHAPMAN, D. R. 1979 "Computational Aerodynamics Development and Outlook," *AIAA J.* **17**, 1293–1313.

CHILÉS, J. P. 1988 "Fractal and Geostatistical Methods for Modeling of a Fracture Network," *Math. Geol.* **20**(6), 631–654.

COLES, D. 1956 "The law of the wake in the turbulent boundary layer," *J. Fluid Mech.* **1**, 191–226.

COLLINS, D. J., COLES, D. E. & HICKS, J. W. 1978 "Measurements in the Turbulent Boundary Layer at Constant Pressure in Subsonic and Supersonic Flow. Part I. Mean Flow," AEDC–TR–78–21.

CONSTANTIN, P. 1989 "Remarks on the Navier-Stokes equations," in *New Perspectives in Turbulence* (L. Sirovich, Ed., Springer-Verlag, NY, 1991), 229–261.

CONSTANTIN, P. 1990 "Navier-Stokes Equations and Area of Interfaces," *Comm. Math. Phys.* **129**, 241–266.

CONSTANTIN, P. 1994a "Geometric Statistics in Turbulence," *SIAM Rev.* **36**(1), 73–98.

CONSTANTIN, P. 1994b "Geometric and Analytic Studies in Turbulence," *Trends and Perspectives in Applied Mathematics* (L. Sirovich, Ed., Springer-Verlag, NY), 21–54.

CONSTANTIN, P. & PROCACCIA, I. 1994 "The geometry of turbulent advection: sharp estimates for the dimensions of level sets," *Nonlinearity* **7**, 1045–1054.

CONSTANTIN, P., PROCACCIA, I. & SREENIVASAN, K. R. 1991 "Fractal Geometry of Isoscalar Surfaces in Turbulence: Theory and Experiment," *Phys. Rev. Lett.* **67**(13), 1739–1742.

DAHM, W. J. A. & DIMOTAKIS, P. E. 1987 "Measurements of Entrainment and Mixing in Turbulent Jets," *AIAA J.* **25**, 1216–1223.

DAHM, W. J. A., SOUTHERLAND, K. B. & BUCH, K. A. 1991 "Direct, high resolution, four-dimensional measurements of the fine scale structure of $Sc \gg 1$ molecular mixing in turbulent flows," *Phys. Fluids A* **3**(5, Pt. 2), 1115–1127.

DIMOTAKIS, P. E. 1987 "Turbulent shear layer mixing with fast chemical reactions," US-France Workshop on *Turbulent Reactive Flows* (Springer-Verlag, New York, 1989), 417–485.

DIMOTAKIS, P. E. 1991 "Fractals, dimensional analysis and similarity, and turbulence," *Nonlinear Sci. Today* #2/91, pp. 1, 27–31.

DIMOTAKIS, P. E. 1993 "Some issues on turbulent mixing and turbulence," GALCIT Report FM93–1a.

DIMOTAKIS, P. E. 1996 "Turbulence, Fractals, and CCD's," *Engineering & Science* **59**(3), 22–34.

DIMOTAKIS, P. E., MIAKE-LYE, R. C. & PAPANTONIOU, D. A. 1983 "Structure and Dynamics of Round Turbulent Jets," *Fluid Dyn. Trans.* **11**, 47–76.

ECKART, C. 1948 "An Analysis of the Stirring and Mixing Processes in Incompressible Fluids," *JMR* **VII**, 265–275.

FALCONER, K. 1990 *Fractal Geometry: Mathematical Foundations and Applications* (Wiley, Chichester, England).

FEDER, J. 1988 *Fractals* (Plenum Press, New York).

FEYNMAN, R. P., LEIGHTON, R. B. & SANDS, M. 1964 *The Feynman Lectures on Physics* **2** (Addison-Wesley Publishing Co, Reading, MA).

FLOHR, P. & OLIVARI, D. 1994 "Fractal and multifractal characteristics of a scalar dispersed in a turbulent jet," *Physica* D **76**, 278–290.

FRIEHE, C. A., VAN ATTA, C. W. & GIBSON, C. H. 1971 "Jet turbulence: Dissipation rate measurements and correlations," AGARD *Turbulent Shear Flows* CP–93, 18.1–7.

FRISH, U. 1995 *Turbulence. The Legacy of Kolmogorov* (Cambridge U.P., Cambridge U.K.).

GIBSON, C. H. 1968 "Fine Structure of Scalar Fields Mixed by Turbulence. I. Zero-Gradient Points and Minimal Gradient Surfaces," *Phys. Fluids* **11**(11), 2305-2315.

GILBRECH, R. J. 1991 *An Experimental Investigation of Chemically-Reacting, Gas-Phase Turbulent Jets*, Ph.D. thesis, California Institute of Technology.

GILBRECH, R. J. & DIMOTAKIS, P. E. 1992 "Product Formation in Chemically-Reacting Turbulent Jets," *AIAA* 30$^{\text{th}}$ *Aerospace Sciences Meeting*, Paper 92–0581.

GIRIMAJI, S. S. & POPE, S. B. 1992 "Propagating surfaces in isotropic turbulence," *J. Fluid Mech.* **234**, 247–277.

GLUCKMAN, B. J., WILLAIME, H. & GOLLUB, J. P. 1993 "Geometry of isothermal and isoconcentration surfaces in thermal turbulence," *Phys. Fluids* **5**(3), 647–661.

HAMMER, J. A. 1993 *Lifted Turbulent Jet Flames*, Ph.D. thesis, California Institute of Technology.

HESLOT, F., CASTAIGN, B. & LIBCHABER, A. 1987 "Transitions to turbulence in helium gas," *Phys. Rev.* A **36**, 5870–5873.

HINZE, J. O. 1975 *Turbulence* (2nd ed., McGraw-Hill).

JIMENEZ, J., WRAY, A. A., SAFFMAN, P. G. & ROGALLO, R. S. 1992 "The structure of intense vorticity inhomogeneous isotropic turbulence," *Studying Turbulence Using Numerical Simulation Databases — IV*, Proceedings, 1992 Summer Program (Center for Turbulence Research, NASA Ames & Stanford U.), 21–45.

KAILASNATH, P. & SREENIVASAN, K. R. 1993 "Zero crossings of velocity fluctuations in turbulent boundary layers," *Phys. Fluids* A **5**(11), 2879–2885.

KARAGOZIAN, A. R. & MARBLE, F. E. 1986 "Study of a Diffusion Flame in a Stretched Vortex," *Combust. Sci. and Technol.* **45**, 65–84.

KERSTEIN, A. R. 1991 "Linear-eddy modeling of turbulent transport. Part V: Geometry of scalar interfaces," *Phys. Fluids* A **3**(5), Pt. 2, 1110–1114.

KOLMOGOROV, A. N. 1941a "Local Structure of Turbulence in an Incompressible Viscous Fluid at Very High Reynolds Numbers," *Dokl. Akad. Nauk SSSR* **30**, 299.

KOLMOGOROV, A. N. 1941b "The logarithmically normal law of distribution of dimensions of particles when broken into small parts," *Akad. Nauk SSSR* **31**(2), 99–101.

KOLMOGOROV, A. N. 1962 "A refinement of previous hypotheses concerning the local structure of turbulence in a viscous incompressible fluid at high Reynolds number," *J. Fluid Mech.* **13**, 82–85.

KONRAD, J. H. 1976 *An Experimental Investigation of Mixing in Two-Dimensional Turbulent Shear Flows with Applications to Diffusion-Limited Chemical Reactions*, Ph.D. thesis, California Institute of Technology.

KOOCHESFAHANI, M. M. & DIMOTAKIS, P. E. 1986 "Mixing and chemical reactions in a turbulent liquid mixing layer," *J. Fluid Mech.* **170**, 83–112.

KUZNETSOV, V. R. & SABEL'NIKOV, V. A. 1990 *Turbulence and Combustion* (Hemisphere Publishing, New York).

LAHERRÈRE, J. 1996 "Distributions de type 'fractal parabolique' dans la Nature," *C. R. Acad. Sci. Paris* **322**(IIa), 535–541.

LANE-SERFF, G. F. 1993 "Investigation of the fractal structure of jets and plumes," *J. Fluid Mech.* **249**, 521–534.

LASHERAS, J., LIÑAN, A. & WILLIAMS, F. 1996 "Turbulent Combustion," NATO Advanced Studies Institute series, *Mixing: Chaos and Turbulence* Cargèse (Corsica, France), 7–20 July 1996(to appear).

LATHROP, D. P., FINEBERG, J. & SWINNEY, H. L. 1992a "Turbulent flow between Concentric Rotating Cylinders at Large Reynolds Number," *Phys. Rev. Lett.* **68**, 1515–1518.

LATHROP, D. P., FINEBERG, J. & SWINNEY, H. L. 1992b "Transition to shear-driven turbulence in Couette-Taylor flow," *Phys. Rev.* A **46**, 6390–6405.

LIEPMANN, D. & GHARIB, M. 1992 "The role of streamwise vorticity in the near-field entrainment of round jets," *J. Fluid Mech.* **245**, 643–668.

LIEPMANN, H. W. 1949 "Die Anwendung eines Satzes über die Nullstellen Stochasticher Funktionen auf Turbulenzmessungen," *Helv. Phys. Acta* **22**, 119.

LOPEZ, R. E. 1977 "The lognormal distribution and cumulus cloud populations," *Mon. Wea. Rev.* **105**, 865–872.

MANDELBROT, B. B. 1967 "How long is the coast of Britain? Statistical self-similarity and fractional dimension," *Science* **155**, 636–638.

MANDELBROT, B. B. 1975a "On the geometry of homogeneous turbulence, with stress on the fractal dimension of the iso-surfaces of scalars," *J. Fluid Mech.* **72**(2), 401–416.

MANDELBROT, B. B. 1975b *Les objets fractals: forme, hasard et dimension* (Flammarion, Paris).

MANDELBROT, B. B. 1977 *Fractals. Form, Chance, and Dimension* (W. H. Freeman & Co., San Fransisco).

MANDELBROT, B. B. 1982 *The Fractal Geometry of Nature* (W. H. Freeman & Co., NY).

MANDELBROT, B. B. 1989 "Fractal geometry: What is it and what does it do?," in *Fractals in the Natural Sciences* (M. Fleischmann, D. J. Tildesley, R. C. Ball, Eds., Princeton), 7.

MARK, D. M. & ARONSON, P. B. 1984 "Scale-Dependent Fractal Dimensions of Topographic Surfaces: An Empirical Investigation, with Applications in Geomorphology and Computer Mapping," *Math. Geol.* **16**(7), 671–683.

MATSUURA, S., TSURUMI, S. & IMAI, N. 1986 "Crossover behavior for Brownian motion," *J. Chem. Phys.* **84**(1), 539–540.

MCCOMB, W. D. 1991 *The Physics of Fluid Turbulence* (Clarendon Press, Oxford).

MERKEL, G. J., DRACOS, T. & RYS, P. 1996 "Two-dimensional and three-dimensional imaging of passive scalar fields in a turbulent jet," *Atlas of Visualization* (Eds., Nakayama, Y., Tanida, Y., CRC Press), 67–78.

MIKHAILOV, A. S. & LOSKUTOV, A. Y. 1991 *Foundations of Synergetics* **II**: *Complex Patterns* (Springer-Verlag, Berlin).

MILLER, P. L. & DIMOTAKIS, P. E. 1991a "Stochastic geometric properties of scalar interfaces in turbulent jets," *Phys. Fluids A* **3**, 168–177.

MILLER, P. L. & DIMOTAKIS, P. E. 1991b "Reynolds number dependence of scalar fluctuations in a high Schmidt number turbulent jet," *Phys. Fluids A* **3**, 1156–1163.

MONIN, A. S. & YAGLOM, A. M. 1975 *Statistical Fluid Mechanics: Mechanics of Turbulence* **II** (Ed. J. Lumley, MIT Press, Cambridge, MA).

OBOUKHOV, A. M. 1962 "Some specific features of atmospheric turbulence," *J. Fluid Mech.* **13**, 77–81.

OTTINO, J. M. 1989 *The kinematics of mixing: stretching, chaos, and transport* (Cambridge U.P., Cambridge, UK).

OTTINO, J. M. 1990 "Mixing, Chaotic Advection and Turbulence," *Ann. Rev. Fluid Mech.* **22**, 207–253.

POPE, S. B. 1988 "The evolution of surfaces in turbulence," *Int. J. Engng. Sci.* **26**(5), 445-469.

POPE, S. B., YEUNG, P. K. & GIRIMAJI, S. S. 1992 "The curvature of material surfaces in isotropic turbulence," *Phys. Fluids A* **1**(12), 2010–2018.

PRASAD, R. R. & SREENIVASAN, K. R. 1989 "Scalar interfaces in digital images of turbulent flows," *Exps. in Fluids* **7**, 259–264.

PRASAD, R. R. & SREENIVASAN, K. R. 1990a "The measurement and interpretation of fractal dimensions of the scalar interface in turbulent flows," *Phys. Fluids A* **2**(5), 792–807.

PRASAD, R. R. & SREENIVASAN, K. R. 1990b "Quantitative three-dimensional imaging and the structure of passive scalar fields in fully turbulent flows," *J. Fluid Mech.* **216**, 1–34.

PRASKOVSKY, A. A., FOSS, J. F., KLEIS, S. J. & KARYAKIN, M. Y. 1993 "Fractal properties of isovelocity surfaces in high Reynolds-number laboratory shear flows," *Phys. Fluids A* **5**(8), 22038–2042.

PRESS, W. H., FLANNERY, B. P., TEUKOLSKY, A. A. & VETTERLING, W. T. 1986 *Numerical Recipes. The Art of Scientific Computing.* (Cambridge Univ. Press).

PROCACCIA, I., BRANDENBURG, A., JENSEN, M. H. & VINCENT, A. 1992 "The fractal dimension of isovorticity structures in 3-dimensional turbulence," *Europhys. Lett.* **19**(3), 183–187.

STEIN, J. (Ed. in Chief) 1971 *The Random House Dictionary of the English Language* (Random House, NY).

RICHARDSON, L. F. 1926 "Atmospheric diffusion shown on a distance-neighbour graph," *Proc. Roy. Soc. London* A **110**, 709–737.

RICHARDSON, L. F. 1961 "The problem of contiguity: an appendix of statistics of deadly quarrels," *General Systems Yearbook* **6**, 139–187.

RIGAUT, J.-P. 1991 "Fractals, semi-fractals, and biometry," in *Fractals: Non-integral Dimensions and Applications* (G. Cherbit, Ed., Wiley, Chichester, UK), 151–187.

ROM-KEDAR, V., LEONARD, A. & WIGGINS, S. 1990 "An analytical study of transport, mixing and chaos in an unsteady vortical flow," *J. Fluid Mech.* **214**, 347–394.

ROSHKO, A. 1954 "On the development of turbulent wakes from vortex sheets," NACA Report 1191.

ROSHKO, A. 1992 "Perspectives on bluff body aerodynamics," 2nd *Int. Coll. on Bluff Body Aerodynamics*, Melbourne, Australia.

RUSS, J. C. 1994 *Fractal Surfaces* (Plenum, NY).

SADDOUGHI, S. G. & VEERAVALLI, S. V. 1994 "Local isotropy in turbulent boundary layers at high Reynolds number," *J. Fluid Mech.* **268**, 333–372.

SHEN, S. F. 1954 "Calculated amplified oscillations in plane Poiseulle and Blasius flows," *J. Aeronaut. Sci.* **21**, 62–64.

SREENIVASAN, K. R. 1984 "On the scaling of the turbulent energy dissipation rate," *Phys. Fluids* **27**, 1048–1050.

SREENIVASAN, K. R. 1991 "Fractals and Multifractals in Fluid Turbulence," *Ann. Rev. Fluid Mech.* **23**, 539–600.

SREENIVASAN, K. R. 1994 "Fractals in Fluid Mechanics," *Fractals* **2** (2), 253–263.

SREENIVASAN, K. R. & MENEVEAU, C. 1986 "The Fractal Facets of Turbulence," *J. Fluid Mech.* **173**, 357–386.

SREENIVASAN, K. R., PRASAD, R. R., MENEVEAU, C. & RAMSHANKAR, R. 1989 "The Fractal Geometry of Interfaces and the Multifractal Distribution of Dissipation in Fully Turbulent Flows," *Pure & Appl. Geoph.* **131**(1–2), 43–60.

SREENIVASAN, K. R., PRABHU, A. & NARASIMHA, R. 1983 "Zero-crossings in turbulent signals," *J. Fluid Mech.* **137**, 251–272.

SUZUKI, M. 1984 "Finite-Size Scaling for Transient Similarity and Fractals," *Prog. Theor. Phys.* **71**(6), 1397–1400.

TAKAYASU, H. 1982 "Differential Fractal Dimension of Random Walk and Its Applications to Physical Systems," *J. Phys. Soc. Japan* **51**(9), 3057–3064.

TAKAYASU, H. 1992 *Fractals in the Physical Sciences* (Wiley, Chichester, UK).

TAYLOR, G. I. 1921 "Diffusion by Continuous Movements," *Proc. London Math. Soc.* **20**, 196–212.

TRICOT, C. 1995 *Curves and Fractal Dimension* (Springer-Verlag, New York).

VAN DYKE, M. 1982 *An Album of Fluid Motion* (Parabolic Press, Stanford, CA).

VICSEK,T. 1992 *Fractal Growth Phenomena* (2nd Ed., World Scientific, Singapore).

VILLERMAUX, E. & GAGNE, Y. 1994 "Line Dispersion in Homogeneous Turbulence: Stretching, Fractal Dimensions, and Micromixing," *Phys. Rev. Lett.* **73**(2), 252–255.

VINCENT, A. & MENEGUZZI, M. 1991 "The spatial structure and statistical properties of homogeneous turbulence," *J. Fluid Mech.* **225**, 1–20.

VON KARMAN, T. 1937 "Turbulence," *J. R. Aero. Soc.* **41**, 1109–1143.

WELANDER, P. 1955 "Studies on the General Development of Motion in a Two-Dimensional, Ideal Fluid," *Tellus* **7**(2), 141–156.

WIENER, N. 1949 *Extrapolation, Interpolation and Smoothing of Stationary Time Series* (Wiley, New York).

WYGNANSKI, I. & CHAMPAGNE, F. H. 1973 "On transition in a pipe. Part I: The Origin of Puffs and Slugs and the Flow in a Turbulent Slug," *J. Fluid Mech.* **59**, 281–335.

YEE, E., CHAN, R., KOSTENIUK, P. R., CHANDLER, G. M., BILTOFT, C. A. & BOWERS, J. F. 1995 "Measurements of level-crossing statistics of concentration fluctuations in plumes dispersing in the atmospheric surface layer," *Bound. Layer Met.* **73**, 53–90.

YODA, M., HESSELINK, L. & MUNGAL, M. G. 1994 "Instantaneous 3-dimensional concentration measurements in the self-similar region of a round high-schmidt-number jet," *J. Fluid Mech.* **279**, 313–350.